Joana Filipa Duarte Almeida

Chalcone derivatives: promising starting points for the discovery of new diarylpentanoids with p53-MDM2/X inhibitory activity

Dissertation presented to the Faculdade de Farmácia da Universidade do Porto, to obtain the degree of Master in Pharmaceutical Chemistry

Work developed under the scientific supervision of Professor Honorina Maria de Matos Cidade and Professor Lucília Helena Ataíde Saraiva

U.PORTO
FACULDADE DE FARMÁCIA
UNIVERSIDADE DO PORTO

July 2019

This work was developed in Laboratório de Química Orgânica e Farmacêutica, Departamento de Ciências Químicas, and Laboratório de Microbiologia, Departamento de Ciências Biológicas, Faculdade de Farmácia da Universidade do Porto. This research was partially supported by the Strategic Funding UID/Multi/04423/2019, UID/QUI/50006/2019 and by the Projects PTDC/MAR-BIO/4694/2014 (reference POCI-01-0145-FEDER-016790; Project 3599–PPCDT), PTDC/SAU-PUB/28736/2017 (reference POCI-01-0145-FEDER-028736) and PTDC/DTP-FTO/1981/2014 (POCI-01-0145-FEDER-016581, through national funds provided by FCT – Foundation for Science and Technology and European Regional Development Fund (ERDF), through the COMPETE – Programa Operacional Factores de Competitividade (POFC) programme in the framework of the programme PT2020.

Some results presented in this dissertation are part of the following scientific communications:

- **Poster communications**

Almeida J.*,#; Moreira J.#.; Soares J; Pinto M.; Saraiva L.; Cidade H. Identification of new MDM2-p53 interaction inhibitors using yeast cell-based models. 12th IJUP – Encontro de Investigação Jovem da Universidade do Porto, Porto, Portugal, 13-15 February 2019 (P-314).

Almeida J.*,#; Moreira J.#; Soares J; Pinto M.; Saraiva L.; Cidade H. Bischalcones targeting MDM2-p53 interaction: synthesis and biological activity. 4th Escola de Inverno de Farmácia, Porto, Portugal, 18-27 March 2019 (P-50).

* Presenting author

# Authors contributed equally to this work

Acknowledgements

É muito difícil conquistar algo na vida sozinho. Por isso, gostaria de aqui agradecer a todas as pessoas que me acompanharam e apoiaram até ao final desta caminhada. Existem, no entanto, pessoas a quem gostaria de expressar a minha mais profunda gratidão, nomeadamente:

À Professora Doutora Honorina Maria de Matos Cidade, minha orientadora, pelos seus ensinamentos, pela sua paciência, pelos seus incentivos e por toda a ajuda. Obrigada ainda pela sua dedicação e por me introduzir à Química Orgânica, bem como pela sua presença incansável.

À Professora Doutora Lucília Helena Ataíde Saraiva, minha co-orientadora, pelos seus conselhos, pela sua disponibilidade, pelas revisões científicas e pela oportunidade que me deu de aprofundar os meus conhecimentos e *know-how* da Biologia Celular e Molecular. Obrigada por toda a motivação e apoio.

À Doutora Joana Soares, por me teres acompanhado afincadamente desde o meu primeiro dia no laboratório até ao dia da tua saída, por me introduzires às "bichas" e por me ensinares novas técnicas e novas formas de trabalhar. Obrigada pela tua paciência e pela tua amizade, por todas as gargalhadas que partilhámos juntas e por todo o convívio.

À Mestre Joana Moreira, por teres sintetizado a maioria dos compostos testados nesta dissertação, mas mais importante do que isso, por me acompanhares com toda a paciência no laboratório e me ensinares todas as sínteses que fiz. Obrigada também pelas conversas e desabafos e pela nossa "relação de simbiose".

Às minhas queridas colegas do 3DUnit, por todo o apoio nas técnicas, pelas conversas dos mais variados assuntos e conselhos, e pela amizade e convívio, tanto dentro como fora do laboratório.

Ao Doutor José Miguel Oliveira, meu ex-orientador, por teres sido o grande impulsionador do meu gosto pela Biologia Celular ainda nos tempos da licenciatura e me dares os conhecimentos-base, que tanto jeito me deram para esta dissertação. Obrigada principalmente pela amizade que ainda mantemos.

A todos os docentes e às colegas do mestrado com quem passei estes dois anos e em especial com quem partilhei o laboratório de Química Orgânica e Farmacêutica, pela colaboração e por todos os momentos que passámos juntas. Em particular, agradeço à Joana Teixeira, por sempre me acompanhares, por aturares as minhas fantasias lunáticas e me compreenderes como ninguém, e acreditares piamente nas minhas capacidades.

Obrigada também por me ensinares a postura de um engenheiro pelo tal fator de 20%, e nunca te esqueças: “relaxa que encaixa”!

Aos meus queridos pais, irmão e avó, a minha família mais próxima, pela ajuda e pelo carinho.

Por fim, a ti, Max Newton, meu querido amigo canino, pela tua lealdade sem igual.

“The heart may be weak. And sometimes it may even give in. But I've learned that deep down, there's a light that never goes out!”

Tetsuya Nomura, *Kingdom Hearts*

Abstract

The p53 protein is one of the most important tumor suppressors. As a transcription factor, p53 regulates the expression of many pro-apoptotic genes, as well of genes involved in cell cycle arrest, senescence and DNA repair. It therefore prevents the accumulation of abnormal cells that can lead to carcinogenesis. p53 is frequently inactivated in cancer cells, either because the *TP53* gene is mutated or deleted, or due to the inhibition of p53 protein by endogenous negative regulators like murine double minute (MDM) 2 and MDMX, in cells that retain the wild-type (wt) form. The disruption of these interactions leads to increased p53 levels and to the recovery of p53 transcriptional activity, indicating a great therapeutic potential for antagonists of the p53-MDM2/MDMX binding.

Chalcones are naturally occurring compounds found in a large variety of plants with a wide array of biological activities. These natural products have been described as potential antitumor agents, inducing cell cycle arrest and apoptosis through several mechanisms, including those involving the p53 pathway. Chalcones can also block the interaction between p53 and MDM2, by binding to a subsite of the p53 binding cleft of human MDM2, releasing p53 from the MDM2-inhibitory effect. Therefore, chalcones may represent a promising starting basis for the development of optimized inhibitors of the p53-MDM2 complex with antitumor properties.

Diarylpentanoids are a class of compounds structurally related to curcumin that consist of two aromatic rings connected by a five carbon bridge. These synthetic compounds are reported to have several pharmacological properties, and the antitumor activity is one of the most extensively studied, being in some cases associated with an activation of the p53 pathway.

Considering the restoration of wt p53 activity by disrupting its interaction with its main inhibitors MDM2 and MDMX, 7 diarylpentanoids were synthesized and tested for their p53-MDMs inhibitory activity along with 11 other structure related compounds that were previously synthesized.

The synthesis of diarylpentanoids was achieved by reacting the building blocks through the Claisen-Schmidt condensation in basic conditions at room temperature. The structure elucidation of the synthesized compounds was established through IR and NMR techniques.

A library of 18 diarylpentanoids were initially evaluated through a yeast-based assay. The obtained results showed that **BP-C4** and **BP-M245** were able to inhibit the growth of yeast cells co-expressing p53 and MDM2 without displaying cytotoxicity towards control

yeasts. **BP-C4** also inhibited the growth of yeast cells co-expressing p53 and MDMX, indicating potential dual-inhibitory activity. The results obtained in yeast cells were then validated in human tumor cells HCT116 $p53^{+/+}$ and MDA-MB-231, and in normal HFF-1 cells. In HCT116 $p53^{+/+}$ cells **BP-C4** caused cell cycle arrest and apoptosis, increased the p53 levels, upregulated p21 and PUMA, and caused PARP cleavage.

Altogether, the results presented in this dissertation pave the way to the identification of a new potential p53-MDM2/MDMX interaction inhibitor.

Keywords: chalcones, diarylpentanoids, p53, p53/MDM2, p53/MDMX.

Resumo

A proteína p53 é um dos supressores de tumores mais importantes. Sendo um fator de transcrição, a p53 regula a expressão de muitos genes pro-apoptóticos, bem como de genes envolvidos na paragem do ciclo celular, senescência e reparação de DNA. Esta proteína previne a acumulação de células anormais que possam conduzir à carcinogénese. A p53 está frequentemente inativada nas células tumorais, ou porque o gene *TP53* sofreu mutações ou deleção ou porque a proteína p53 está inativada por inibidores endógenos como a Murine Double Minute (MDM) 2 (MDM2) ou a Murine Double Minute X (MDMX), nas células que retêm a forma *wild-type* (wt). A disrupção destas interações conduz ao aumento dos níveis de p53 e à recuperação da sua atividade transcricional, indicando um grande potencial terapêutico para os antagonistas da ligação p53-MDM2/MDMX.

As calconas são compostos naturais encontrados numa grande variedade de plantas com um vasto conjunto de atividades biológicas. Estes produtos naturais foram descritos como potenciais agentes antitumorais, sendo capazes de induzir paragem do ciclo celular e apoptose através de vários mecanismos, incluindo aqueles envolvidos na via da p53. As calconas podem também bloquear a interação entre a p53 e a MDM2 ligando-se a um sublocal da bolsa de ligação da p53 que existe na MDM2 humana, libertando a p53 do efeito inibidor da MDM2. Assim, as calconas podem representar uma base promissora para o desenvolvimento de inibidores otimizados do complexo p53-MDM2 com propriedades antitumorais.

Os diarilpentanoides são uma classe de compostos estruturalmente relacionados com a curcumina, que consistem em dois anéis aromáticos ligados por uma ponte de pentano. Estes compostos sintéticos foram descritos como tendo várias propriedades farmacológicas, sendo a atividade anti tumoral uma das mais extensivamente estudadas, com alguns casos em que modulam a via da p53.

Tendo como objetivo a restauração da wt p53 pela disrupção da interação com os seus inibidores principais MDM2 e MDMX, foram sintetizados 7 diarilpentanoides inspirados em calconas, que foram depois testados de forma a avaliar a sua capacidade de inibir a interação p53-MDM2/MDMX, juntamente com 11 outros diarilpentanoides sintetizados anteriormente.

A síntese dos diarilpentanoides foi realizada pela reação dos blocos construtores através da condensação de Claisen-Schmidt em condições básicas à temperatura ambiente.

A elucidação estrutural dos compostos sintetizados foi realizada através de técnicas de espectrofotometria no Infravermelho (IV) e de ressonância magnética nuclear (RMN).

Inicialmente, uma biblioteca de 18 diarilpentanoides foi testada em ensaios de leveduras. Os resultados obtidos demonstraram que os derivados **BP-C4** e **BP-M245** foram capazes de inibir o crescimento de leveduras que co-expressavam a p53 e MDM2 sem interferir no crescimento das leveduras-controlo. Adicionalmente, o derivado **BP-C4** inibiu o crescimento das leveduras que co-expressavam a p53 e a MDMX, indicando uma potencial atividade inibidora dual. Os resultados obtidos em leveduras foram depois validados nas linhas celulares humanas tumorais HCT116 e MDA-MB-231, bem como na linha HFF-1 de fibroblastos humanos. O derivado **BP-C4** demonstrou ter uma ligeira seletividade para a via da wt p53 e provocou a paragem do ciclo celular e indução da apoptose, assim como o aumento dos níveis de p53, p21 e PUMA, e quebra de PARP.

Em resumo, os resultados apresentados nesta dissertação abrem as portas a uma potencial descoberta de um novo inibidor dual das interações p53-MDM2/MDMX.

Palavras-chave: calconas, dirarilpentanoides, p53, p53/MDM2, p53/MDMX

Table of Contents

Table of figures

Table of tables

Abbreviations and Symbols

^{13}C NMR – Carbon-13 Nuclear Magnetic Resonance

^{1}H NMR – Proton Nuclear Magnetic Resonance

AML – Acute Myeloid Leukemia

ANS – Anthocyanidin Synthase

ARF – Alternative Reading Frame

ASPP – Apoptosis-Stimulating of p53 protein

ATP – Adenosine Triphosphate

CBP – CREB Binding Protein

CD95 – Cluster of Differentiation

CDK – Cyclin-Dependent Kinase

CFU – Colony Formation Unit

CHI – Chalcone Flavone Isomerase

Chk2 – Checkpoint Kinase 2

CLL – Chronic Lymphocytic Leukemia

CREB – CAMP Response Element Binding Protein

CSH – Chalcone Synthase

CTD – Carboxyl-Terminal Domain

Cyt C – Cytochrome *C*

d – Doublet

DBD – DNA-Binding Domain

dd – double of doublets

DFR – Dihydroflavonol Reductase

DMSO – Dimethyl Sulfoxide

DN – Dominant Negative

DR – Death Receptor

EGR-1 – Early Growth Response Protein 1

ELISA – Enzyme-Linked Immunosorbent Assay

EMSA – Electrophoretic gel Mobility Shift Assay

EMT – Epithelial-mesenchymal Transition

F3H – Flavanone 3-hydroxylase

GAPDH – Glyceraldehyde 3-phosphate dehydrogenase

GI_{50} – Concentration for 50% of maximal inhibition of cell proliferation

GOF – Gain of Function

GST – Glutathione S-Transferase

HMBC – Heteronuclear Multiple Bond Correlation

HRMS – High Resolution Mass Spectroscopy

HRP – Horseradish-peroxidase

HSP – Heat Shock Protein

HSQC – Heteronuclear Single Quantum Coherence Spectroscopy

IC_{50} – Concentration that causes an inhibitory effect of 50%

IMiD – Immunomodulatory Imide Drug

IR – Infrared

iv - Intravenous

Leu – Leucine

LOF – Loss of Function

m – Multiplet

MDM2 – Murine Double Minute 2

MDMX – Murine Double Minute X

MDR1 – Multidrug Resistance 1

Met – Methionine

miRNA – microRNA

MMP – Matrix Metalloproteinase

MMP – Mitochondrial Membrane Permeabilization

MTT – 3-(4,5-dimethylthiazol-2-yl)-2,5-diphenyltetrazolium bromide

mutp53 – mutant p53

NEDD – Neural precursor cell Expressed, Developmentally Downregulated 8

NES – Nuclear Export Signal

NF-Kb – Nuclear Factor kapa B

NLS – Nuclear Localization Signal

NoLS – Nucleolar Localization Signal

OD – Oligomerization Domain

OD_{600} – Optical Density at 600 nm

PARP – Poly ADP Ribose Polymerase

PCAF – p300/CBP Associated Factor

PCNA96 – Proliferating Cell Nuclear Antigen

Phe – Phenylalanine

PICT1 – Protein Interacting with Carboxyl Terminus 1

PP – Proline rich region

PROTAC – PROteolyzis Targeting Chimeras

PTEN – Phosphatase and Tensin Homolog

PUMA – p53 Upregulated Modulator of Apoptosis

q – Quadruplet

qRT-PCR – Quantitative Real Time Polymerase Chain Reaction

Rb – Retinoblastoma Protein

RING – Really Interesting New Gene

RNA-Seq – RNA Sequencing

ROS – Reactive Oxygen Species

RT-PCR – Real Time Polymerase Chain Reaction

s – Singlet

SDS-PAGE – Sodium Dodecyl Sulphate-Polyacrilamide Gel Electrophoresis

SEM – Standard Error of Mean

Ser – Serine

SNP – Single Nucleotide Polymorphism

SRB - Sulforhodamine B

STAT3 – Signal Transducer and Activator of Transcription

STS – Stilbene Synthase

t – Triplet

TAB1 – TGF-beta Activated kinase 1

TAD – Transactivation Domain

TCA – Trichloroacetic Acid

TLC – Thin Layer Chromatography

Try – Tryptophan

Tyr – Tyrosine

UCH-L1 – Ubiquitin Carboxyl-terminal Hydrolase L1

UFGT – UDP Glucose-Flavonoid-3-*O*-Glucosyl Transferase

USP2a – Ubiquitin-Specific Cystein Protease 2a

VEGF – Vascular Endothelial Growth Factor

wt – Wild-type

YY1 – Yin Yang 1

Outline of the dissertation

This dissertation is organized into five chapters:

CHAPTER I – Introduction

The first chapter covers the theoretical foundation for the developed work in this dissertation and is divided into four subchapters. The first subchapter focuses on a review about p53 and its role, its inhibitors MDM2 and MDMX and their structures. It also covers some of the reported targeting strategies for this pathway. The second subchapter reviews some chalcone derivatives that were reported to modulate the p53 pathway, and derivatives that disrupt the p53-MDM2 interaction. The third subchapter deals with diarylpentanoids and gives some examples of diarylpentanoids reported to target the p53 pathway. The fourth subchapter establishes the aims of this work.

CHAPTER II - Results and Discussion

The second chapter focuses on the results and discussion of the developed research work, being sub-divided into two subchapters, which cover the synthesis of the obtained compounds and their biological evaluation. These subchapters are followed by the discussion of the obtained results.

CHAPTER III - Experimental

The third chapter covers the experimental procedures taken for the synthesis of eight diarylpentanoids, and for the performed biological activity assays.

CHAPTER IV - Conclusions and Perspectives

The fourth chapter presents the main conclusions of the work, as well as future work for a better understanding of the obtained results.

CHAPTER V - References

The fifth chapter presents a list of the references used in this dissertation. The references followed the American Chemical Society style guide. The main bibliographic research motors were Scopus, PubMed, Science Direct, Web of Science and Google.

CHAPTER I

Introduction

1. The p53 tumor suppressor protein

Initially, p53 was identified in transformed rodent cells in complex with the simian virus 40 T antigen[1,2] and was recognized as a tumor suppressor for the first time in 1989[3,4]. This protein is deeply involved in the DNA damage response, and as such, it is often called as the "guardian of the genome". *TP53*, which is the gene that codes p53, was subsequently found to be most frequently mutated gene in cancer[5,6]. It is located at the short arm of chromosome 17 (17p13.1)[7,8] and is 20 kb in size, having a non-coding exon 1 and a long first intron of 10 kb[9].

1.1. Structure of p53

The p53 protein is a transcription factor that consists of several well-characterized functional domains (Figure 1). At the amino terminus there are two tandem transcription activation domains (TAD1 and TAD2) that together constitute the TAD region[10–12]. Both TADs are necessary for proper p53 target gene induction in response to DNA damage and p53 tumor suppressor function in mice[13]. However, there are some differences in how mutations in each TAD affect gene expression. Overall, a TAD1 mutant has greater effects on target-gene expression than a TAD2 mutant. Nevertheless, the TAD1 mutant maintains expression of some genes, like *Bax*, that were lost after inactivation of both TADs, indicating their role in determining p53 target gene selection[13]. The TADs also mediate the interaction with the histone acetyltransferases CBP/p300 and PCAF and with the E3 ubiquitin ligase murine double minute (MDM) 2[14].

The TADs are followed by a proline-rich domain (PP), which contributes to transcription activation and is required for restricting cell growth (Figure 1[15,16])[17]. The PP interacts with the Sin3 corepressor and ensures the stability and transcriptional activity of p53, and also induces transcription-independent apoptosis[14]. This region is then followed by the DNA-binding domain (DBD) or core domain[18], which has been crystalized complexing with DNA[19–21] and is p53's most frequently mutated region (Figure 1)[18]. This region is linked by a flexible linker to the tetramerization domain (Tet), which regulates the oligomerization state of p53 and gives it biological activity as a homotetramer (Figure 1). Although the core domain of p53 is able to tetramerize on its own after complexation with DNA and is able to form stable interactions[22], the OD facilitates these interactions[23].

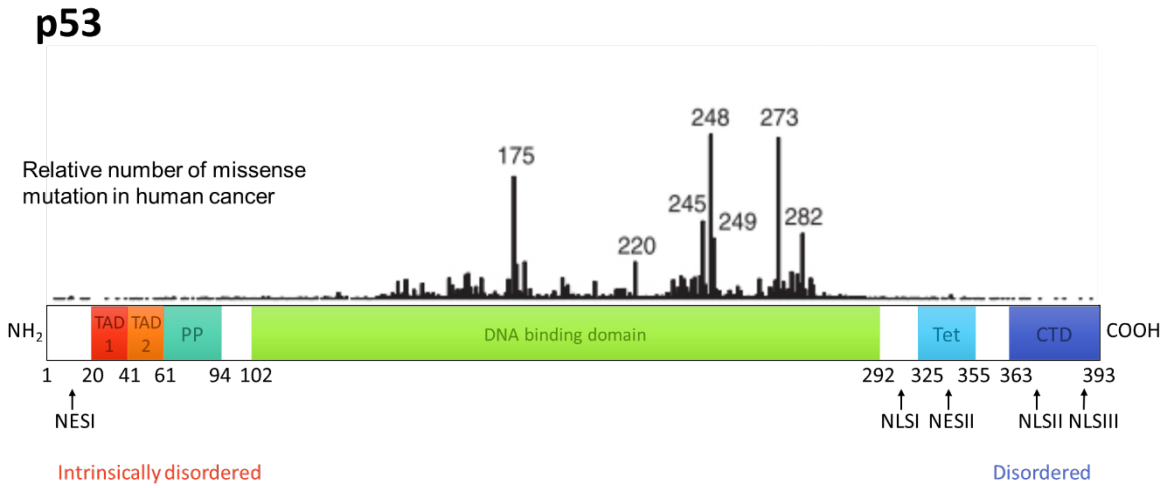

***Figure 1**: Schematic domain structure of p53. The N-terminal region (residues 1-101) includes the transactivation domain (TAD), which can be divided into two subdomains (TAD1 and TAD2); a proline-rich region (PP) which contains five PXXP sequence motifs critical for induction of apoptosis; and a Nuclear Export Signal (NES) between residues 11 and 27. The central domain (residues 102-292) encompasses the DNA binding domain. The majority of p53 missense mutations occur in this region, as indicated by the vertical bars for each residue. The C-terminal region (residues 292-393) contains a flexible linker region (residues 292-324) connecting the core domain to the tetramerization domain (Tet, residues 325-355). It also contains a basic regulatory domain (CTD, residues 363-393), as well as NES and Nuclear Localization Signals (NLS) sequences. Adapted from Joerger* et al. *2010[15] and Karni-Schimidt* et al. *2016[16]).*

Mutations in the OD have been reported to impair the DNA-binding ability of p53, leading to the loss of its transcriptional activity, as demonstrated by crystal structures[24–26].The remaining region is the carboxy-terminal domain (CTD) (Figure 1). The role of this domain is still unknown. The CTD is highly unstructured[27] and post-translationally modified, being the main site of acetylation[28]. Initially it was thought that the CTD had a negative regulatory role due to the fact that recombinant p53 would bind weakly to its targets[29] and this binding could be improved with antibodies against the CTD or by phosphorylation[29] or acetylation[28,30] of this region. This hinted at the existence of allosteric inhibition of p53 DNA binding by the CTD, which could be released by certain signals. Nonetheless, the lack of CTD conformational change after DNA binding[31] and strong p53 DNA binding *in vitro* in the absence of competing DNA[32] has questioned this theory. Regardless, the CTD is essential for *in vitro* DNA binding and transcription activity[33], and other roles have been suggested, such as promotion of p53 linear diffusion along DNA[34–36], binding to nonlinear DNA[37,38] and binding to nucleosomes[39].

1.2. Regulation of p53 activity

The p53 protein seems to be quite unstable in normal cells, with a half-time ranging from 5 to 30 minutes. Therefore, p53 is kept at very low levels and in its inactive state in normal conditions[40]. However, when cells start to experience stress, p53 stabilizes and

becomes active in response to the intra- and extracellular stress signals. The accumulation of p53 in the cell nucleus may lead to apoptosis, cell-cycle arrest and DNA repair[41]. Regardless of cellular context, the levels and activity of p53 are under tight control through numerous mechanisms. Some of these mechanisms include stabilization, anti-repression, acetylation, methylation, sumoylation, neddylation, regulation by the ASPP family, 53BP1 and other cofactors[42]. Among these, the regulation by MDM2 and MDMX (also known as MDM4) has been recognized as a very important mechanism for the discovery of new potential anticancer drugs.

1.2.1. MDM2 and MDMX

1.2.1.1. Structural features

MDM2 is an E3 ubiquitin-protein ligase and is the main negative regulator of p53[43]. It is a complex and highly regulated protein, with 491 residues comprising numerous functional domains, signal sequences and sites of modification (Figure 2A). It can also be expressed as different isoforms generated by alternative splicing[44]. The N-terminal region is important for the interaction with p53 and for the inhibition of the p53 ability to be transcriptionally active. This region is followed by a linker in which there is a nuclear localization signal (NLS) and a nuclear export signal (NES), at positions 178 and 192 respectively. The central acidic domain contributes to the degradation of p53[45,46], and is followed by the zinc-finger domain, which is involved in the interaction with several proteins, like ribosomal and nucleolar proteins, as well as the tumor suppressor p14^{ARF}[47]. Lastly, the MDM2 C-terminus includes a RING domain (Really Interesting New Gene; amino acids 436-482), which has a cryptic nucleolar localization signal (NoLS; residues 466-473) and residues at the extreme C-terminus (aminoacids 485-491) that have a role in interactions between RING domains[48,49]. The MDM2 RING domain is responsible for the E3 ligase activity of this protein, and this is critical for MDM2 to be able to restrain p53 during the early stages of embryogenesis. Point mutations in the RING domain of MDM2 promote p53-dependent mortality in a very similar way to that caused by the deletion of the entire gene that codes MDM2, indicating the importance of the RING region[50].

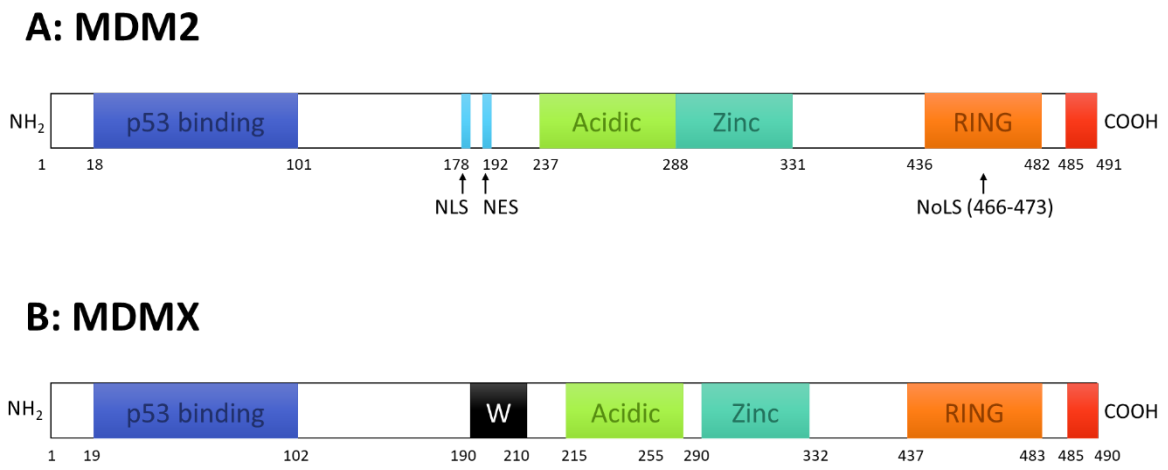

***Figure 2**: Schematic domain structures of MDM2 and MDMX. (A) MDM2 structure includes the N-terminal p53 binding domain (residues 18-101), the acidic domain that binds to ARF and also plays a role in ubiquitinating p53 (residues 237-288), and the zinc finger motif (residues 289-331) which interacts with ribosomal proteins. The MDM2 C-terminus contains the RING region, which is responsible for its E3 ligase activity, and the carboxyl terminus tail, which regulates the RING motif through MDM2 homodimer formation and MDM2 and MDMX heterodimerization. MDM2 also contains NLS, NES and Nucleolar Localization Signal (NoLS) sequences in its structure. (B) MDMX is structurally similar to MDM2, also containing a N-terminal p53 binding region (residues 19-102), a central acidic (residues 215-255) and zinc-finger (residues 290-332) domains and a RING domain (residues 437-483) located at the C-terminus. However, unlike MDM2, MDMX lacks NES, NLS or NoLS sequences, but has a unique WWW motif (W, residues 190-210) that inhibits interaction with p53. MDMX also lacks E3 ligase activity, unlike MDM2. The carboxyl-terminal tail (residues 485-490) is necessary for the heterodimerization of MDM2 and MDMX. Adapted from Karni-Schimidt* et al. *2016*[16].

Three regions of interaction between p53 and MDM2 have been identified (Figure 3). The first documented interaction occurs between TAD 1 and MDM2 p53 N-terminal domain. This interaction is responsible for the inhibition of p53 binding to the transcriptional systems[51]. In 1996, a crystal structure analysis of a p53 peptide bound to the MDM2 N-terminus (which comprised amino acids 15-29) identified a specific hydrophobic pocket in MDM2 that included the amino acids phenylalanine 19, tryptophan 23 and leucine 26 in p53[52]. Some studies have suggested that p53 may adopt a helical conformation upon binding to MDM2[51,53]. The two large hydrophobic amino acids of p53 Phe19 and Trp23 are located face to face on the same side of the helix, and along with Leu26, they point towards the MDM2 protein, surrounded by several hydrophobic residues from MDM2. Afterwards, some studies indicated an interaction between the DBD of p53 and the central acidic domain of MDM2[54–57], which is essential for an efficient p53 ubiquitination. Additionally, the acidic region of MDM2 was reported to inhibit the p53 interaction with DNA due to the promotion of a conformational change in p53[58]. In 2010, a third interaction was described between the p53 C-terminus and MDM2 N-terminus, indicating that the p53-MDM2 interaction is decreased after deletion of the p53 C-terminus, and that modifications of this region can indeed regulate the interaction between MDM2 and p53[59].

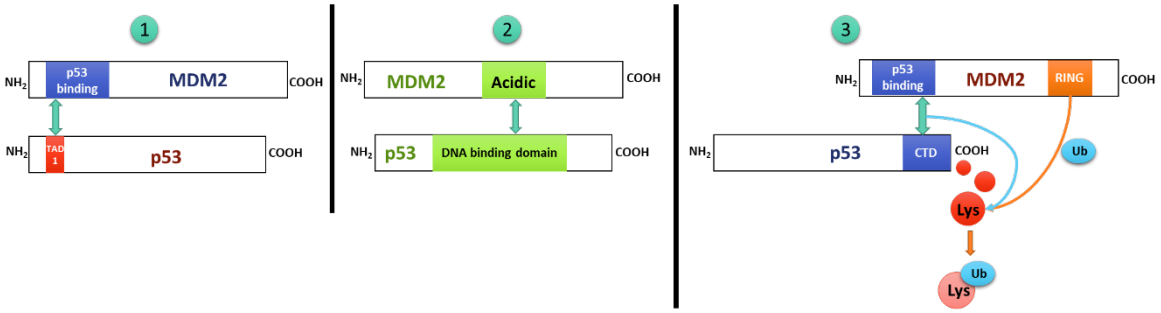

***Figure 3**: The interactions between p53 and MDM2 involve three regions of each protein. (1) The main interactions occur between MDM2 N-terminal region and p53 N-terminal TAD1. (2) The acidic domain of MDM2 can interact with p53 DNA-binding domain. (3) MDM2 N-terminal domain can also interact with the p53 C-terminal domain, which harbors lysines that are ubiquitinated through the MDM2 RING region.*

The MDMX protein consists of 490 amino acids (Figure 2B) and its overexpression inhibits p53 transcriptional activity. This effect is dependent on the p53 binding domain of MDMX[60]. MDMX lacks the NLS, NoLS and NES sequences and is mainly localized in the cytoplasm. However, after association with different partners, particularly MDM2, and after DNA damage, MDMX may be found in the nucleus. Interestingly, the precise amino acids required for interacting with the p53 N-terminus in MDM2 and MDMX are identical. Still, even though MDM2 and MDMX share high homology between their p53-binding pockets, a structural analysis revealed important differences between these two pockets, namely two different residues in MDMX's binding pocket[61]. Unlike MDM2, MDMX does not exhibit E3 ligase activity in its RING domain, nor directly promotes p53 degradation. However, it interacts with MDM2 through its RING motif, affecting levels of both p53 and MDM2[62–64]. Additionally, both MDM2 and MDMX have P-loop regions in their RING domains, which allows them to bind specifically to ATP[48,65–68].

In 2013, an auto-inhibitory sequence motif was described in MDMX, near the residues Trp200 and Trp201, and was given the name of WWW element[69]. The absence of this region increases the interaction with p53 by 32-fold. The WWW element binds to the MDMX own N-terminal domain, preventing binding to p53. This region may justify the existence and the oncogenic impact of alternatively spliced MDMX proteins that lack this motif and that are present in some aggressive tumors, raising the possibility of another level of regulation.

1.2.1.2. The p53-MDM2 interaction and its effects

MDM2 has a critical role in regulating the levels of p53, whether cells are under normal or stress conditions[70–72]. After being ubiquitinated, p53 is degraded by the 26S proteasome (Figure 4[73]). This ubiquitination occurs at several lysine amino acids located at

the C-terminus, and it requires MDM2 E3 ubiquitin-ligase function. Additionally, MDM2 has a postubiquitination role in enabling the direct interaction of p53 with the proteasome[74]. MDM2 is also essential for regulating p53 activity through mediation of p53 export from the nucleus, which involves monoubiquitination and sumoylation[74].

The *MDM2* gene contains two promoters: P1 and P2. In many cells, the P1 promoter is constitutively active, though at low levels. The P2 promoter has two p53 binding sites and is activated in response to cellular stress in a p53-dependent way[75,76]. By interacting with these sites, p53 mediates the transcription of the *MDM2* gene, becoming part of the p53-MDM2 negative-feedback loop. This auto-regulatory system between the two proteins is essential not only for keeping p53 in check, but also for increasing the levels of p53 after the cells start to experience mild forms of stress. These interactions result in oscillation of cellular levels of both proteins, which has been observed both in populations of cells[77] as well as in individual cells[78]. However, this oscillation is altered in cells that express high levels of MDM2, due to the fact that the promoter region of their MDM2 proteins has a single nucleotide polymorphism (SNP)[78].

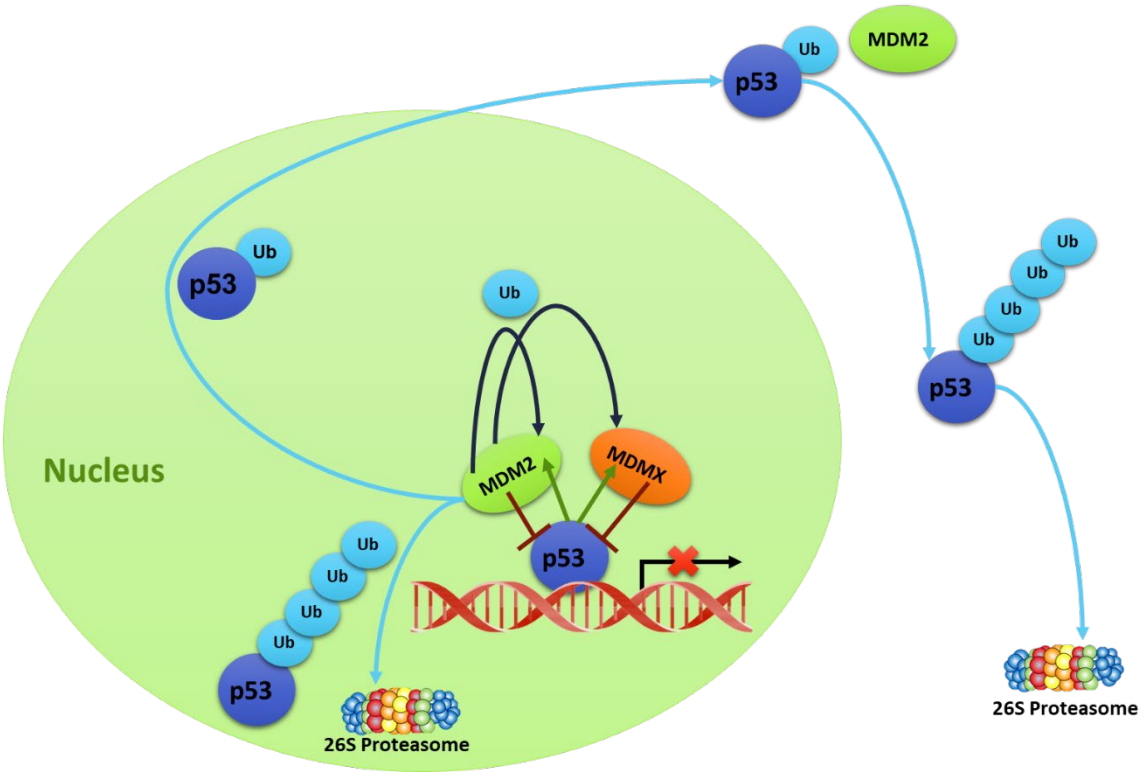

***Figure 4**: Regulation of p53 by MDM2 and MDMX. p53 regulates MDM2 and MDMX transcription levels (green arrows), while MDM2 and MDMX inhibit p53's transcriptional function. MDM2 can also promote p53 nuclear export to the cytoplasm for ubiquitin-mediated degradation by the proteasomes. It can also promote the nuclear degradation of p53 (polyubiquitination), MDMX ubiquitination and its own ubiquitination and degradation. Ub: ubiquitin. Adapted from Soares* et al. *2017*[73].

Interestingly, it has been observed *in vivo* that this feedback loop is important in hematopoiesis for the regulation of p53 activity (especially in response to DNA damage), but not for homeostasis, longevity or development[77]. In mice, point mutations in the two p53-binding sites of the MDM2 promoter introduced into the endogenous MDM2 locus induced an increased response to DNA damage, although p53 degradation in different tissues remained similar to the wt control. This implies that MDM2 has different roles in different tissues, and it also highlights the importance of their understanding.

Furthermore, a p53-response element has been identified in the MDMX promotor, which adds more complexity to the understanding of p53 regulation, since it has the potential to form another negative-feedback loop[79]. Like MDM2, MDMX also has a promoter named P2, which is responsive to p53 and produces a longer human MDMX transcript called HDMX-L, with 18 extra residues in N-terminus. This transcript has a critical role in MDM2-mediated p53 ubiquitination by turning p53 levels down to normal after stress activation[60]. It is still unknown when and under what conditions p53 regulates MDMX through its P2 promoter.

In addition to these mechanisms, MDM2 is regulated by many other partners, such as Alternative Reading Frame (ARF) tumor suppressor protein ($p14^{ARF}$)[80–83], microRNAs (miRNAs)[84–86], miR-605, a small nucleolar RNA-derived miRNA50[87,88], 14-3-3σ[89], the Ubiquitin-Specific Cystein Protease 2a (USP2a)[90], the ribosomal protein L11 (RPL11)[91,92], Protein Interacting with Carboxyl Terminus 1 (PICT1)[93], Yin Yang1 (YY1)[94], AKT recruited by survival signals[95], Neural precursor cell Expressed, Developmentally Downregulated 8 (NEDD8)[96] and others (Figure 5[43]).

The MDM2 interaction with its diverse protein partners indicates that its activity occurs under a complex regulatory network that ultimately modulates the ubiquitination and proteasomal degradation of p53 in a cell context-dependent manner. Adding to these partners, two other distinct regulatory mechanisms influence the p53/MDM2 axis under normal and pathological conditions (Figure 6). The level of MDM2 in cells is one of these mechanisms. A low level of MDM2 can monoubiquitinate p53 and to induce nuclear export of p53. But, on the other hand, a high level of MDM2 leads to polyubiquitination of p53 and nuclear degradation[17]. The second mechanism is activated when the monoubiquitinated p53 moves to the cytoplasm and recruits another set of proteins called polyubiquitin ligase (E4) enzymes[76]. The presence of these enzymes in the cytoplasmic compartment is essential for the polyubiquitination of p53 for downstream proteasomal degradation. The p300 and cAMP-response element-binding protein (CREB) are two ubiquitination factors with E3 and E4 activities required for endogenous p53 polyubiquitination and proteasomal

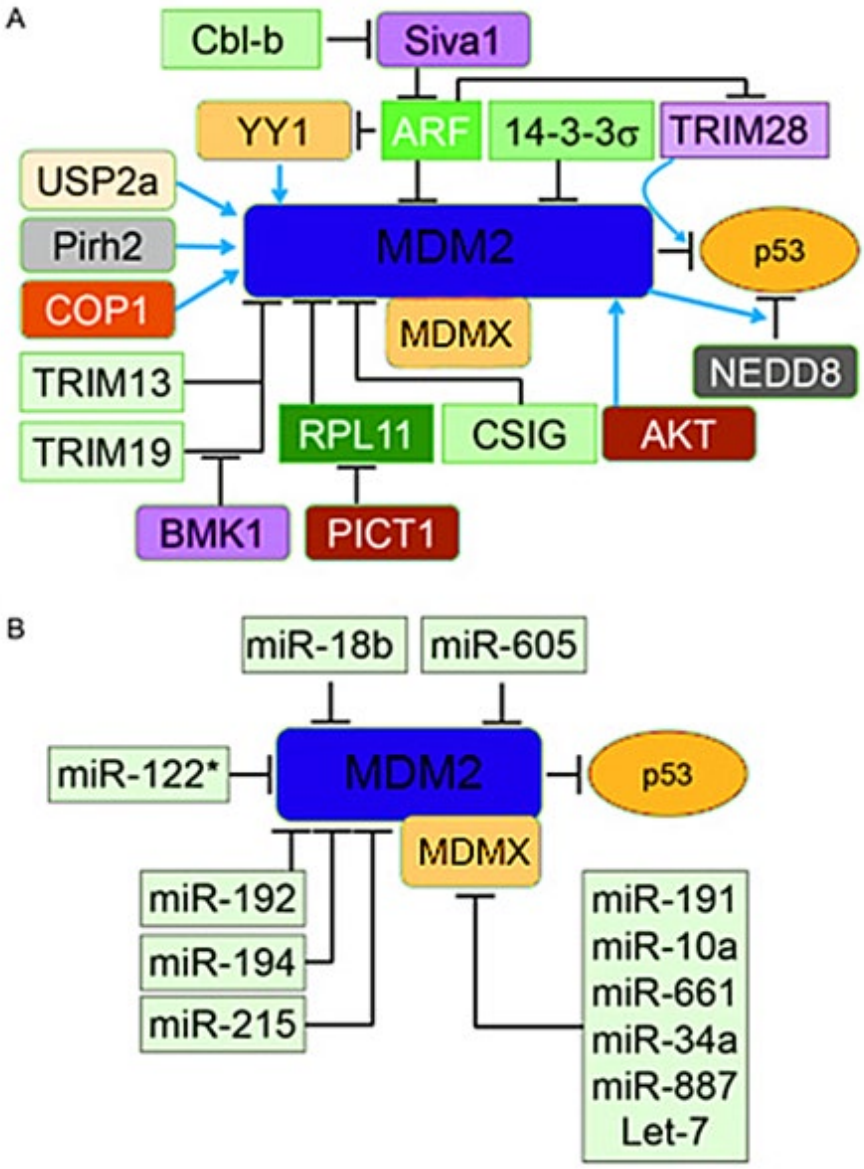

***Figure 5**: Regulation of MDM2 protein. By binding to p53, MDM2 promotes ubiquitination of p53. The presence of MDMX and its binding to MDM2 enhances ubiquitination and proteasomal degradation of p53. The activity of MDM2 and MDMX is modulated by several regulatory proteins expressed as part of oncogenic events. Understanding the role of MDM2 and MDMX regulators in different grades of human tumors can open a new therapeutic window for a subset of cancer patients. Panels A and B illustrate the proteins and microRNA partners of MDM2 and MDMX proteins, respectively. Induction of gene expression or protein activation is shown by pink arrows and inhibition of gene expression or block protein activity is shown by T-bars. Cbl-b, Casitas B-cell lymphoma-b; RPL11, ribosomal protein L11; COP1, constitutive photomorphogenesis protein 1; Pirh2, p53-induced protein with a RING-H2 domain; ARF, alternative reading frame (p14ARF); NEDD8 neural precursor cell expressed, developmentally down-regulated 8; USP2a, Ubiquitin-specific cysteine protease 2a; PICT1, protein interacting with carboxyl terminus 1. Adapted from Sane* et al. *2017*[43].

degradation of p53 in unstressed cells. P300 and CREB are exclusively cytoplasmic and cannot be found in nuclear extracts[77,78]. E4B (also called UBE4B) is another E3 and E4 ubiquitin ligase. E4B binds to p53 and MDM2, promoting ubiquitination and proteasomal degradation of p53, which results in the inhibition of p53-dependent transactivation and apoptosis. E4B is particularly overexpressed in human brain tumors and leads to inactivation of p5379.

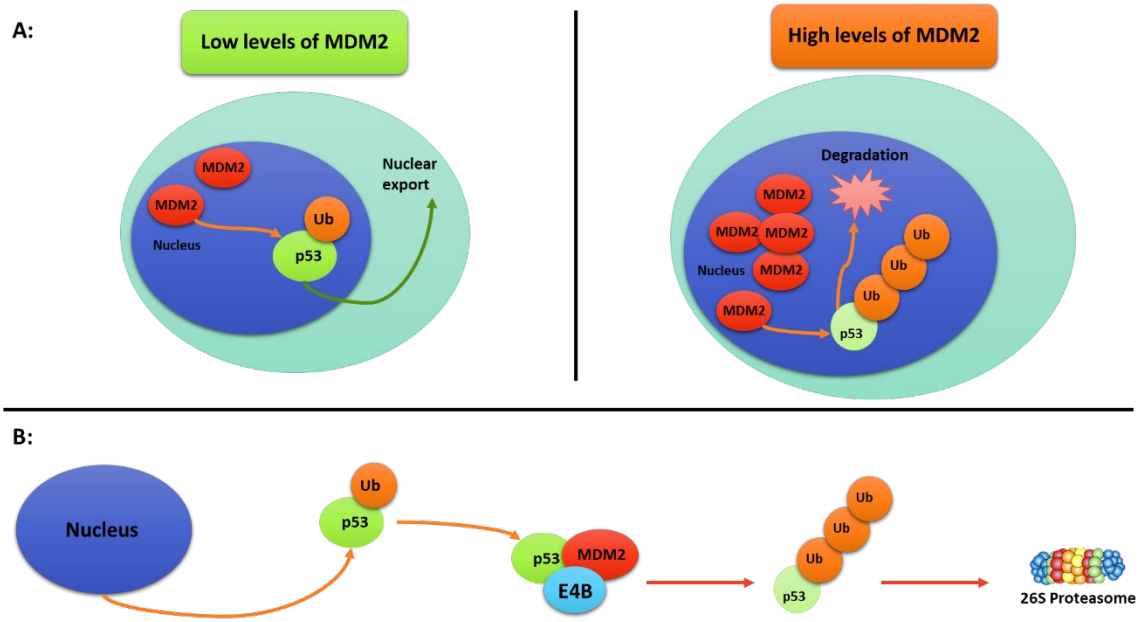

***Figure 6**: Two regulatory mechanisms that influence the p53/MDM2 axis. (A) A low level of MDM2 can monoubiquitinate p53 and induce nuclear export of p53. High levels of MDM2 lead to polyubiquitination of p53 and nuclear degradation. (B) The monoubiquitinated p53 moves to the cytoplasm and recruits E4B, which binds to p53 and MDM2, promoting ubiquitination and proteasomal degradation of p53. This results in the inhibition of p53-dependent transactivation and apoptosis.*

1.2.1.3. The p53–MDM2/MDMX Axis

The most studied, and probably the most important, role of MDM2 and MDMX in oncogenesis is through their interaction with p53. There are two primary models that have been proposed for this interaction[64]. One of these models suggests that MDM2 and MDMX independently regulate some specific activities of p53; MDM2 is responsible for the control of the cellular levels of p53, and MDMX only modulates the transcriptional activity of p53. The other model, however, states that MDM2 and MDMX regulate each other by interaction, and together they modulate the p53 function. Even though the second model is the most supported – for example, the inhibition of the p53 function by MDM2 has been shown to be enhanced through interaction with MDMX[97] – this scenario is more complex than it seems, as revealed by *in vivo* studies in mice. MDMX has proven to be as important as MDM2 during embryonic development, since both MDM2- and MDMX- knockout mice exhibit p53-

dependent embryonic lethality that can be reversed by p53 loss, though MDM2-null mice die in the preimplantation stage and MDMX-null embryos die later, around the embryonic days 7.5-9.5[98,99]. This embryonic lethality resulting from the individual loss of either MDM2 or MDMX suggests that they are not functionally redundant. Nevertheless, p53 and MDMX double-null mice that overexpress MDM2 are viable, which indicates that MDM2 can compensate for the phenotype observed with the loss of MDMX when expressed at high levels[100]. Overall, the literature on these two proteins indicates that they seem to work together to restrain p53.

The RING-finger regions of both MDM2 and MDMX are essential for their activity towards each other and towards p53. When they interact with each other, MDM2 and MDMX form a complex[62,63]. Some quantitative assays have showed that there is 5-10 times more cellular MDM2 than MDMX in mammary epithelial cell and normal human fibroblasts. This indicates that most MDMX binds to MDM2, since the binding affinity for establishing a heterodimer is higher than for forming MDM2 homodimers[63,101]. Wang *et al* reported that the heterodimerization of the RING domains of MDM2 and MDMX results in a complex that has the ability to mediate p53 polyubiquitination by MDM2, which mainly monoubiquitinates p53 by itself[102]. This work also suggests that the previous observations of MDM2 polyubiquitinating p53 were caused by artificial activation due to the use of glutathione S-transferase (GST) -tagged MDM2 in *in vitro* assays.

Some studies have demonstrated that the binding of MDM2 and MDMX through their RING domains is crucial for efficient p53 degradation in adult tissues[103,104]. Moreover, MDM2 has been suggested to regulate, albeit indirectly, the stress-induced levels of p53 by downregulating MDMX levels. More specifically, MDM2 can induce nuclear localization and E3-dependent degradation of MDMX after gamma irradiation of cancer cell lines, and the downregulation of MDMX contributes to p53 activation by irradiation[105–107].

Additionally, the extreme five residues at the C-terminus of MDM2 have been reported to play a crucial role in E3 ligase function both *in vivo* and *in vitro*[48,49]. The formation of the MDM2-MDMX heterodimer seems to be essential for embryonic development, as shown in mouse models in which either a single missense mutation within, or deletion of the MDMX RING domain (which prevents interaction with MDM2) results in early embryonic lethality[108,109]. However, the requirement of MDM2 E3 ligase activity during embryogenesis for regulating p53 has been questioned in the last years. In 2014, a study using a mouse model with a MDM2 that lacked E3 ligase activity but retained the ability to bind to MDMX (Y487Aknockin) showed that in normal conditions, the development of these mice into

adulthood was normal[110]. This discrepancy between recent and earlier reports is still not resolved.

Even though MDM2 and MDMX share a high degree of homology, they have some distinct functions. MDM2 is able to inhibit the interactions between p53 and DNA through its acidic domain, while MDMX only slightly mitigates this interaction[58]. However, MDMX is able to induce a p53 conformational change, protecting it from proteasomal degradation after DNA damage in an ubiquitin- and MDM2-independent manner, which is an effect not observed with MDM2[111]. Additionally, despite the high similarity between them, the MDM2 and MDMX binding pockets for p53 have some differences, as shown by a structural analysis of these domains bound to a p53 N-terminal peptide[61]. The precise amino acids essential for interaction with p53 are identical, but the Met53 and Tyr99 residues in MDMX protrude into its p53-binding pocket, blocking it slightly. The WWW inhibitory region present in MDMX, but not in MDM2 (as mentioned earlier), indicates that there might be a mechanism of regulation in which this domain competes with the p53 TAD1 region for binding to the MDMX N-terminal domain. This may emphasize the potential oncogenic capacity of MDMX splice variants that lack the WWW region, which are present in some aggressive tumors. Furthermore, it has been demonstrated in many human cancers expressing wt p53 that functional deactivation is a result of overexpression and amplification of either MDM2 or MDMX. Tumors that overexpress MDM2 (like liver tumors) are different from those that overexpress MDMX (for example colon tumors), which implies that MDM2 and MDMX have distinct roles in cancer[112,113]. Regardless of these differences, there is evidence that MDM2 and MDMX work together, and this cooperation is what probably makes them both required to effectively inhibit p53 during embryogenesis.

It is worth mentioning that many tumors exhibit either a p53 mutation or MDM2 and/or MDMX amplification. For example, in 2014, a study analyzed samples of infiltrating ductal breast carcinoma, where it was observed an overexpression of either MDM2 or MDMX in more than half the cases; however, this overexpression was rarely present in the samples with a p53 dysfunction[114]. Curiously, the overexpression of MDMX has been observed in a wide variety of human cancers and can prevent the p53 tumor suppression effect[114].

Intriguingly, it has also been reported that MDMX may have a potential tumor suppressor role, which can be either p53-dependent or -independent, in different experimental settings. MDMX is able to suppress tumorigenesis in a p53-independent way by promoting centrosome clustering and bipolar mitosis[115,116]. MDMX and p53 double-null mice overexpressing MDM2 show fast rates of tumor formation, which are not observed in

mice that have both MDMX alleles, indicating that MDMX has a context-dependent tumor-suppressive function[100]. Also, in response to DNA damage, MDMX has been shown to translocate to the mitochondria, promoting p53 phosphorylation at serine 46, contributing to p53-mediated apoptosis in cisplatin-treated cells[117] in way that requires TAB1's activity[117]. It remains to be discovered if these unexpected effects of MDMX are relevant to human cancer as a disease or not.

1.3. p53 and cancer development

One common aspect among the different types of human cancers is the loss of the tumor suppressor function of p53. In theory, the pharmacological restoration of p53 should result in tumor regression, as supported by several studies[118,119].

In about half of human cancers, p53 is inactivated through mutations, most of which occur in the DNA-binding domain (Figure 1). There are two types of mutations that may occur: "contact", which eliminate an essential DNA contact (like R273H and R248Q), and "structural", which cause structural faults, like formation of internal (V143A and F270L) or surface cavities (Y220C) and even structural distortion in many parts of the DNA-binding surface (G245S, R249S and R282W).

1.3.1. Dominant negative activity of mutp53

The *TP53* gene is frequently inactivated by a single mono-allelic missense mutation, and the mutant p53 protein (mutp53) is normally overexpressed in the full-length form in human tumors[120]. Several evidences suggest that mutp53 not only loses its tumor suppressive ability, but also has dominant negative activity on the remaining wt allele[120] (Figure 7[120]). Some *in vitro* experiments showed that mutp53 inhibits the activity of wt p53 by binding to p53-responsive elements, inhibiting endogenous target genes and stimulating growth in the presence of mutp53[121]. Genetic knock-in mouse models support these conclusions. $p53^{+/-}$ mice bearing A135V p53 mutant transgene vector exhibited accelerated tumor development when compared to $p53^{+/-}$ mice without the transgene[121]. Since p53 binds to DNA as a tetramer, a mechanism for the dominant negative activity involves wt p53 proteins forming hetero-oligomers with mutp53 proteins, which results in impaired DNA binding and transcriptional activity[122,123].

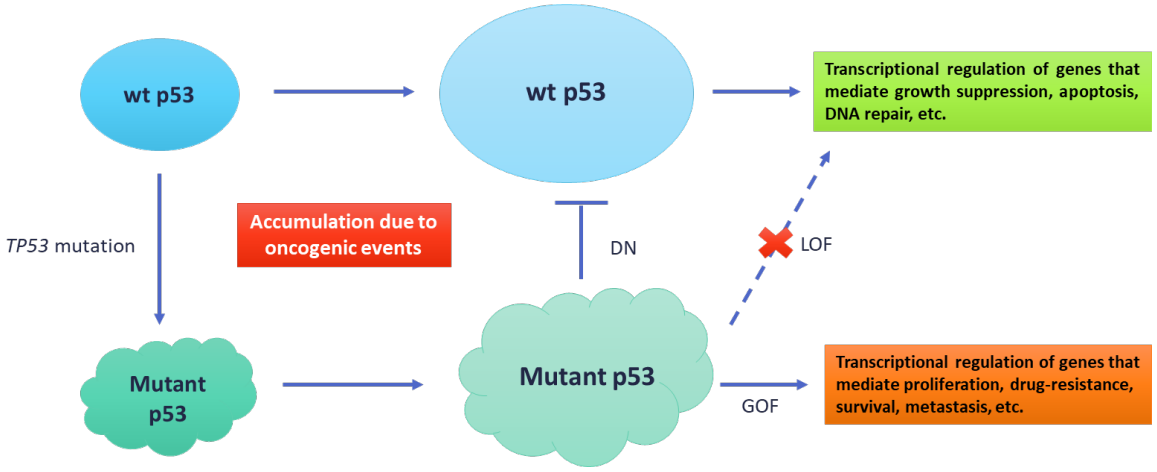

***Figure 7**: Functional impact of TP53 mutations. In addition to losing its tumor suppression function, mutp53 has a negative effect on the remaining wt p53. It is also able to bind to cellular proteins, like transcription factors, and it is believed that most of its gain-of-function properties, like promotion of proliferation and metastasis, come from this binding. Adapted from Brosh* et al. *2009[120]); DN: Dominant Negative effect; LOF: Loss Of Function; GOF: Gain Of Function.*

1.3.2. Oncogenic properties of mutp53

In addition to its dominant negative activity, mutp53 may acquire oncogenic properties that lead to "gain of function"[120]. Initially, p53 was identified as an oncogene, since early studies wrongly used mutp53 sequences with oncogenic function[124]. *In vitro* studies indicated that transfection of mutp53 into p53-null cancer cells can suppress the promoter of p53 target genes and decrease p53 target genes expression[125]. Down-regulation of mutp53 by siRNA increases the expression of p53 target proteins and suppresses cancer cell growth[126–128]. *In vivo* studies in mice expressing mutp53 (R172H and R270H) showed that both p53R172H- and p53R270H-expressing mice have developed highly aggressive carcinoma, while $p53^{-/-}$ mice only developed lymphoma and sarcoma, but never carcinoma. In over 43% of p53R270H-expressing mice and 57% of p53R172H-expressing mice developed multiple tumors, while only 32% of $p53^{-/-}$ mice developed numerous tumors[129]. Clinical evidence shows that p53 mutations are related with poor prognosis in various cancer types[130]. Multiple mechanisms are involved in the oncogenic activity of mutp53 (Figure 7). First, mutp53 can inhibit the function of the p53 family proteins p63 and p73 by protein-protein interaction. Moreover, it was found that mutp53 only inhibits p73 and p63 when it is present in large excess compared to p63/p73, which normally occurs in tumors[131,132]. Second, the regulation of gene transcription by mutp53 is an important mechanism for gain-of-function. Mutp53 is able to activate the transcription of the *Multidrug Resistance 1* (*MDR1*) gene, which causes drug resistance in mutp53-expressing cancer cells[133]. In addition to *MDR1*, mutp53 has been involved in the transcriptional regulation of

several genes, including *PCNA96*, *C-MYC97, FAS98, BCL-XL99 and VEGF*[134]. Third, the inhibition of DNA repair pathways by mutp53 is another gain of function mechanism.

1.3.3. p53 targeting strategies

p53 has a critical role in cancer, controlling apoptosis, cell cycle, senescence and DNA repair. Therefore, it represents a very important drug target. p53 is inactivated in 50% of human cancers, and some elements of the p53 signaling pathway, like MDM2 and $p14^{ARF}$, are often misappropriate in the other 50% of cases. Besides that, molecular epidemiological analyses have shown that numerous cancers, like breast, head and neck, liver and hematopoietic malignancies, have a significant association between *TP53* mutations and lower patient survival chances[130]. Based on the importance that p53 has in tumorigenesis, numerous strategies have been developed to recover p53-induced cell cycle inhibition, pro-apoptotic and pro-senescence roles in p53 mutant cells and tumors. Figure 8[135,136] summarizes the p53 targeting strategies that are in pre-clinical or clinical development stages, and even those that represent novel approaches to enable p53 signaling in human cancers.

1.3.3.1. Targeting the p53-MDM2 interaction

The vital role of the p53-MDM2 axis in cancer prompted cell culture-based and xenograft studies. These studies confirmed potent cytostatic, pro-apoptotic and tumor suppressive functions of small molecule-based and polypeptidylic inhibitors of MDM2, especially Nutlin-3 (**1**)[137], MI-17 (**2**)[138] and MI-43 (**3**)[138].

Nutlin-3 (**1**) (Figure 13) is a *cis*-imidazoline that acts as MDM2 antagonist[139], which mimics critical residues in the transactivation domain of p53 essential for MDM2 binding, like Phe19, Trp23 and Leu26. Some pre-clinical data in hematological, neurological and bone cancers showed strong pro-apoptotic, anti-tumorigenic and anti-metastatic functions with subtle adverse side effects. This favorable activity may reflect the ability of nutlin-3 (**1**) to induce apoptosis, inhibit autophagy and even promote pro-senescence responses specifically in tumors, but not in normal cells, where the MDM2 blockage by nutlin-3 (**1**) is linked mainly to cell cycle inhibition[140]. Notably, nutlin-3 (**1**) shows synergism with conventional chemotherapeutic drugs, like doxorubicin and cytarabine, radiation, TRAIL and inhibitors of XIAP, g-secretase, Cdks, JNK, PI3K and aurora kinases, suggesting the possibility of combinatorial therapies for the treatment of advanced blood, brain and bone cancers[140]. Currently, there is a more detailed understanding about the cellular responses

induced by nutlin-3, which can help in the optimization of drug combinations for preclinical and clinical testing.

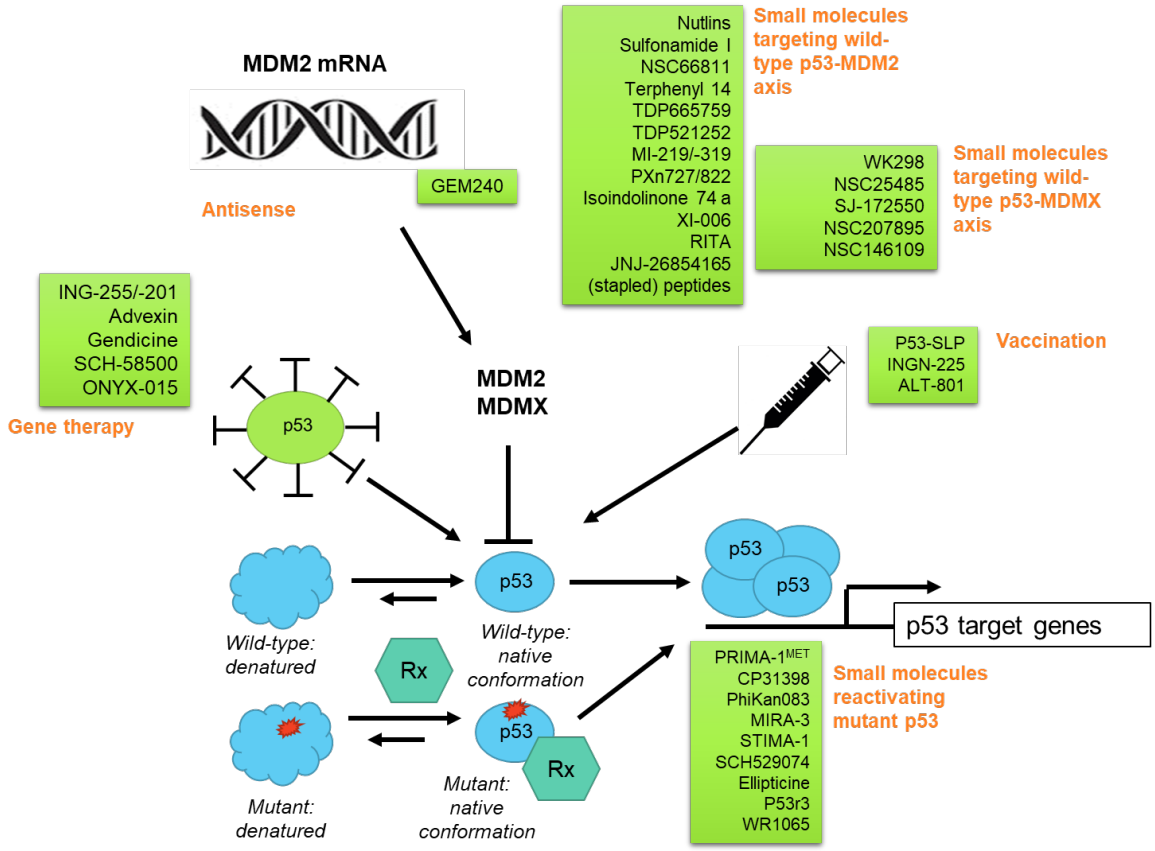

***Figure 8**: Therapeutics targeting the p53-signaling pathway. Depicted are the five classes of p53-targeting therapeutics: gene therapeutic agents to deliver p53 via adenoviral transduction into p53-deficient cancer cells; antisense oligonucleotides targeting MDM2; small molecules targeting wild-type p53 (i.e., compounds that release p53 from inhibitory p53:MDM2/X complexes); small molecules targeting mutp53 to restore its native conformation and transactivational activity; and vaccination approaches (i.e., p53-SLP, a mixture of overlapping p53 peptides representing amino acids 70 to 248 used in conjunction with montanide, a water-in-oil emulsion as adjuvant; INGN-225, a vaccine using p53-peptide transfected dendritic cells; and ALT-801, an interleukin-2-T cell receptor fusion protein directed against MHC-presented p53 peptides). MIRA-1: Mutp53 reactivation and induction of rapid apoptosis; PRIMA: p53 reactivation and induction of massive apoptosis-1; RITA: Reactivation of p53 and induction of tumor cell apoptosis; STIMA: SH group targeting and induction of massive apoptosis. Adapted from Stegh* et al. *2012*[135] *and Liu* et al. *2019*[136].

Some reports suggested that the treatment through nutlin-3 (**1**) leads to p53-dependent upregulation of Notch-1 in leukemia and chronic lymphocytic leukemia (CLL) B cells[141] Notch-1 activates the PI3K-mTOR signaling pathway, which then limits the pro-death activity of p53. Therefore, the rational combination of nutlin-3 (**1**) with the g-secretase inhibitors N-[N-(3,5-fluorophenacetyl)- L-alanyl]-S-phenylglycine t-butyl ester (DAPT) and L-685458 potentiated nutlin-3 action[141]. Finally, besides inducing apoptosis specifically on tumor cells, nutlin-3 (**1**) also seems to induce pro-senescence responses, since it potentiated tumor regression through phosphatase and tensin homolog-loss induced cellular senescence[142].

The spiro-oxindoles MI-17 (**2**) and its derivative MI-43 (**3**) (Figure 13) represent another class of MDM2 inhibitors that, like nutlin-3 (**1**), block the interaction of p53 with MDM2 by mimicking critical residues of the p53-MDM2 complex interface. MI-17 (**2**) mimics the p53 residues Phe19, Trp23 and Leu19, while MI-43 (**3**), besides being able to mimic these three residues, also mimics the p53 residue Leu22[138]. Thus, MI-43 (**3**) triggered apoptosis in wild-type p53, but not in cells with mutp53.

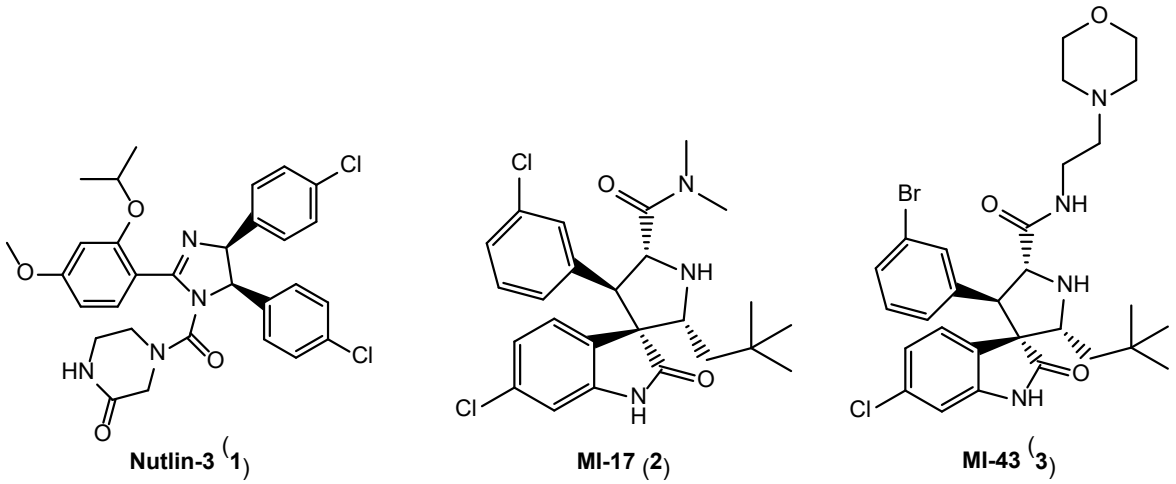

***Figure 9**: Chemical structures of **Nutlin-3** (**1**), **MI-17** (**2**) and **MI-43** (**3**).*

Other small-molecule inhibitors of the p53-MDM2 interaction have entered clinical trials for the treatment of various cancer types (Figure 10), but so far, they have shown mixed response rates. The doses of these inhibitors have been reduced due to hematological toxicity, as well as neutropenia, prolonged cytopenia, bone marrow failure and even gastrointestinal toxicity[143–148].

Another approach to the disruption of this interaction is through targeted protein degradation. This method involves the use of chimeric molecules known as PROTACs (PROteolysis Targeting Chimeras), which simultaneously bind to a target protein and to a E3 ligase. This causes ubiquitination and signals the target for degradation by the 26S proteasome[149,150]. The pharmacological consequences arising from this strategy could be outstandingly different from those obtained from reversible or covalent inhibition. Additionally, it has been demonstrated that it is possible to design PROTACs with picomolar activity[151] from binding partners of low affinity due to the formation of a cooperative complex and the catalytic nature of these bispecific molecules. Thus, aiming for targeted degradation of the p53-MDM2 interaction could result in improved potency when compared to the traditional inhibitors.

In 2018, Li *et al* have reported the structures of potent MDM2 degraders[152]. Using the p53-MDM2 interaction inhibitor MI-1061 (**10**) and IMiDs as ligase binders (which, in this case, target the CRL4-CRBN E3 ubiquitin ligase, also known as cereblon) the authors aimed to obtain potent degraders of MDM2 after linker optimization of MD-224 (**11**) (Figure 11).

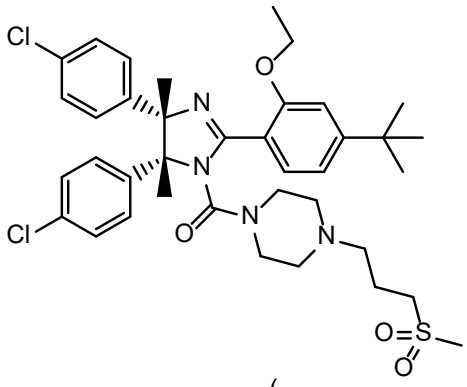

RG7112 (4)
Hoffmann-La Roche

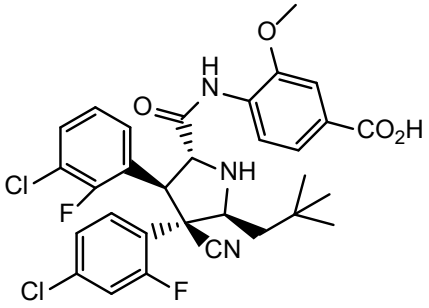

RG7388 (5)
Hoffmann-La Roche

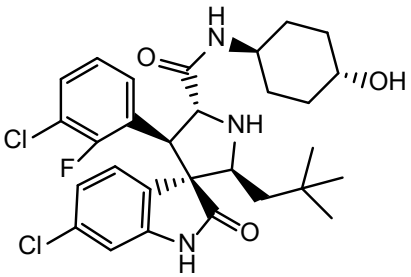

MI-77301 (6)
Univ. Michigan, Sanofi

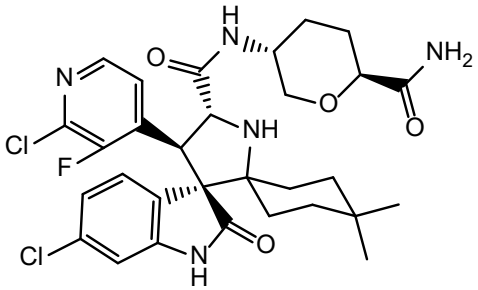

S-3032b/Milademetan (7)
Daiichi-Sankyo

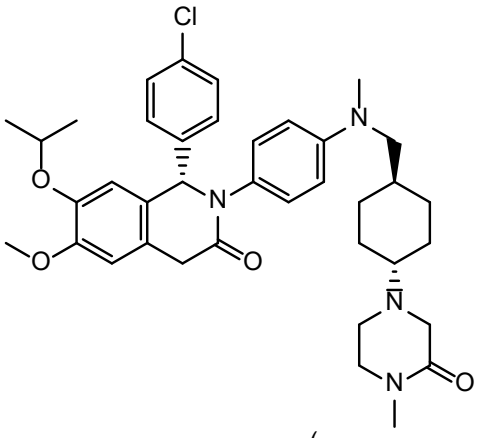

NVP-CGM097 (8)
Novartis

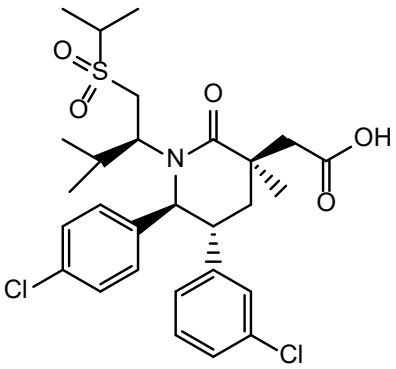

AMG 232 (9)
Amgen

***Figure 10**: Six representative p53-MDM2 inhibitors that have entered human clinical trials.*

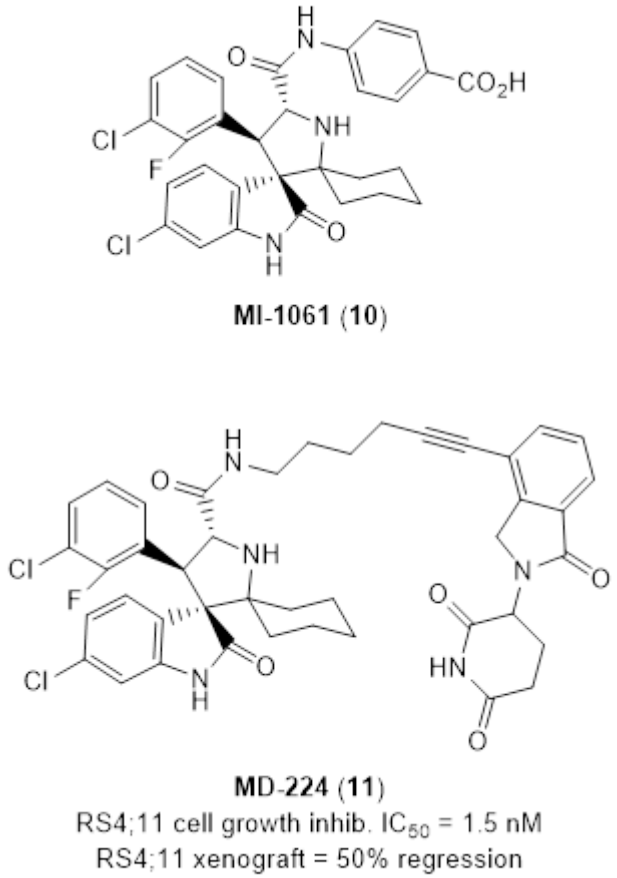

***Figure 11**: Structures of **MI-1061 (10)** and PROTAC **MD-224 (11)**.*

Experiments with MD-224 (**11**) confirmed that its mechanism was related to MDM2 degradation, as the co-treatment with lenalidomide (a cereblon binder), blocked the MDM2 degradation through displacement of cereblon from the ternary complex. The pre-incubation with proteasome inhibitors or with a neddylation inhibitor also blocked MDM2 degradation by MD-224 (**11**), further confirming the targeted degradation mechanism. MD-224 (**11**) is 10-50 times more potent than its parent compound MI-1061 (**10**) in induction of p53 activation and also in inhibition of cell growth in the MV-4-11 (biphenotypic B myelomonocytic leukemia) and RS4;11 (acute lymphoblastic leukemia) cell lines.

Compared to MD-224 (**11**) in RS4;11 cells, MI-1061 (**10**) showed increased MDM2 levels, as shown by Western Blot analysis, as well as the desired increase in free p53. Additionally, analysis by qRT-PCR (6 hours) revealed transcription upregulation of *MDM2*, *p21* and *PUMA*, but not of *TP53.* MD-224 (**11**) also induced upregulation of *MDM2*, but, unlike MI-1061 (**10**), a complete depletion of MDM2 protein was observed.

MD-224 (**11**) showed nanomolar inhibitory activity in cell growth on a panel of AML (Acute Myeloid Leukemia) cell lines, which suggests that this degradation approach could be applied in AML. As theoretically expected, two AML cell lines expressing mutp53 were

unresponsive to MD-224 (**11**). In the RS4;11 xenograft model, a single 25 mg/kg iv (intravenous) dose of MD-224 (**11**) showed a time-dependent reduction in MDM2 levels, with some depletion noticeable by 3 hours and near complete depletion by 24 hours. However, there is no pharmacokinetic profile for MD-224 (**11**) available to this date. Multiple intravenous dosing of MD-224 (**11**) at 24 mg/kg every second day showed up to 50% tumor regression without significant weight loss or other signs of toxicity. These results are favorably different from the oral dosing at 100 mg/kg (5 days/week via oral gavage) of MI-1061, which resulted in only modest tumor growth inhibition in this model.

1.3.3.2. Targeting the p53-MDMX interaction

Some works have highlighted the importance of MDMX inhibitors for anticancer therapy. For example, in melanoma, in which most of the cases express wt p53, MDMX is abnormally upregulated[153,154]. Notably, the inhibition of the interaction between p53 and MDMX has been shown to restore the function of p53. This can indicate that, at least in melanoma, p53 is the main target of MDMX. These melanoma studies have a big clinical relevance because MDMX overexpression seems to be predominant in these tumors and they have a very low frequency of p53 mutations.

There are reports of many small molecules able to target MDMX. One of them is called WK 298 (**12**) (Figure 12). It disrupts the interaction between p53 and MDMX by mimicking the binding of a p53 peptide. Specifically, it fills the Trp23 subpocket of MDMX with its 6-chloroindole group[155]. Another small molecule is SJ-172550 (**13**) (Figure 12). It targets the MDMX N-terminus-p53 interaction pocket. A more attentive analysis of SJ-172550 (**13**) revealed that it affects the conformation of MDMX instead of acting as a competitive inhibitor[156]. Additionally, some small molecules prevent MDMX transcription, such as the benxofuroxan derivative NSC 207895 (**14**)[157] (Figure 12) or indirectly destabilize MDMX through the inhibition of heat shock 90, like 17-AAG, also called tanespimycin (**15**)[158] (Figure 12). XI-011 (**16**) is another small molecule capable of interfering with the p53-MDMX interaction by acting synergistically with cisplatin[159]. XI-006 (**17**) (also known as NSC207895) was also reported to downregulate MDMX and upregulate p53 and pro-apoptotic genes like *PUMA* and *BAX*[160]. Adding to this list is CTX1 (**18**), which binds directly to MDMX, preventing the formation of the p53-MDMX complex and inducing apoptosis in a panel of cancer cell lines[161].

Since many tumors overexpress MDMX, the molecules that only target MDM2 might not be effective for these types of tumors. For this reason, many compounds targeting both MDM2 and MDMX, with disruption of both p53-MDM2 and p53-MDMX interactions, were

generated and are currently being tested. They include the small molecule RO-5963 (**19**), which interferes with the p53-MDM2-MDMX interaction by promotion of the homo- and heterodimerization of MDMX and MDM2[162]. Other inhibitors of both MDMX and MDM2 include some synthetic peptide compounds, like SAH-p53-8, PMI peptide, and pDI peptide[163–166]. Interestingly, one study demonstrated that high levels of SAH-p53-8 were effective in a melanoma mouse model expressing high levels of MDMX, increasing the effect of treatment with cisplatin and vemurafenib, a BRAF-V600E inhibitor[153]. This study is an example of how combination therapy may reduce cancer resistance and allow cancer treatment strategies to be adapted to each patient[167].

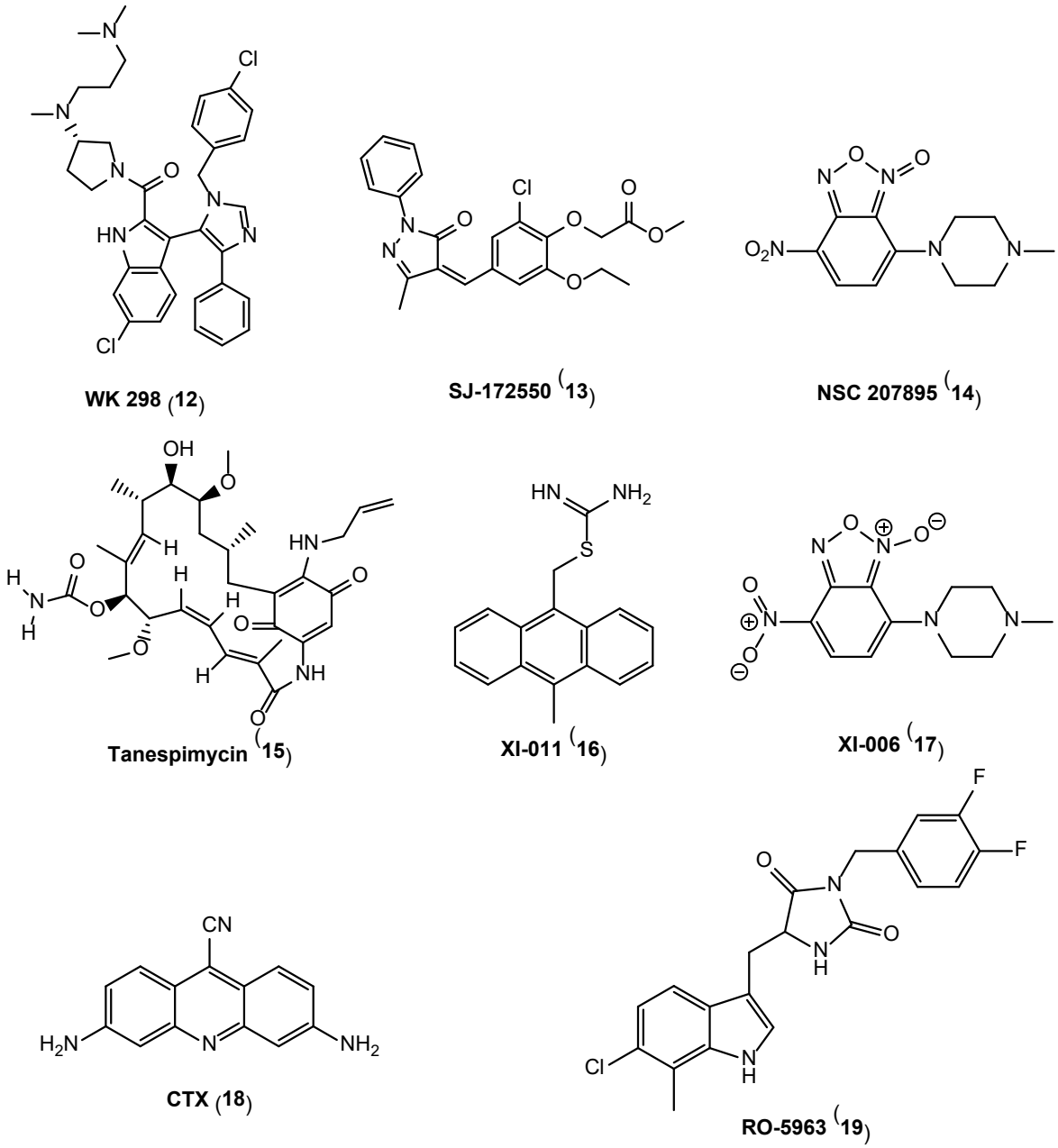

***Figure 12**: Chemical structures of **WK 298 (12)**, **SJ-172550 (13)**, **NSC 207895 (14)**, **tanespimycin (15)**, **XI-011 (16)**, **XI-006 (17)**, **CTX1 (18)** and **RO-5963 (19)**.*

1.3.3.3. Restoration of wt-like activity to mutp53

The high-throughput screening of chemical libraries and *in silico* screens with computational techniques identified a large number of small molecules that could restore wt-like function of mutp53. These include PRIMA-1 (**20**)[168] and its derivative, PRIMA-1^{MET} (**21**)[169], MIRA-1 (**22**)[170], STIMA-1 (**23**)[171], PhiKan083 (**24**)[172], NSC319726 (**25**)[173], CP31398 (**26**)[174], SCH529074 (**27**)[175], ellipticine (**28**)[176] and p53R3 (**29**)[177] (Figure 13). Other small molecules targeting mutp53 include PK11007 (**30**)[178], stictic acid (**31**)[178], PK7088 (**32**)[179], R-goniothalamin (**33**)[180], MB725 (**34**)[181], COTI-2 (**35**)[182], PEITC (**36**)[183], RETRA (**37**)[184], SAHA (**38**)[185], chetomin (**39**)[186], KSS-9 (**40**)[187] and SLMP53-1 (**41**)[188] (Figure 14).

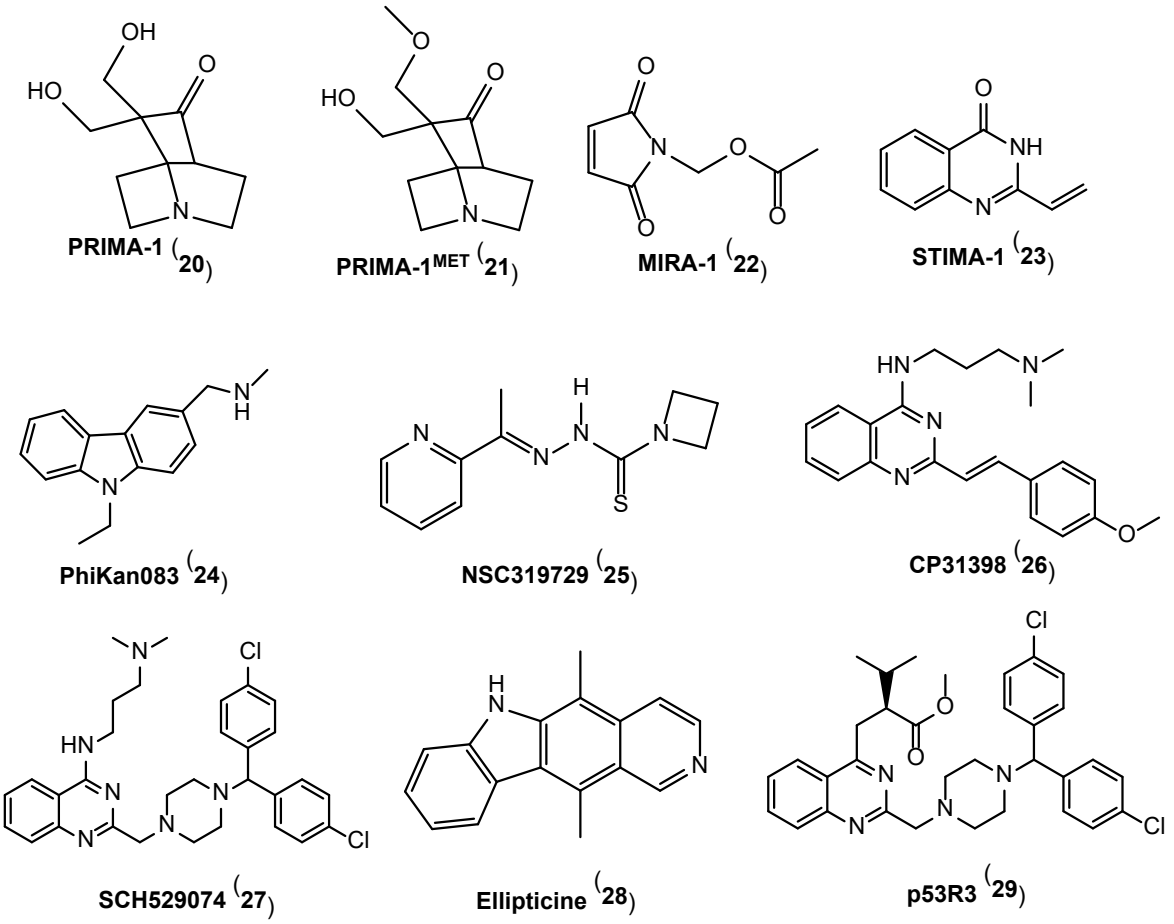

***Figure 13**: Chemical structures of **PRIMA-1** (20), **PRIMA-1^{MET}** (21), **MIRA-1** (22), **STIMA-1** (23), **PhiKan083** (24), **NSC319726** (25), **CP31398** (26), **SCH529074** (27), **ellipticine** (28) and **p53R3** (29).*

The PRIMA-1 (**20**) derivative PRIMA-1^{MET} (**21**) (Figure 13), was the first compound to enter into clinical trial. PRIMA-1 (**20**) and its optimized derivative PRIMA-1^{MET} (**21**) has been tested in phase I trial. PRIMA-1 (**20**) seems to specifically inhibit the growth of mutant p53-expressing cells. This small molecule was first identified through screening a library of 2,000 compounds in a SAOS-2 cell model (human osteosarcoma) expressing the R273H

mutp53[168], and it restores both DNA contact and structural p53 mutants by restoring the wt p53 conformation and its sequence-specific DNA binding *in vitro*. An *in vivo* study showed strong antitumor activity of PRIMA-1 (**20**) alone or in combination with cisplatin with no apparent toxicity in lung and osteosarcoma xenografts[168]. The phase I trial of PRIMA-1^{MET} (**21**) was completed in patients with acute myeloid leukemia and prostate cancer. According to these studies, PRIMA-1 (**20**) showed a favorable pharmacokinetic profile and was well tolerated. Treatment of PRIMA-1^{MET} (**21**) in patients induced cell-cycle arrest, apoptosis and transcription of p53 target genes *NOXA*, *PUMA* and *BAX*. One of the patients, having AML with a p53 core domain mutation showed a reduction of blast percentage from 46% to 26% in the bone marrow after treatment with PRIMA-1^{MET} (**21**)[169]. However, in 2015, PRIMA-1^{MET} (**21**) was reported to be rather unspecific, as it inhibited proliferation of colorectal cancer cells, independent of p53 status[189] and targeted MEK and thioredoxin reductase 1 a (**21**)[190,191].

The carbazole derivative PhiKan083 (**24**) (Figure 13) was identified by an *in silico* analysis of the p53 Y220C mutant crystal structure using virtual screening and rational drug design. PhiKan083 (**24**) was able to selectively bind to a unique pocket in mutp53 Y220C, stabilizing it. PhiKan083 (**24**) increases the melting temperature of the Y220C mutant and slows its rate of denaturation. Like PhiKan083 (**24**), PK7088 (**32**) (Figure 14) also binds to Y220C pocket, stabilizing its structure and raising its melting point[179]. However, the biological activity of these compounds has still to be assessed[172].

Based on the same screening approach used to identify PRIMA-1 (**20**), a maleimide-derived molecule, MIRA-1 (**22**) was observed to exert mutp53 reactivating activity *via* covalent binding[192]. Later studies showed that MIRA-1 (**22**) was actually toxic to normal cell lines that were hoped to be insensible to this potential mutp53 reactivator[193].

NSC319726 (**25**) (Figure 13) was identified by an *in silico* analysis of US National Cancer Institute (NCI) using 60 human tumor cell line anticancer drug screen (NCI60). This compound restored wtp53 activity in mutant p53R175H-expressing cell lines[173]. It also displayed antitumor activity specifically in mutant p53 R172H (equivalent to human R175H) genetically engineered mice, and inhibited xenograft tumor growth of mutant p53R175H-expressing cells[173].

Other compounds that target mutp53 include STIMA-1 (**23**), CP31398 (**26**), SCH529074 (**27**), ellipticine (**28**), p53R3 (**29**), PK11007 (**30**), stictic acid (**31**), PK7088 (**32**), *R*-goniothalamin (**33**), MB725 (**34**), COTI-2 (**35**), PEITC (**36**), RETRA (**37**), SAHA (**38**), chetomin (**39**), KSS-9 (**40**) and SLMP53-1 (**41**) (Figures 13 and 14). CP31398 (**26**) stabilizes the core domain of mutp53 protein, increases DNA binding and transcriptional activity, and

also shows antitumor activity in colon cancer and melanoma mice models[174]. However, in 2002, it was reported that this compound intercalates with DNA and alters and destabilizes the p53-DNA complex[178]. STIMA-1 (**23**) is a CP-31398 (**26**) derivative, which also induced suppression of mutp53-dependent tumor growth[171]. SCH529074 (**27**) is another compound able to target mutp53. It binds to the DNA binding domain of mutp53, stabilizes it and induces p53-dependent apoptosis[175]. Ellipticine (**28**) restores the transcriptional activity of mutp53[176]. p53R3 (**29**) restores DNA binding of R175H and R273H p53 mutants, induces DR5 expression, and makes cancer cells more sensitive to TRAIL-induced apoptosis[177]. *R*-goniothalamin (**33**) (Figure 14), the R-enantiomer of goniothalamin (which was toxic to coronary artery smooth muscle cells by activating the p53 pathway[194]), was reported to selectively kill human breast cancer cells by reactivating the R175H mutant[180].

The 2-sulfonylpyrimidine, PK11007 (**30**) (Figure 14), designed to stabilize mutant p53Y220C, is actually an alkylator of p53 cysteines[195]. The alkylation of cysteine residues in p53 may prevent the formation of disulfide bonds that induce protein misfolding, thus creating new DNA contacts which allow more efficient DNA binding and promote correct protein folding[196]. Computational studies identified an open pocket in p53 DBD as a critical target for the reactivation of mutp53[197]. The residues Cys124, Cys135 or Cys141 in this pocket are thought to be the binding sites of STIMA-1 (**23**) and MIRA-1 (**22**) through Michael addition[197]. However, for PK11007's (**30**), the crystal structure indicates that it alkylates the residues Cys182 or Cys277 through nucleophilic aromatic substitution[195]. Nonetheless, the mechanisms by which these compounds act to stabilize mutp53 still need further investigation.

A virtual screening based on the pocket formed by mutp53 indicates that stictic acid (**31**) (Figure 14) is a potential mutp53 reactivator. Furthermore, it exhibited strong induction of p21 in SAOS-2 (human osteosarcoma) cells expressing the R175H mutant[197].

By binding tightly to the Y220C pocket and stabilizing this mutant, MB725 (**34**) was able to induce selective reduction of viability in several Y220C-expressing cancer cell lines while having little effect on control cell lines[181]

COTI-2 (**35**) was first identified through the computational platform CHEMSAS, which is a system that predicts target biological activity from molecular structures[182]. This compound inhibits the growth of a wide group of cancer cell lines, especially those expressing p53 mutants[182], and it seems to work by reactivating mutp53 and also inhibiting the PI3K/Akt pathway[182].

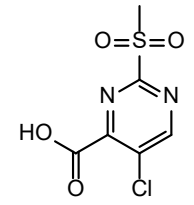

PK11007 (30)

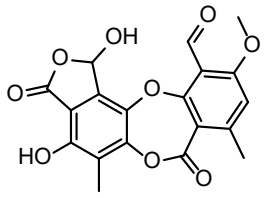

Stictic acid (31)

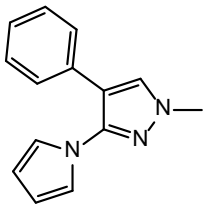

PK7088 (32)

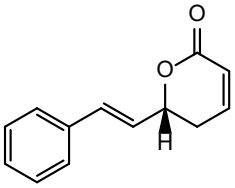

***R*-goniothalamin (33)**

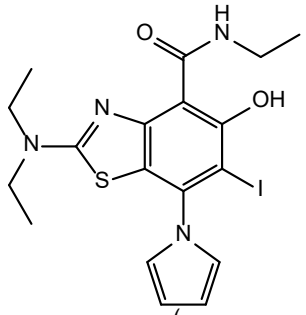

MB725 (34)

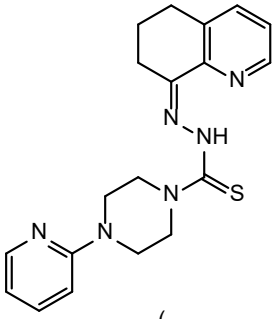

COTI-2 (35)

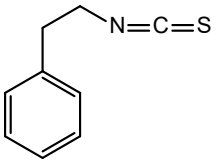

PEITC (36)

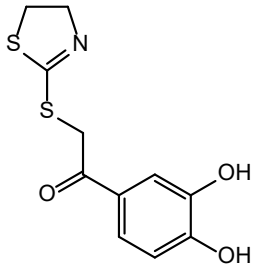

RETRA (37)

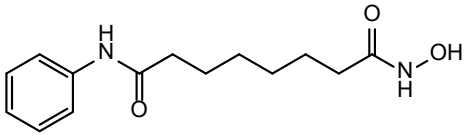

SAHA (38)

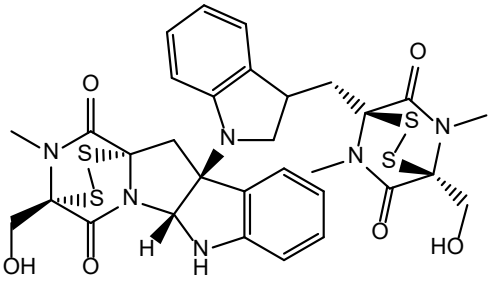

Chetomin (39)

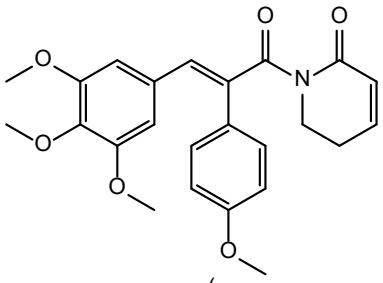

KSS-9 (40)

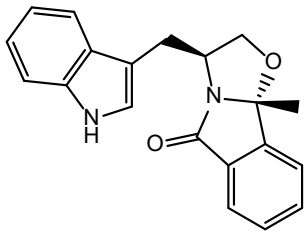

SLMP53-1 (41)

***Figure 14**: Chemical structures of **PK11007 (30)**, **stictic acid (31)**, **PK7088 (32)**, **R-goniothalamin (33)**, **MB725 (34)**, **COTI-2 (35)**, **PEITC (36)**, **RETRA (37)**, **SAHA (38)**, **chetomin (39)**, **KSS-9 (40)** and **SLMP53-1 (41)**.*

Phenethyl isothiocyanate, also known as PEITC (**36**), is a low MW compound derived from edible cruciferous plants (like cabbages and broccoli) that was reported to reactivate mutp53, particularly mutp53R175H[183]. The authors of this work claimed that PEITC (**36**) functions by chelating zinc, and it is now in clinical trials for the treatment of cancer through a variety of effects, including inhibition of cytochrome P450s, induction of Phase II detoxifying enzymes, cell cycle arrest and apoptosis[183].

RETRA (**37**) was identified as a mutp53 reactivator by using a reporter assay on A431 (epidermal carcinoma) cells expressing the mutp53 R273H. The treatment of cells expressing mutp53 with this compound leads to an increase in p73, which yields tumor suppressive effects, similar to mutp53 reactivation[184].

Vorinostat (also known as SAHA (**38**)) was approved by the Food and Drug Administration (FDA) as a histone deacetylase inhibitor. SAHA (**38**) seems to exhibit preferential cytotoxicity to mutp53-expressing cells, rather than wt p53 and p53-null cancer cells. A mechanistic study suggested that, by inhibiting histone deacetylase 6 (a critical positive regulator of HSP90), SAHA (**38**) is able to indirectly release mutp53 from the mutp53-HSP90 complex, thus facilitating the degradation of mutp53[185]. Additionally, this compound sensitizes cancer cells expressing mutp53 to chemotherapy[185].

The fungal natural product chetomin (**39**) was identified through high-throughput screening as a reactivator of mutp53R273H. However, it seems to rescue mutp53 indirectly, as it interacts with HSP40, increasing its activity on mutp53R273H. This induces a conformational change of this mutant to a wt-like p53, with activation of a downstream p53 signalling[186].

KSS-9 (**40**) is a hybrid molecule composed of two natural compounds: piperlongumine (an alkaloid that is able to produce ROS in cancer cells[198]) and CA4 (a known antimicrotubule[199]). This compound exhibited strong tumor-suppressive effects in breast cancer cells, especially those expressing the mutp53R273H. Additionally, KSS-9 (**40**) restored the activity and conformation of mutp53, an effect that neither piperlongumine nor CA4 had individually[187].

SLMP53-1 (**41**) was identified as a new reactivator of the mutp53R280K through a yeast-based screening, also increasing the inhibitory effect of wt p53 on yeast growth[188]. It exhibited antiproliferative effects in both wt and mutp53-expressing tumor cells, and also triggered apoptosis mediated by p53 transcription and mitochondrial pathways. SLMP53-1 (**41**) also inhibited migration and showed synergistic effects with conventional chemotherapeutics like doxorubicin and etoposide in a p53-dependent manner[188]. However, the mechanism by which SLMP53-1 reactivates the mutp53R280K is still unknown.

2. Chalcones

Chalcones are natural products with a great distribution in many plant species[200–204], possessing the common chemical scaffold of a 1,3-diaryl-2-propen-1-one, also called chalconoid, that may exist as *trans* and *cis* isomers, being the *trans* isomer thermodynamically more stable[203,205] (Figure 15).

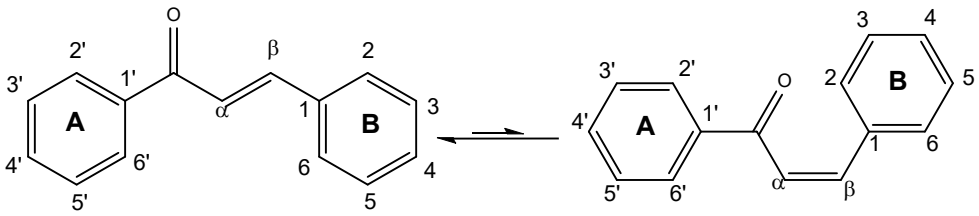

***Figure 15**: Structures of chalcone.*

A great number of natural chalcones are polyhydroxylated. Other common substituents include methoxy and prenyl groups, being also reported the isolation of bischalcones, like rhuschalcone (**42**) from *Rhus pyroides*, which contains two chalcone moieties in a single structure[206].

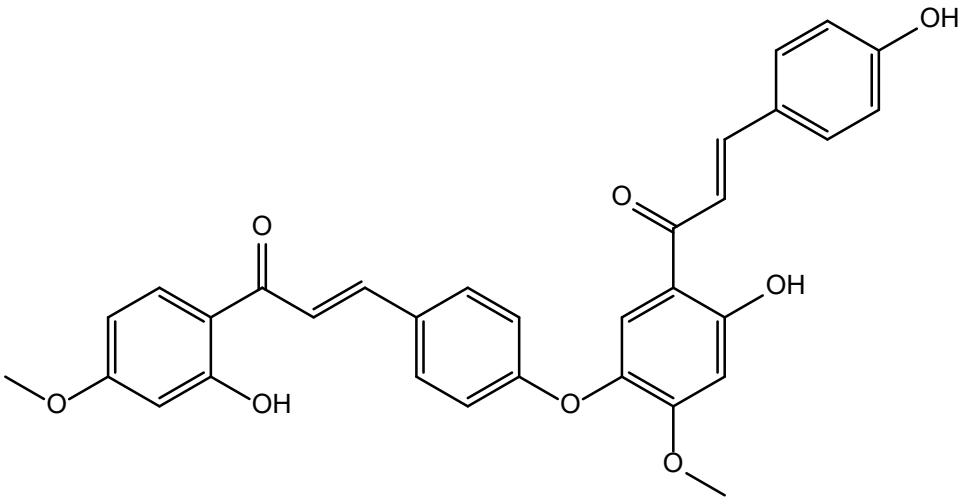

Rhuschalcone I (**42**)

***Figure 16**: Structure of rhuschalcone I (**42**).*

Chalcone synthase (CSH) is a member of the plant polyketide synthase superfamily, which also includes stilbene synthase (STS), acridone synthase, pyrone synthase, bibenzyl synthase, and *p*-coumaroyltriacetic acid synthase[207]. Chalcone synthases provide the

starting materials for a varied set of metabolites, like the flavonoid family, which includes chalcones[208].

Flavonoids are synthesized *via* the phenylpropanoid and polyketide pathway, which starts with the condensation of one molecule of CoA-ester of cinnamic acid or derivatives such as coumaric or ferulic acid, and three molecules of malonyl-CoA, yielding a naringenin chalcone as the major product. This reaction is carried out by CSH. The chalcone is isomerized to a flavanone by the enzyme Chalcone Flavanone Isomerase (CHI). From these central intermediates, the pathway diverges into several branches, each resulting in a different class of flavonoids. Flavanone 3-hydroxylase (F3H) catalyzes the stereospecific 3β-hydroxylation of (2*S*)-flavanones to dihydroflavonols. For the biosynthesis of anthocyanins, dihydroflavonol reductase (DFR) catalyzes the reduction of dihydroflavonols to flavan-3,4-diols (leucoanthocyanins), which are converted to anthocyanidins by anthocyanidin synthase (ANS). The formation of glucosides is catalyzed by UDP glucose-flavonoid 3-*O*-glucosyl transferase (UFGT), which stabilizes the anthocyanidins by 3-*O*-glucosylation. An overview of the flavonoid pathway is presented in Figure 17.

Due to their relatively easy synthesis and to their large number of replaceable hydrogens, chalcones have attracted the attention of many organic medicinal chemistry groups worldwide. There is a large number of research publications dedicated to the synthesis and biological activities of chalcones, and every year there are new insights about these flavonoids exploring their wide array of properties, such as antioxidant[209], anticancer[210,211], anti-tubercular[212], anti-inflammatory[211,213], antimalarial[214], antifungal and antiviral[215,216].

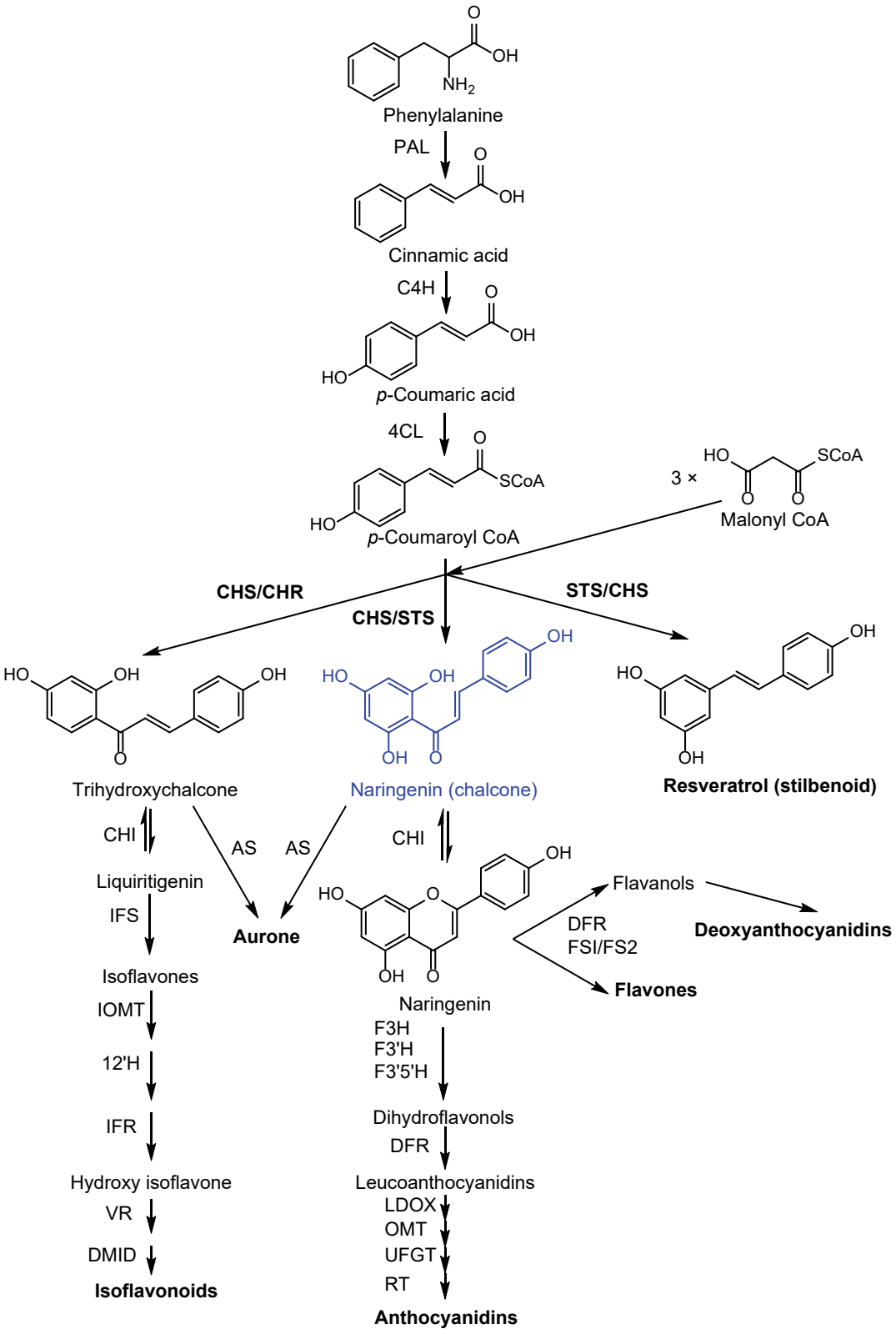

***Figure 17**: Flavonoid biosynthetic pathway. ANS anthocyanidin synthase; AS aureusidin synthase; C4H cinnamate-4-hydroxylase; CHR chalcone reductase; DFR dihydroflavonol 4-reductase; DMID 7,20- dihydroxy, 40- methoxyisoflavanol dehydratase; F3H flavanone 3-hydroxylase; F30H flavonoid 30 hydroxylase; F3050H flavonoid 3050 hydroxylase; FS1/FS2 flavone synthase; I20H isoflavone 20-hydroxylase; IFR isoflavone reductase; IFS isoflavone synthase; IOMT isoflavone O-methyltransferase; LCR leucoanthocyanidin reductase; LDOX leucoanthocyanidin dioxygenase; OMT O-methyltransferase; PAL phenylalanine ammonia- lyase; RT rhamnosyl transferase; UFGT UDP flavonoid glucosyl transferase; VR vestitone reductase; STS stilbene synthase; FLS flavanol synthase. Adapted from Dao et al. 2011.*

2.1. Chalcones as modulators of the p53 pathway

2.1.1. Natural chalcones

Several natural chalcones are reported as inducers of p53-mediated apoptosis and cell cycle arrest (Table 1). The effect of the chalcone itself (**43**) was investigated in terms of viability reduction, induction of apoptosis and alteration of gene expression of p53 and Sp1 in the human osteosarcoma U2OS cell line through *in vitro* assays[217]. Treatment with *trans*-chalcone (**43**) induced growth inhibition of these cells in a time- and dose-dependent manner, especially at the concentration of 10 μM after 48 hours[217]. It also induced apoptosis in a dose-dependent way, and caused Sp1 downregulation at the transcriptional level, while up-regulating p53 expression at the post-translational level[217]. Recently in 2018, Silva *et al.* further investigated the effects of *trans*-chalcone (**43**) on the transcriptomes altered by p53 expression through RNA-Seq analysis. This study was once again performed on the U2OS cell line, which were treated with 50 μM *trans*-chalcone (**43**) for 24 hours. After the treatment, the RNAs were isolated and subjected to RNA-Seq. This assay allowed Silva *et al.* to conclude that the p53 pathway was one of the most highly affected pathways by *trans*-chalcone (**43**) treatment. The *DNAJB1* (*HSP40* family) and *ATF3* genes, which play a role in enhancing stability and activation of p53 by interacting with MDM2, were highly upregulated. This result was further confirmed by RT-PCR and Western Blot. Also, in order to evaluate *trans*-chalcone ability to modify the expression of these two genes in other types of tumor cells, HCT116, FaDu and SJSA1 cells were treated in the same way as the U2OS cells were. The *DNAJB1* gene was upregulated in all cells, and the *ATF3* gene was upregulated in the HCT-116 and FaDu cells, but not in the SJSA1 cells. These results may suggest that the *DNAJB1* gene, might be a target of *trans*-chalcone (**43**)[218].

Besides this unsubstituted chalcone, other natural chalcones, with different substitution patterns, including chalcones with hydroxyl, methoxy, and prenyl groups, were reported for their apoptotic activities, as well as for their ability to induce cell cycle arrest through a p53-mediated pathway.

Isoliquiritigenin (**44**) and HTMC (**45**) are naturally occurring chalcones reported to induce cell cycle arrest and apoptosis in some cell lines, particularly in the lung A549 tumor cell line[219–221]. The cell cycle arrest ability of these chalcones showed to be mainly associated with an increase in p53 and p21 expression, which is a required element in the p53-dependent cell cycle arrest. In fact, p21 is regulated by p53, so it depends on p53 expression in order to perform its role, which is the inhibition of CDKs and subsequent cell cycle arrest[220].

When A549 cells were treated with 20 μmol/L isoliquiritigenin (**44**), over 46% of cells were arrested in G_1 phase, being this percentage increased to 60% with 40 μmol/L of **44**[219]. p53 was up-regulated after 6 hours treatment and it reached its maximum after 12 hours. Isoliquiritigenin (**44**) also induced apoptosis due to its ability to enhance the expression of p53 downstream targets, specifically Fas and its two ligands, namely membrane-bound Fas ligand (mFasL) and soluble Fas ligand (sFasL), in A549 cells[219]. This compound was tested again by the same authors a year later in 2005, in Hep G2 cells[222]. The treatment with 20 μg/mL isoliquiritigenin (**44**) induced cell cycle arrest at the G_2/S phase, and also caused DNA fragmentation at a concentration of 10 μg/mL after 48 hours of treatment, which triggered apoptosis. This concentration also increased p53 levels after 3 hours and reached maximum levels after 6 hours of exposition[222]. In 2009, Hsu *et al.* tested this chalcone on HeLa cells[223]. The results were similar, showing cell cycle arrest in the G_2/S phase and induction of apoptosis, with an IC_{50} value of 9.8 μM. Furthermore, the authors observed that the exposure of cells to 20 μM isoliquiritigenin (**44**) enhanced the phosphorylation of p53 on residues Ser15 and Ser392, and increased one of p53 downstream targets, p21. A more recent work published by Kim *et al.* in 2017 demonstrated that isoliquiritigenin (**44**) generated ROS in Caki cells[224]. This, in turn, would stabilize and activate p53, increasing its levels. It also downregulated MDM2, which contributed to the increase of p53 expression.

HTMC (**45**) caused reduction of cell proliferation in the lung A549 tumor cell line by 59% with the concentration of 50 μM for 24 hours. It also increased the G_1 population of cells from 62.5% to 83.4% and decreased the S population from 31.1% to 13.3% after treatment with 12.5 μM HTMC (**45**) for 24 hours[220]. This cell cycle arrest ability was caused by the effect of HTMC (**45**) on the p21 upregulation, therefore implying p53 upregulation as well, which in turn would inhibit cdc2, causing cell cycle arrest at G_1 phase. When it comes to apoptosis induction by p53, however, the authors that tested HTMC (**45**) stated that it was unclear whether this chalcone could induce DNA damage, which can be required for p53 to execute its pro-apoptotic role[220].

Flavokawin A (**46**) and B (**47**) are two natural chalcones which only differ in the substitution pattern of B ring. In 2008, a study conducted by Tang *et al.* showed that flavokawin A (**46**) induced cell cycle arrest in the G_2/M phase in six p53-mutant papillary bladder tumor cell lines[225]. In RT4 bladder tumor cells that express wt p53, flavokawin A increased the levels of p21/WAF1, suggesting that p53 activated the transcription of the p21 gene[225]. It also caused cell cycle arrest, but the increase in p21/WAF1 levels, which are related to cell cycle arrest, was observed independent of cell cycle phase. The treatment of human squamous carcinoma KB cells with 5-20 μM of flavokawin B (**47**) induced the upregulation of p21/WAF, p53 and Wee1[225]. This upregulation resulted in cell cycle arrest

at the G_2/M phase, since p21/WAF is able to inhibit CDKs and Wee1 prevents the cell from entering into the mitotic stage by catalyzing the inhibitory tyrosine phosphorylation of Cdc2-cyclin B kinase. Also, there was a decrease in the levels of cyclin A, cyclin B1, Cdc2 and Cdc25C, which contributed for the cell cycle arrest. The apoptotic effects of flavokawin B (**47**) were mainly associated with the decrease in Bcl-2 levels and increase in Bax levels, disrupting the Bcl-2:Bax ratio, as well as the activation of caspase-9, -3 and -8, cleavage of poly ADP ribose polymerase (PARP) and Bid in KB cells[225].

The prenylated chalcone isolespeol (**48**), isolated from *Artocarpus communis*, revealed a potent growth inhibitory effect in SW 872 human liposarcoma cells (IC_{50} value of 3.8 μM)[226]. Western blotting revealed that isolespeol (**48**) increased p53 levels at a concentration of 3 μM after 3 hours of exposition.

The treatment of lung adenocarcinoma A549 cells with xanthohumol (**49**) induced apoptotic cell death after treatment for 48 hours with 5 μM and reached a maximum effect with 20 μM. Xanthohumol (**49**) also induced cell cycle arrest at the G_1 phase. The first noticeable differences in cell cycle arrest were observed after treatment with 10 μM xanthohumol (**49**) and the maximum percentage of cells in G_1 phase was observed after treatment with 20 μM xanthohumol [227]. The induction of cell cycle arrest was associated with the upregulation of key cell cycle regulators p53 and p21 as well as downregulation of cyclin D1, while the induction of apoptosis was related with the activation of caspase-3.[228]

***Table 1**: Natural chalcones inducers of p53-dependent apoptosis and/or cell cycle arrest.*

Chalcones	Molecular targets in apoptotic/cell cycle cellular processes	Cytotoxic effect (IC_{50})/ p53 activation (Ref) (Method)
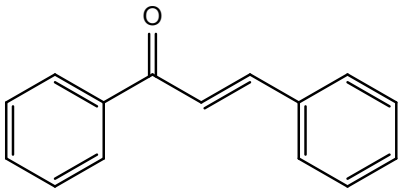 ***trans*-Chalcone (43)**	Decrease of Sp1, Sp3 and Sp4 expression Downregulation of Top2A and MMP-2 transcripts (Sp1 target genes)[217], and MN1[218] Upregulation of Gadd45A, p21[217] DNAJB1, ATF3[218] (p53 target genes), TP53AIP1 and PLK2[218] Increase of p53 expression	U2OS[217,218]: IC_{50} = n.d p53 activity* = 50 µM (Western Blot)[217]; (RNA-Seq, RT-PCR and Western Blot)[218] HCT116[218]: IC_{50} = n.d. p53 activity* = 50 µM (Western Blot) FaDu[218]: IC_{50} = n.d. p53 activity* = 50 µM (Western Blot) SJSA1[218]: IC_{50} = n.d. p53 activity = 50 µM (Western Blot)

Table 1 *(cont.)*

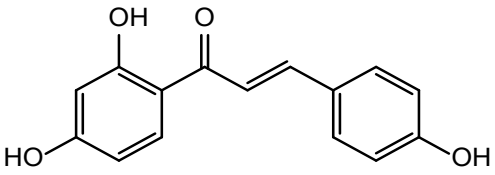 **Isoliquiritigenin** (**44**)	Increase of p53 expression, p21/WAF1 levels, Fas-ligand and Fas-receptor expression, Bax and NOXA expression, Bak levels and caspase-9 activity Decrease of Bcl-2 and Bcl-X_L, PCNA, MDM2, p-GSK-3β, p-Akt, p-c-Raf and p-PTEN expression levels	Hep G2[222]: IC_{50} = n.d. p53 activity* = 10 µg/mL (ELISA) A549[219]: IC_{50} = n.d. p53 activity* = 20 µmol/L (ELISA) HeLa[229]: IC_{50} = 9.8 µM p53 activity* = 10 µM (ELISA) Caki[224]: IC_{50} = n.d. p53 activity* = 50 µM (Western Blot)

Table 1 *(cont.)*

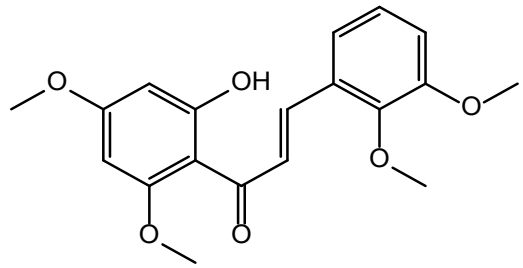 **2'-Hydroxy-2,3,4',6'-tetramethoxychalcone** (HTMC, **45**)	Inhibition of phosphorylation of cdc2 (Tyr15 and Tyr161) and Rb (Ser795 and Ser807/811) Increase of p53 and p21 expression	A549[220]: IC_{50} = 47 µM p53 activity* = 6.25 µM (Western Blot)
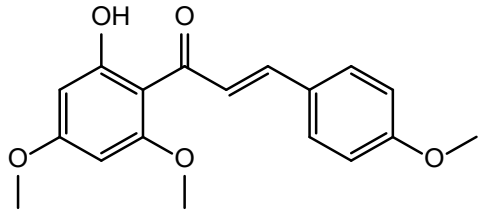 **Flavokawin A** (**46**)	Increase in p21/WAF1, p27/KIP1 Decrease of CDK2 activity	RT4[225]: IC_{50} = 20.8 µM p53 activity = 40 µmol/L (Flow Cytometry)
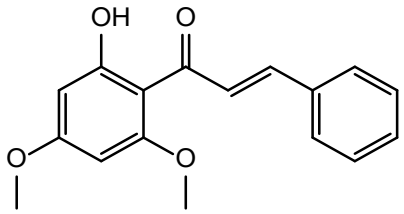 **Flavokawin B** (**47**)	Increase in p53, p21/WAF1, Wee1 and Bax levels Activation of caspase-9, -3 and -8 PARP cleavage Bid cleavage Decrease of Bcl-2, cyclins A and B1, Cdc2 and Cdc25C levels Release of cytochrome *c*	KB[228]: IC_{50} = 30.0 µg/mL[#] p53 activity* = 5 µg/mL (Western Blot)

Table 1 *(cont.)*

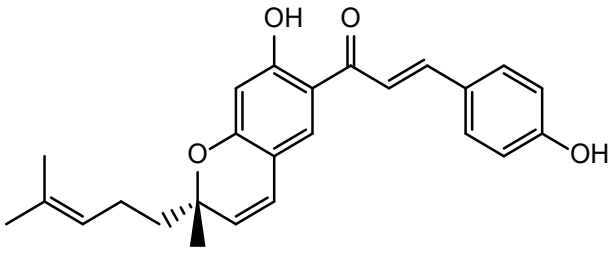 **Isolespeol** (**48**)	Increase of p53, Fas, FasL, and Bcl-2 family proteins expression Increase of caspases -3, -8 and -9 expression PARP cleavage Release of cytochrome C	SW 872[226]: IC_{50} = 3.8 µM p53 activity = 5 µM (Western Blot)
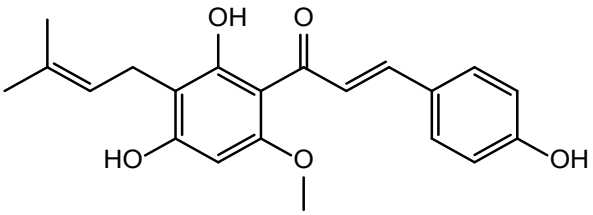 **Xanthohumol** (**49**)	Suppression of ERK1/2 and p90RSK kinases Inhibition of phosphorylation and activation of the CREB protein Increase in p53 and p21 expression Downregulation of cyclin D1	A549[227]: IC_{50} = 20.9 µM** p53 activity* = 20 µM (RT-PCR; Western Blot)
*IC_{50}: concentration that causes a growth inhibitory effect of 50% **After 48 hours n.d.: not determined. *Lowest tested concentration that induced p53 activity.		

2.1.2. Synthetic chalcones

The wide range of promising biological activities described for natural chalcones encouraged the synthesis of structure-related chalcones in order to obtain new promising drug candidates for the treatment of several diseases, namely cancer. Table 2 summarizes some synthetic chalcones with antitumor activity through a p53-mediated apoptosis and cell cycle arrest. Pedrini *et al.*[230] synthesized a series of chalcones derived from 2-naphtaldehyde. A preliminary screening of this series using L-1210 lymphoblastic leukemia cells showed that chalcone **50** had the most promising cytotoxic effect. It induced apoptosis through the increase of Bax, p53 and cleaved caspase 3 expression. This chalcone also caused a significant increase of cells in G_0/G_1 phase (45.59%) and in G_2/M phase (42.05%), which the authors claimed that could be associated with the increase in p53 expression[230].

A small library of imidazo[2,1-b]thiazole chalcone derivatives were synthesized and evaluated for their antitumor activity in a panel of 60 cell lines. Among the studied compounds, derivatives **51** and **52** showed to be the most potent growth inhibitors of human tumor cell lines. Compound **51** showed a strong cytotoxicity effect with GI_{50} values ranging from 0.26 to 4.74 μM in a wide range of tumor cell lines, including leukemia (CCRF-CEM, K-562, RPMI-8226, SR), colon (HCC-2998, HCT-15, KM12), prostate (PC-3, DU-145), breast (MCF-7, T-47D, MDA-MB-468), non-small cell lung (NCI-H23, NCI-H460, NCI-H522), CNS (SF-295, U251), ovarian (IGROV1, NCI/ADR-RES, OVCAR-8), renal (UO-31), and melanoma (MDA-MB-435, SK-MEL-2, SK-MEL-5). Compound **52** had a more modest activity against the SR leukemia and HCT116 colon tumor cell lines, with GI_{50} values of 0.53 μM and 1.00 μM, respectively. The comparison of the results obtained for all compounds allowed to conclude that the presence of a trifluoromethyl group and a 2-thienyl ring at position 6 was associated with an enhancement of the antiproliferative effect. In order to evaluate the effect of these chalcone derivatives, flow cytometry analysis was performed at the concentration of 4 μM for 24 hours. Compounds **51** and **52** caused G_0/G_1 phase cell cycle arrest, being this effect related with the decrease of cyclins D1, A and E1 levels and the increase of CDK4 levels, as well as the upregulation of p53, p21, p27 and chk2. Moreover, **51** and **52** elicited the characteristic features of apoptosis in MCF-7 cells such as enhancement in the levels of p53, p21, and p27, suppression of NF-κB, and upregulation of caspase-9[231].

CH027 (**53**) was identified as a potent growth inhibitor of LNCaP, C4-2 and 22Rv1 human tumor cell lines, with IC_{50} values in nanomolar range[232]. Using these prostate tumor cells, it was demonstrated that CHO27 at low nanomolar levels has antiproliferative activity through cell cycle arrest and caspase-dependent apoptosis, being also observed an

upregulation of p53. The authors of this work evaluated the *in vivo* effects of CH027 (**53**) in mice with established 22Rv1 xenograft tumors, as well as its pharmacokinetic parameters. CHO27 (**53**) treatment retarded the growth of 22Rv1 xenograft tumors and decreased the final tumor weight by 30 %. After one dose of administration (1 mg per mouse, approx. 40 mg/kg body weight), the plasma levels of CHO27 (**53**) achieved a peak of approx. 850 nM by 1 hour, then decreased to over 400 nM by 2 hours and to 200 nM by 4 hours. CH027 (**53**) was able to phosphorylate p53 and therefore to up-regulate $p21^{Cip1}$, and this effect was responsible for the antiproliferative and pro-apoptotic activities of this compound[232].

A series of six chalcone derivatives with a 2-acetyl thiophene A ring were synthesized and evaluated for their antiproliferative activity in HT-29 human colon adenocarcinoma cells. C06 (**54**) up-regulated p53 and p21 expression in HT-29 cells, especially at the concentration of 40 μM, causing G_2/M cell cycle arrest. The treatment of these cells with 40 μM C06 (**54**) was also associated with a high percentage of cells in early or late apoptosis, indicating that it was able to induce apoptosis, mainly through the increase of caspase-9 mRNA levels[233]. On the contrary, the structurally related chalcone C09 (**54**) increased p53 at 40 μM, showing no changes in p21 transcription levels. Like C06 (**54**), C09 (**55**) also induced a similar late apoptosis and a higher early apoptosis at 40 μM, while revealing a lower cytotoxic effect when compared to C06 (**54**). Together, these results indicate that C09 (**55**) may induce cell death though non-apoptotic mechanisms[233].

In 2014, Shin *et al.* synthesized the chalcone derivative HMNC-74 (**56**) and studied its activity on HCT116 cells. This compound inhibited the clonogenicity of these cells and induced cell cycle arrest at the G_2/M phase, as well as apoptosis. The authors of this work further analyzed the cause of this apoptosis induction. They concluded that 10 μM HMNC-74 (**56**) increased p53 levels over time in wild-type HCT116, but not in p53-null HCT116 cells. Also, the cleavage of caspase-7 and its substrate PARP was attenuated on p53-null cells, which suggests that the apoptotic effect could be related to p53 activation[234]. In the same year, Lee *et al.* verified that HMNC-74 (**56**) also promoted the inhibition of clonogenicity, G_2/M cell cycle arrest and induction of apoptosis on SW620 cells. The levels of p53 were increased after 12 hours treatment with 10 μM HMNC-74, as well as the levels of phosphorylated p53, γ-H2AX, p-Chk2 and Bax[235].

SKLB-M8 (**57**), a synthetic derivative of the natural chalcone millepachine, showed *in vitro* growth inhibitory effect in three melanoma cell lines (A2058, CHL-1, and B16F10), being this effect associated with G_2/M cell cycle arrest, downregulation of cdc2 expression, and upregulation of p53, in A2058 and CHL-1 cells treated with 0.1 μM chalcone **57** and 0.5

μM chalcone **57**, respectively. SKLB-M8 (**57**) also induced apoptosis through downregulation of AKT and phosphorylated mTOR (p-mTOR)[236].

As a result of the search for new effective antitumor compounds for human oral squamous cell carcinoma (OSCC), TMC (**58**) was identified as a potent inhibitor of cell proliferation, showing an IC_{50} value of 3 μM. TMC (**58**) promoted an inhibition of cell cycle arrest at G_2/M phase and caused DNA double-strand breaks in the SCC4 cell line. Cells treated with 1 μM **57** also revealed increased expression of caspase -3 and -9, PARP, cytochrome *c* release, calpain-1 and -2, phosphorylation of histone H2AX, phosphorylation of checkpoint kinases 2, p53, BCL2-antagonist/killer and BCL2-associated X protein[237].

Tetramethoxychalcone (TMOC, **59**) inhibited the proliferation and colony formation of cisplatin sensitive human ovarian tumor A2780 cell line. The treatment of these cells with TMOC (**59**) resulted in G_0/G_1 cell cycle arrest through the downregulation of cyclin D1 and CDK4, and the upregulation of p16, p21 and p27 proteins. Apoptosis was also induced through suppression of Bcl-2 and Bcl-xL and induction of the expression of Bax and PARP cleavage. It also up-regulated p53[238].

The study of the mechanism underlying the potent antiproliferative activity of the new coumarin–chalcone hybrid S009-131 (**60**) in HPV positive (HeLa) and HPV negative (C33A) cervical tumor cell lines demonstrated that this chalcone inhibited the proliferation through apoptosis induction and cell cycle arrest at G_2/M phase. Moreover, the S009-131 (**60**) pro-apoptotic effect was associated with an increase in Bax/Bcl-2 ratio, intracellular ROS, release of cytochrome *c* into the cytosol, and activation of capases-9, -3 and -7. p53 was also up-regulated, but only in the C33A cell line, along with its transcriptional target PUMA (in both cell lines), suggesting its role in mediating the apoptotic cell death[239].

Lock-Neckel *et al.*[240] reported that the chalcone-quinoxaline hybrid N9 (**61**) induced the inhibition of cell proliferation, cell death and G_1 cell cycle arrest in U87-MG glioma cells. In addition, an inhibition of cyclins A and E expression and a decrease in the expression of CDK2, CDK6 and phosphorylation of Rb was observed in N9-U87-MG glioma cells. N9 (**61**) also up-regulated p53 and its downstream molecule p21, stabilized p53 and reduced MDM2 levels. Along with the increase in cleaved caspase-9 expression, these effects triggered apoptosis after 24 hours treatment in a dose-dependent manner[240]. Collectively, these results demonstrate that the induction of p53 and p21 proteins, as well as, the activation of mitochondrial apoptosis pathway associated with the inhibition of protein MDM2 is involved in the antitumor activity of N9 (**61**).

Ma *et al.* selected in 2015 a panel of cell lines including p53 wild-type HeLa (cervical), HCT-116 (colon), MCF-7 (breast), A549 (lung), and p53 null HL-60 (leukemia), as well as

normal human lung fibroblast MRC-5 and cisplatin-resistant cells A549cDDP for treatment with chalcoplatin (**62**), a Pt(IV) prodrug. Platinum drugs form Pt-DNA cross-links that inhibit DNA metabolism and trigger apoptosis, and platinum(IV) scaffolds allow the enhancement of the oral availability and antitumor activity. They also contribute to the decrease of the toxicity of platinum(II) drugs, since they are reduced to platinum(II) equivalents only when inside the cells[241]. Chalcoplatin (**62**) showed up to 10.0-fold increased cytotoxicity compared with cisplatin. However, this chalcone showed the same cytotoxicity as cisplatin towards p53-null cells, indicating that its mechanism should be related to an activation of p53[241]. Furthermore, chalcoplatin (**62**) was also very active against cisplatin-resistant A549cDDP, with 31.6-fold increased cytotoxicity in the resistant cells compared with cisplatin. It was also able to induce cell cycle arrest at the G_2/M phase, upregulate p53 at the minimum concentration of 5 μM, and induce apoptosis by disruption of mitochondrial transmembrane potential change[241].

The chalcone based pyrido[b]indole CPI-7c (**63**) activated p53 by phosphorylation at serine 15, serine 46 and serine 392 residues[242]. CPI-7c (**63**) also strongly up-regulated DR4 and DR5 proteins and down-regulated the anti-apoptotic protein XIAP. However, it did not induce significant changes in the expression of Bax, Bak, Bcl2 or cytochrome *c* release. More importantly, this compound was able to promote ubiquitination and degradation of MDM2 by binding directly to its N-terminal and RING domains, allowing p53 to be stabilized and activated[242].

Fu *et al.* synthesized in 2016 a series of 1,2,3-triazole-chalcone hybrids and tested those derivatives on three tumor cell lines, SK-N-SH, HepG2 and MGC-803. Most of these compounds showed moderate to good antitumor activity on the selected cells. The best antiproliferative activity was achieved by **64**, with an IC_{50} value of 1.53 μM on the SK-N-SH cells. This activity was related to cell cycle arrest at the G_1 phase and induction of apoptosis. This effect was further investigated, and the authors concluded that **64** increased the levels of p53 and caspase-3, while also decreasing the levels of pro-caspase-3[243]. In the same year, the same team of researchers tested another group of synthetic chalcones, this time a series of dithiocarbamate-chalcone derivatives[244]. The chalcone **65** exhibited a notorious result on the SK-N-SH cells, with an IC_{50} value of 2.03 μM. It also increased dramatically the p53 and caspase-3 levels and decreased the levels of pro-caspase 3, probably due to the fact that pro-caspase-3 needs to be cleaved to originate caspase 3.

Shin *et al.*[245] investigated the mode of action underlying the antitumor activity of the naphtal chalcone derivative HMP (**66**). HMP (**66**) promoted a sub-G_0/G_1 phase arrest and triggered apoptosis in HCT116 cells. Additionally, HMP (**66**) stimulated the cleavage of

caspase-7 and its substrate PARP, and promoted γ-H2AX formation, production of ROS, and upregulation of p53 expression. It is noteworthy to mention that HMP-induced caspase-7 activation was not completely abolished in p53-null HCT116 cells, which indicates that the observed cell death could be induced by both p53-dependent and -independent mechanisms[245].

The treatment of HepG2 cells with 3MCIC (**67**) caused drastic reduction of cyclin D1 and cyclin B1. 3MCIC (**67**) at 12 μg/mL reduced CDK1, but the reduction of inactivated p-CDK1/2 was only observed after 24 hours treatment. This, in turn, increased significantly the percentage of inactivated CDK1. Moreover, 3MCIC (**67**) downregulated c-Myc, E2F1, Ser567- phosphorylated p-Rb and total Rb, but upregulated p53 and p21[246].

Among 19 synthesized chalcones, SSE14105 (**68**) and SSE14106 (**69**) induced accumulation of p53 in HCT116 cells after 4 and 8 hours treatment like Nutlin-3 (**1**), which is, as referred earlier, a well-known inhibitor of the p53-MDM2 interaction[247].

Cabral *et al.*[248] synthesized LQFM064 (**70**) and studied its effects on MCF-7 cells. It induced cell cycle arrest at G_0/G_1 phase with increased p53 and p21 expressions. Following treatment with LQFM064 (**70**) it was observed externalization of phosphatidylserine, cytochrome *c* release, increased expression of caspases-7, −8 and −9, reduced mitochondrial membrane potential and ROS over-production. LQFM064 (**70**) also increased TNF-R1, Fas-L and Bax levels and reduced Bcl-2 expression, resulting in apoptosis of these cells[248].

A small library of pyrazolo[1,5-a]pyrimidines was synthesized and tested for antiproliferative activity in A549, MDA-MB-231 and DU-145 cell lines. Compounds **71**-**73** showed potent growth inhibitory effect in the above-mentioned lines, with IC_{50} values between 2.6 – 34.9 μM. A549 cells treated with 2 μM of compounds **71**-**73** showed a G_2/M phase cell cycle arrest of 29.6%, 29.5%, and 33.11% respectively. These chalcone hybrids increased the levels of p53, p21 and Bax and decreased the expression of Bcl2 in A549 cells, confirming their ability to trigger an apoptotic cell death.[249].

In 2018, Mu *et al.* synthesized the curcumin-chalcone derivative L6H4 (**74**) and tested its activity on gastric BGC-823 tumor cells[250]. Through MTT and Annexin V assays, the authors concluded that this synthetic chalcone was able to inhibit cell proliferation. It was also able to induce apoptosis by enhancing the expression levels of p53, p21, Bax and Bcl-2, both *in vitro* and *in vivo*. In the *in vitro* assays, p53 expression was increased at the optimum concentration of 10 μmol/L L6H4 (**74**) after 48 hours. On the other hand, the *in vivo* studies on male BALB/c nude mice showed an increase of p53 levels after treatment with 15 μmol/L L6H4 (**74**) for 48 hours[250].

In the same year, D14 (**75**) and D15 (**76**), two 4´-aminochalcones, were studied on the U2OS and SAOS-2 cells by Seba *et al.* in 2018, particularly in terms of anti-metastatic activity[251]. p53 regulates an important process that confers migratory and invasive properties to tumor cells called epithelial-mesenchymal transition (EMT)[251]. Chalcones D14 (**75**) and D15 (**76**) successfully decreased the migration of U2OS cells but had little effect on the migration of SAOS-2 cells. However, both chalcones reduced cell migration in SAOS-2 cells expressing wt p53 (normal SAOS-2 are *TP53*-null[252]). These chalcones seem to be more effective in p53-expressing osteosarcoma cells. Additionally, these authors proposed a model for the action of these chalcones, suggesting that D14 (**75**) and D15 (**76**) upregulated p53 protein levels, thus regulating genes involved in EMT and promoting the inhibition of cell migration and invasion[251].

Mohamed *et al.* synthesized a series of tetrahydro-[1,2,4]triazolo[3,4-a]isoquinolin-3-yl)-3-arylprop-2-en-1-one derivatives and evaluated their cytotoxic activities against MCF7, A549, HCT116, and HepG2 cell lines. The MCF-7 cells revealed the highest sensitivity towards all compounds, especially compounds **77** and **78**, which exhibited the lowest IC_{50} values (50.05, and 27.15 mg/mL, respectively), while having little toxicity towards normal melanocytes HFB). Both compounds up regulated BAX, p53 and caspase-3 genes, and down regulated BCL2, MMP1 and CDK genes. It was also noted that compound **78** was more effective in gene regulation than compound **77**, as well as in induction of apoptosis. Both compounds were able to induce cell cycle arrest at G_1 phase, and both induce death of breast cells of 8.72% and 17.28%, respectively (compared to a control of 0.55%). The authors also claim that compound **78** induced apoptosis by activation of caspase-3[253].

***Table 2**: Synthetic chalcones inducers of p53-dependent apoptosis and/or cell cycle arrest.*

Chalcones	Molecular targets in apoptotic/cell cycle cellular processes	Cytotoxic effect (IC_{50})/ p53 activation (Ref) (Method)
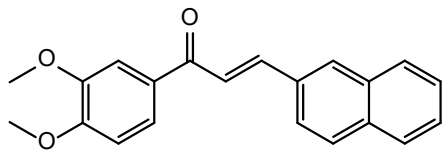 (**50**)	Increase in p53 and Bax expression and in caspase-9 activity	L-1210[230]: IC_{50} = 54 µM p53 activity* = 100 µM (Flow Cytometry)
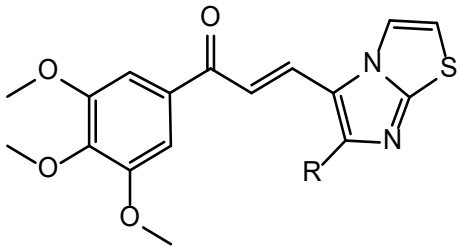 R = 2-thienyl (**51**) R = trifluoromethyl (**52**)	Increase in cyclins D1, A and E1, CDK4 and IKKα levels Decrease in NF-κB Upregulation of caspase-9, p53, p21, p27 and chk2	(**51**) MCF-7[231]: IC_{50} = 0.72 µM p53 activity* = 4 µM (Western Blot) (**52**) MCF-7[231]: IC_{50} = 1.26 µM p53 activity* = 4 µM (Western Blot)
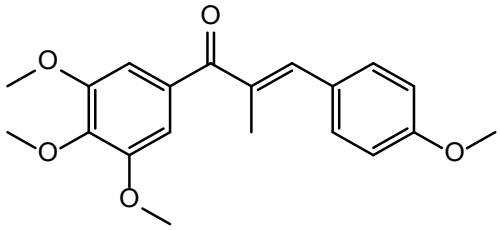 **CH027** (**53**)	Increase in p53 activity Upregulation of p21/WAF1 PARP cleavage	LNCaP[232]: IC_{50} = 13 nM*** p53 activity* = 10 nM (Western Blot) 22Rv1[232]: IC_{50} = 15 nM*** p53 activity* = 10 nM (Western Blot)

***Table 2** (cont.)*

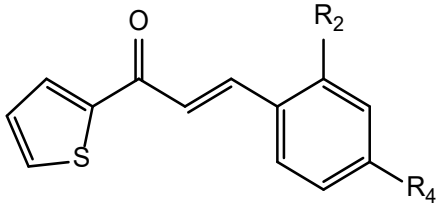 R_2=H, R_4=Br; **C06** (**54**) R_2=NO_2, R_4=H; **C09** (**55**)	Decrease of Bcl-2 expression Increase of Bax expression Upregulation of caspase-9, p53 and p21 Downregulation of survivin	(**54**): HT-29[233]: IC_{50} = 13.4 μM# p53 activity* = 20 μM (RT-PCR) (**55**): HT-29[233]: IC_{50} = 19.5 μM# p53 activity* = 40 μM (RT-PCR)
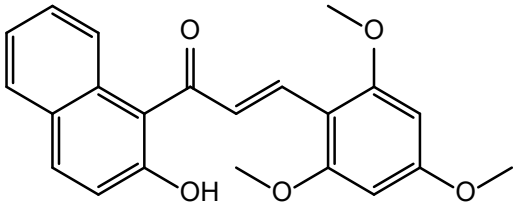 **HMNC-74** (**56**)	PARP and caspase-7 cleavage Increase of p53, γ-H2AX, p-Chk2 and Bax levels	HCT116[234]: IC_{50} = n.d. p53 activity* = 10 μM (Western Blot) SW620[235]: IC_{50} = 14.5 μM p53 activity = 10 μM (Western Blot)

***Table 2** (cont.)*

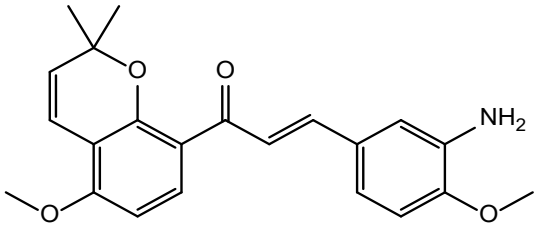 **SKLB-M8** (**57**)	Increase of cleaved caspase-3 Decrease of cleaved procaspase-9 levels and of p-mTOR expression Activation of PARP Downregulation of AKT and cdc2 Upregulation of cyclin B1 and p53	<u>A2058</u>[236]: IC_{50} = 0.07 µM p53 activity* = 0.5 µM (Western Blot) <u>CHL-1</u>[236]: IC_{50} = 0.25 µM p53 activity* = 0.5 µM (Western Blot)
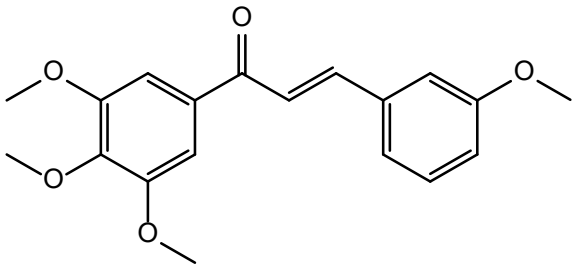 **TMC** (**58**)	Increase of caspase-3 and -9 expressions Increase of PARP, cytochrome c, calpain-1 and -2 expressions Phosphorylation of histone H2AX, checkpoint kinases 2 and of p53	<u>SCC4</u>[237]: IC_{50} = 3 µM p53 activity* = 1 µM (Western Blot)

Table 2 *(cont.)*

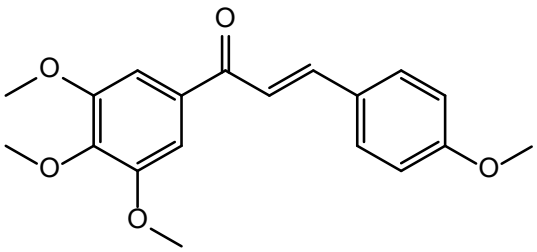 **TMOC** (**59**)	Increase of Bax expression Decrease of Bcl-2 and Bcl-xL Inhibition of phosphorylation of STAT3 and tyrosine kinases c-Src Downregulation of cyclin D1 and c-myc Upregulation of p53 and PTEN	A2780[238]: IC_{50} = 3.5 µM# p53 activity* = 10 µM (Western Blot)
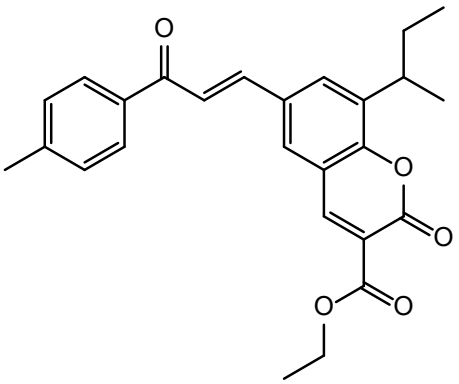 **S009-131** (**60**)	Increase of cytochrome c release Increase of Bax, Bak and p53 expression Decrease of Bcl-2 and Bcl-xL expression Increase of p53 expression Cleavage of caspase-7 and -9	C33A[239]: IC_{50} = 4.7 ± 1.0 µM p53 activity* = 4.7 µM (≥ 12 h exposure) (Western Blot)

***Table 2** (cont.)*

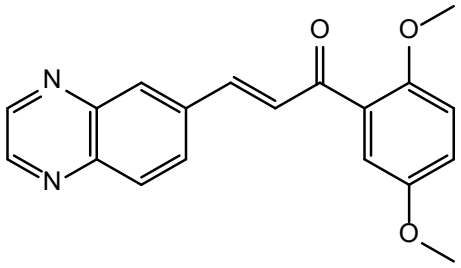 **N9** (**61**)	Inhibition in the expression of cyclins A and E Decrease of CDK2 and CDK6 expression and of MDM2 levels Rb inactivation ROS formation Increase of Bax, p53 and p21 levels Caspase-9 cleavage	U87-MG[240]: IC_{50} = 0.72 µg/mL p53 activity* = 0.1 µg/mL
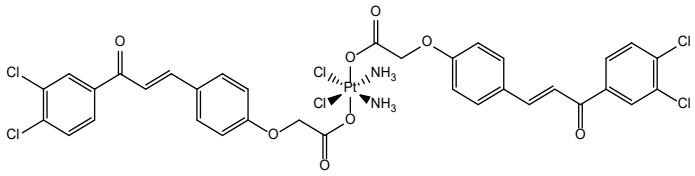 **Chalcoplatin** (**62**)	Increase of p53 expression	MCF-7[241]: IC_{50} = 4.8 ± 1.0 µM p53 activity* = 5 µM (48 h exposure) (Western Blot)

***Table 2** (cont.)*

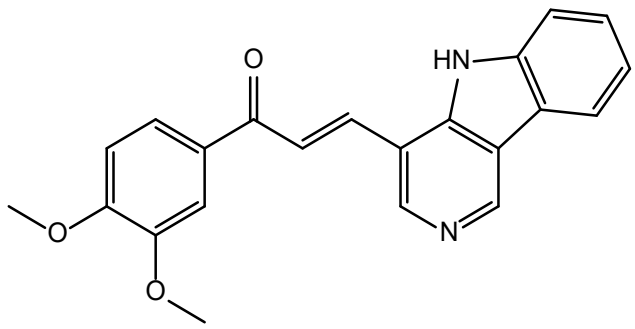 **CPI-7c** (**63**)	Inhibition of the MDM2-p53 interaction Degradation of MDM2 Increase of *DR4* and *DR5* expression	MCF-7[242]: IC_{50} = n.d. p53 activity* = 5 µM (Western Blot)
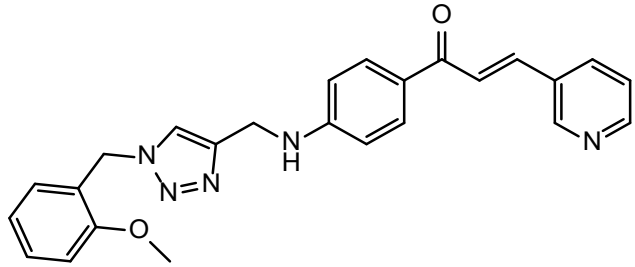 **64**	Increase of p53 and caspase-3 levels Pro-caspase 3 cleavage	SK-N-SW[243]: IC_{50} = 1.53 µM p53 activity = 5 µM (Western Blot)
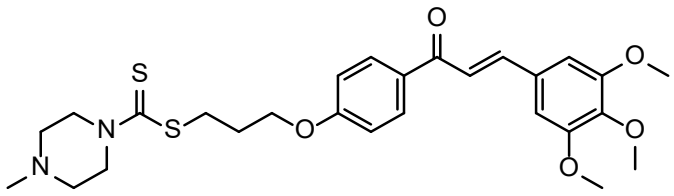 **65**	Increase of p53 and caspase-3 levels Pro-caspase 3 cleavage	SK-N-SW[244]: IC_{50} = 2.03 µM p53 activity = 5 µM (Western Blot)
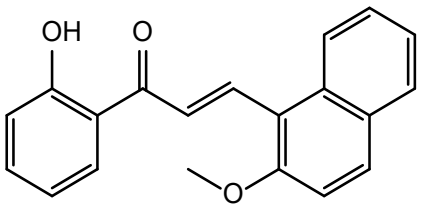 **HMP** (**66**)	Caspase-7 cleavage PARP cleavage γ-H2AX formation ROS formation Upregulation of p53 and Egr-1	HCT116[245]: IC_{50} = n.d. p53 activity* = 50 µM (Western Blot)

***Table 2** (cont.)*

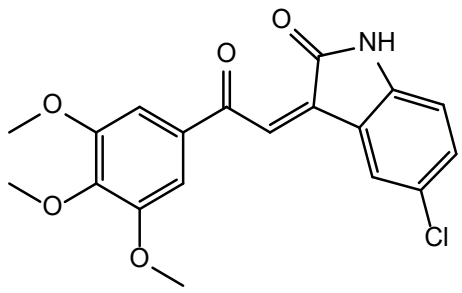 **3MCIC** (**67**)	Reduction of cyclin D1, cyclin B1, CDK1, inactivated p-CDK1/2 (after 24 h) Downregulation of c-Myc, E2F1, Ser567-phosphorylated p-Rb and total Rb Upregulation of p53 and p21	HepG2[246]: IC_{50} = 4.5 µM p53 activity* = 8 µM
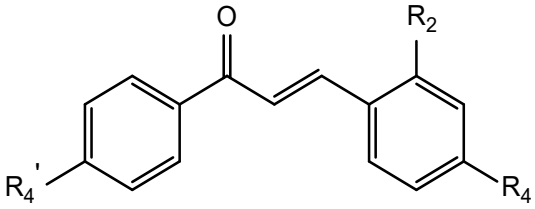 $R_{4'}$ = R_2 = H; R_4 = Cl; **SSE14105** (**68**) $R_{4'}$ = R_2 = H; R_4 = OCH_3; **SSE14106** (**69**)	Accumulation of p53	(**68**): HCT116[247]: IC_{50} = n.d. p53 activity* = 12.5 µM (Western Blot)
	Accumulation of p53	(**69**): HCT116[247]: IC_{50} = n.d. p53 activity* = 6.25 µM (Western Blot)

Table 2 *(cont.)*

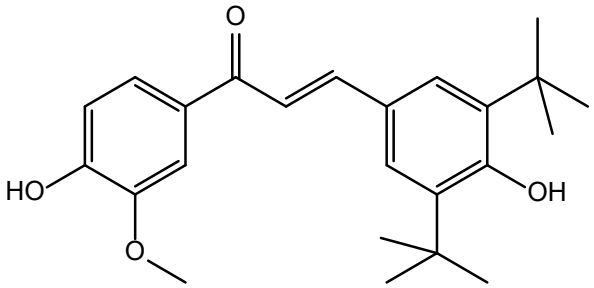 **LQFM064** (**70**)	Increase of p53, p21 and of caspases -7, -8 and -9 expression and of TNF-R1, Fas-L and Bax levels Externalization of phosphatidylserine Release of cytochrome *c* ROS formation Decrease of Bcl-2 expression	MCF-7[248]: IC_{50} = 21 µM p53 activity* = 21 µM (Flow Cytometry)
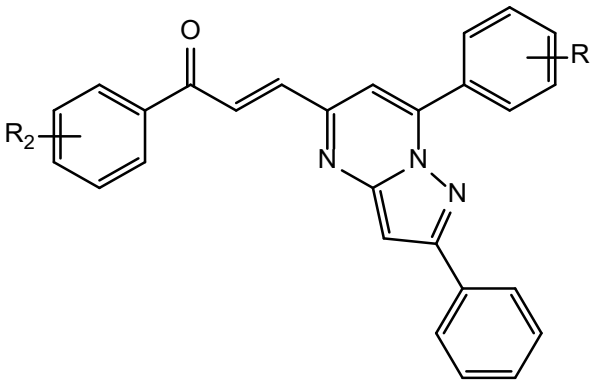 R_2 = 4-OMe, R = 4-OMe (**71**) R_2 = 3,4-diOMe, R = 3,4-diOMe (**72**) R_2 = 3,4-diOMe, R = 3,4,5-triOMe (**73**)	Inhibition of EGFR and STAT3 axis Increase of p53, p21 and Bax levels Decrease of Bcl-2 and procaspase-9 levels	A549[249]: IC_{50} = 2.9 ± 0.3 µM (**71**); 3.9 ± 0.4 µM (**72**); 7.2 ± 0.4 µM (**73**) p53 activity* = 2 µM (RT-PCR, Western Blot)
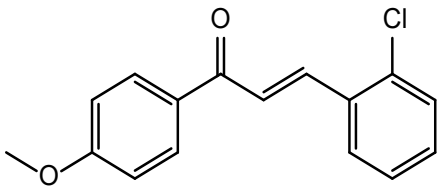 **L6H4** (**74**)	Increase of p53, p21, Bax and Bcl-2 expression	BGC-823[250]: IC_{50} = n.d. p53 activity = 10 µmol/L (*in vitro*); 15 µmol/L (*in vivo*) (Western Blot)

Table 2 *(cont.)*

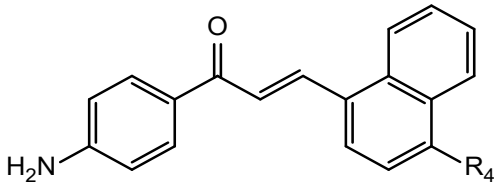 R_4 = H; **D14** (**75**) R_4 = CH_3; **D15** (**76**)	Increase of p53 Downregulation of MMP-2, MMP9, vimetin, Slug, N-cadherin and β-catenin	U2OS[251]: IC_{50} = n.d. p53 activity* = 27 μM SAOS-2[251]: IC_{50} = n.d. p53 activity* = 27 μM
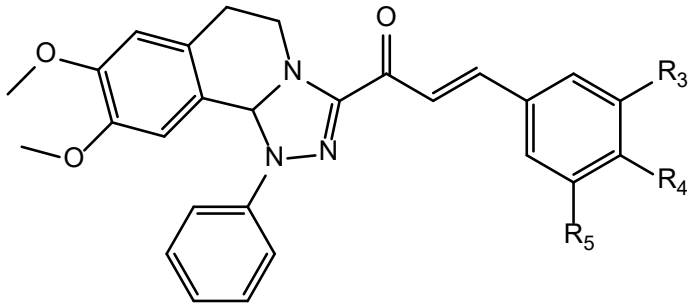 R_3=R_5=H, R_4=NO_2; (**77**) R_3=R_4=R_5=OCH_3; (**78**)	Upregulation of Bax, p53 and caspase-3 Downregulation of BCL2, MMP1 and CDK4	(**77**) MCF-7[253]: IC_{50} = 50.05 μg/mL p53 activity* = 50.05 μg/mL (RT-PCR) (**78**) MCF-7[253]: IC_{50} = 27.15 μg/mL p53 activity* = 27.15 μg/mL (RT-PCR)
*IC_{50}: concentration that causes a growth inhibitory effect of 50% n.d.: not determined. *Lowest tested concentration that induced p53 activity. #After 24 h. ***After 72 h		

2.2. Chalcones as disruptors of the p53-MDM2 interaction

Most chalcones interfere with p53 pathway, being not proven the direct effect on p53 or in the interaction between p53 and its negative regulators MDM2 and MDMX. The first report about the effect of chalcones in p53-MDM2 interaction was conducted by Stoll *et al.* in 2001. After this, about 17 chalcone derivatives have proved to interfere with p53-MDM2 interaction (Table 3). Encouraged by the promising antitumor properties of chalcones, Stoll *et al.* decided to characterize a library of chalcone derivatives at the molecular level for eventual interactions with the p53-MDM2 complex[254]. They proved that chalcone derivatives **79**-**83** inhibited the MDM2 binding to a p53 peptide using ELISA assay. Compounds **80**, **82** and **83** denatured MDM2 and compound **81** lead to MDM2 aggregation.

In addition to this, the authors of this study also tested these compounds for dissociation of preincubated p53/MDM2 complexes and release of p53 active from DNA-binding, using the full-length p53 protein in an electrophoretic gel mobility shift assay (EMSA). Compounds **79** and **82** inhibited the p53/MDM2 complex, but without releasing p53[254]. These interactions seemed to influence the p53 protein, which was not predicted from the ELISA test. Compounds **80**, **82** and **83** partially removed MDM2 from the p53/MDM2 complex[254], while compound **81** completely released active p53 from MDM2 binding.

Using a yeast screening assay, 14 chalcone derivatives (**84**-**97**) were identified as inhibitors of p53–MDM2 interaction[255–257]. These results were validated in human tumor cell lines, namely in human colon adenocarcinoma HCT116 cells expressing wt p53 for compounds **84**, **85**, and **92**-**97**. Chalcones **84**-**91** induced a growth inhibition in yeast cells of 63.7-97.2%. Computational docking studies allowed to predict that, like nutlin-3a, chalcone **85** binds to the p53-binding site of MDM2[256]. Additionally, **84** and **85** induced upregulation of p53, p21 and PUMA on NCI-H460 cells[256]. In HCT116 cells, the prenylated chalcone PC2 (**92**) showed potent growth inhibitory activity related to the activation of the p53 pathway through induction of cell cycle arrest and a mitochondria-dependent apoptosis. Using the co-IP assay, it was also demonstrated that 12 μM PC2 (**92**) caused a significant decrease of the amount of MDM2 co-immunoprecipitated with p53, confirming the disruption of the p53–MDM2 interaction by this chalcone[255]. Chalcone (**96**) showed improved cytotoxicity against human tumor cells expressing wild-type p53, including liver hepatocellular carcinoma HepG2, breast adenocarcinoma MCF-7, and malignant melanoma A375 cells. In HCT116 cancer cells, it was also shown that the growth inhibitory effect of prenylchalcone (**96**) was associated with the induction of cell cycle arrest, apoptosis, and increased protein expression levels of p53 transcriptional targets. Moreover,

computational docking studies predicted the interaction of this chalcone with the p53-binding site of MDM2. Chalcone (**96**) also induced upregulation of MDM2, p21, GADD45 and PUMA, downregulation of Bcl-2 and cleavage of PARP[257].

***Table 3**: Chalcones that interact with the p53/MDM2 complex.*

Chalcone	Cytotoxic effect (IC_{50} / GI_{50}) / Ref
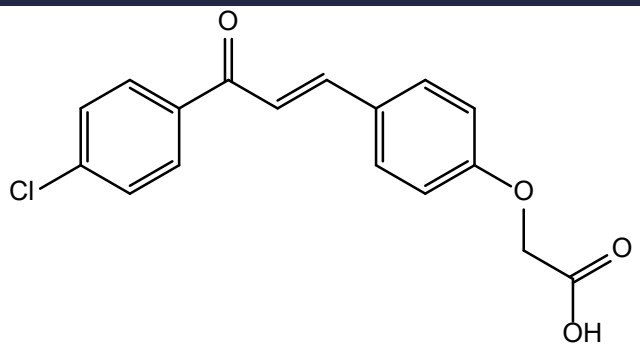 (**79**)	ELISA[254]: IC_{50} = 206 µM
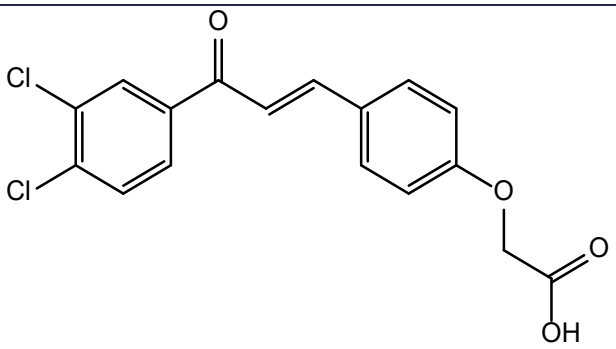 (**80**)	ELISA[254]: IC_{50} = 117 µM
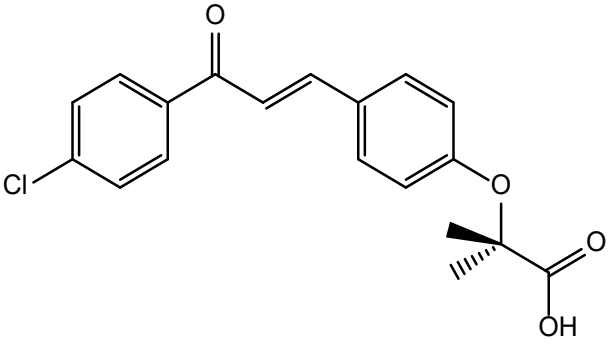 (**81**)	ELISA[254]: IC_{50} = 250 µM
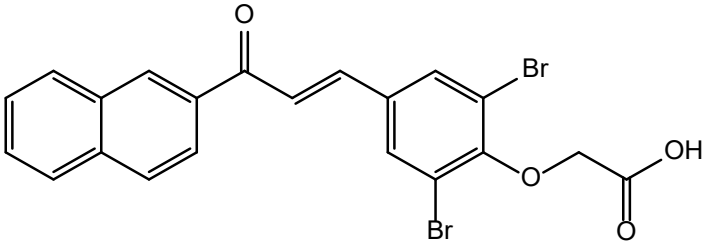 (**82**)	IC_{50} = n.d.[254]

Table 3 *(cont.)*

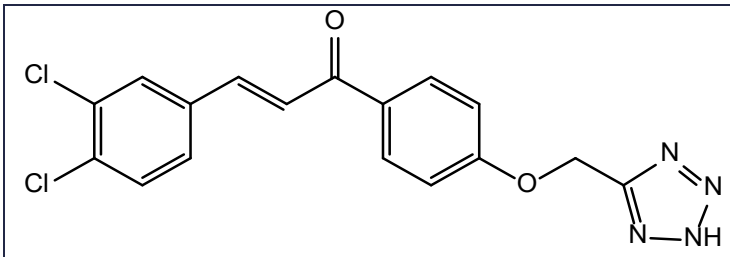 (**83**)	IC_{50} = n.d.[254]
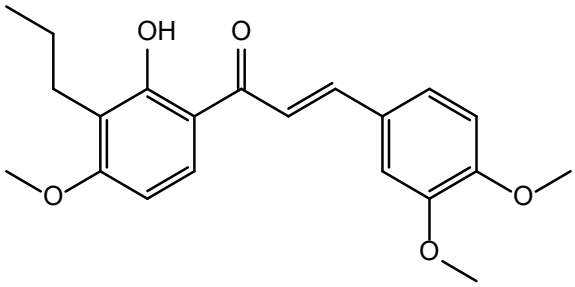 (**84**)	Yeast screening assay[256]: 79.4 % growth inhibition (% of p53 effect) HCT116 p53$^{+/+}$[256]: GI_{50} = 2.6 µM NCI-H460[256]: GI_{50} = 2.1 µM
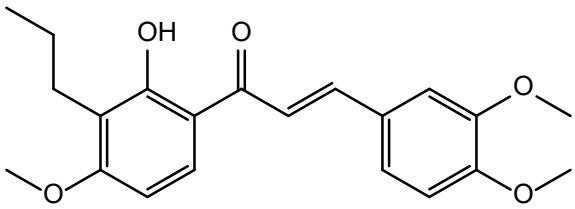 (**85**)	Yeast screening assay[256]: 97.2 % growth inhibition (% of p53 effect) HCT116 p53$^{+/+}$[256]: GI_{50} = 5.9 µM NCI-H460[256]: GI_{50} = 3.3 µM
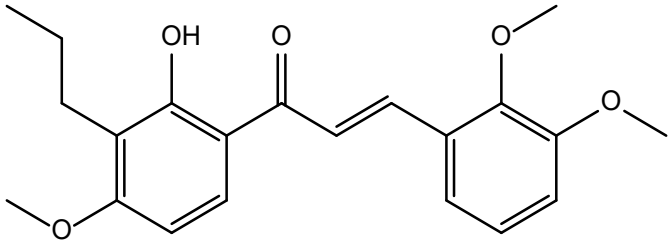 (**86**)	Yeast screening assay[256]: 63.7 % growth inhibition (% of p53 effect)

Table 3 *(cont.)*

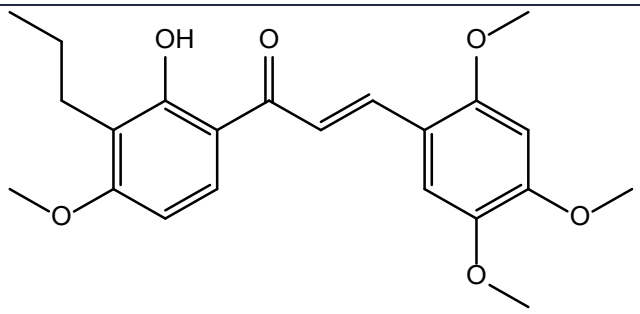 (**87**)	Yeast screening assay[256]: 68.8 % growth inhibition (% of p53 effect)
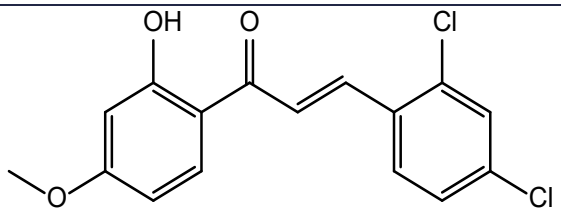 (**88**)	Yeast screening assay[256]: 77.9 % growth inhibition (% of p53 effect)
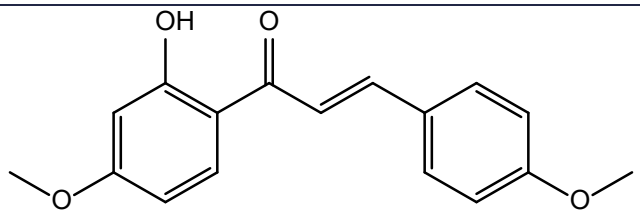 (**89**)	Yeast screening assay[256]: 95.2 % growth inhibition (% of p53 effect)
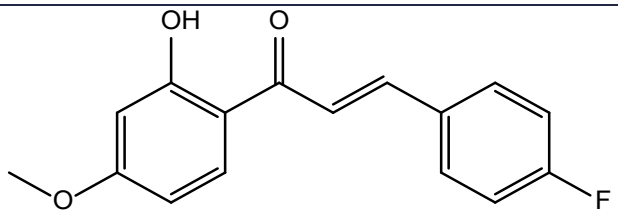 (**90**)	Yeast screening assay[256]: 78.3 % growth inhibition (% of p53 effect)
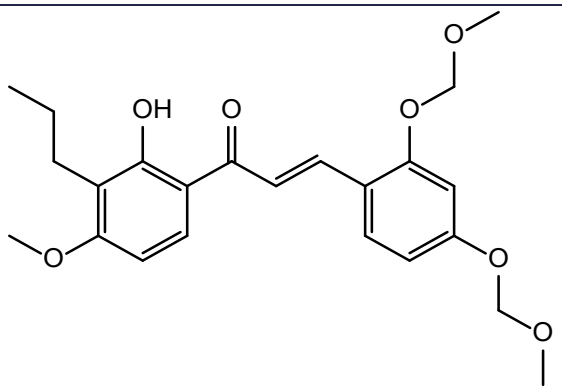 (**91**)	Yeast screening assay[256]: 97.0 % growth inhibition (% of p53 effect)

Table 3 *(cont.)*

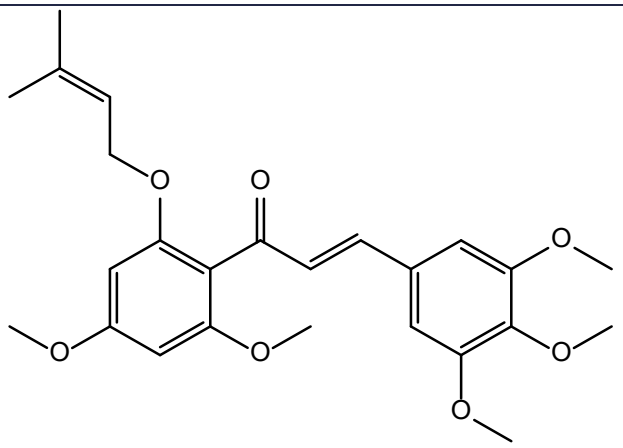 **PC2** (**92**)	HCT116 $p53^{+/+255}$: GI_{50} = 4 µM
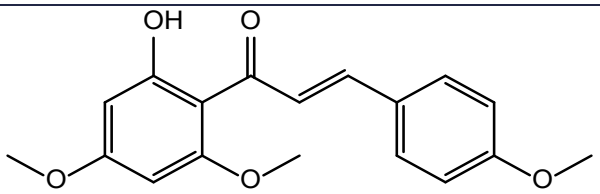 (**93**)	HCT116 $p53^{+/+257}$: IC_{50} = 10.6 µM
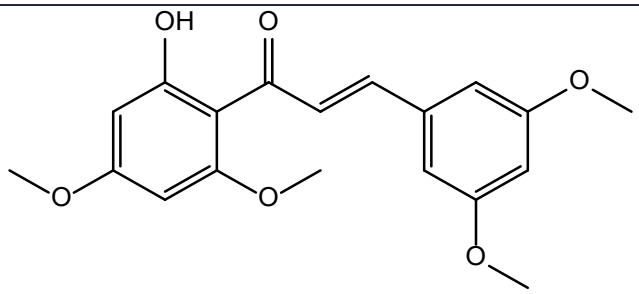 (**94**)	HCT116 $p53^{+/+257}$: IC_{50} = 50.0 µM
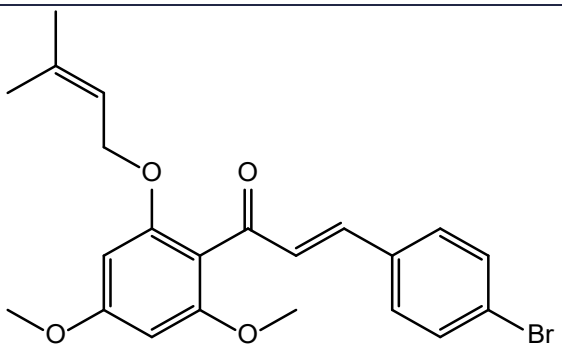 (**95**)	HCT116 $p53^{+/+257}$: IC_{50} = 2.1 µM

Table 3 *(cont.)*

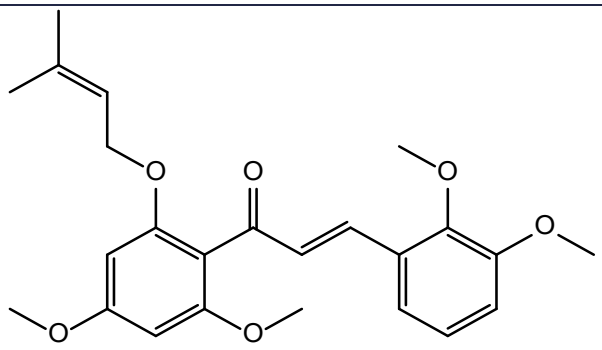 (**96**)	HCT116 p53$^{+/+257}$: IC_{50} = 11.7 µM
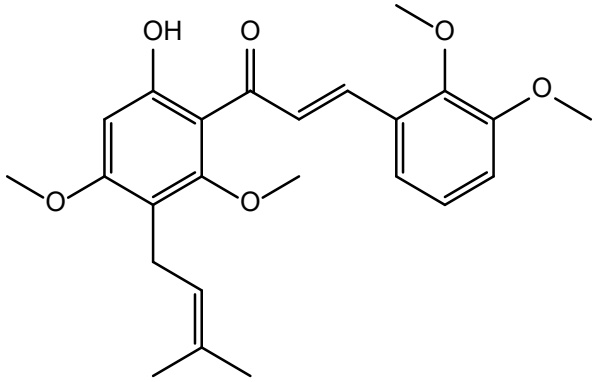 (**97**)	HCT116 p53$^{+/+257}$: IC_{50} = 29.5 µM
IC_{50}: concentration that causes an inhibitory effect of 50%. GI_{50}: concentration for 50% of maximal inhibition of cell proliferation n.d.: not determined	

3. Diarylpentanoids targeting the p53 pathway

Diarylpentanoids comprise a class of compounds possessing two aromatic rings (A and B) linked by a five carbon bridge. Most of these compounds possess a dienone (3-oxo-1,4-pentadiene) moiety in the C5 bridge. Other common moieties include a C5 bridge possessing a cyclic moiety, such as cyclopentanone, cyclohexanone, piperidin-4-one, tetrahydro-4*H*-pyran-4-one, and with tetrahydro-4*H*-thiopyran-4-one (Figure 18).

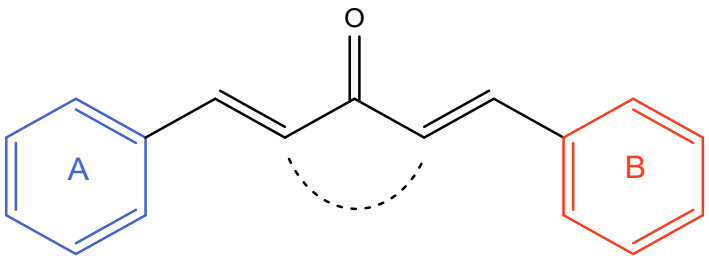

1,5-diaryl-3-oxo-penta-1,4-diene

***Figure 18**: General structure of diarylpentanoids.*

In the last decades, the synthesis of diarylpentanoids have gained increasing attention due to their wide range of pharmacological potential, being the antitumor activity one of the most exhaustively studied. To date more than 600 synthetic diarylpentanoids with antitumor activity have been reported. Among these, some have revealed to interfere with p53 pathway (Table 4).

In 2006, from a series of diarylpentanoids with boronic moieties conducted by Modzelewska *et al.*, diarylpentanoid AM114 (**98**) was identified as a promising antitumor agent. This compound was found to be more cytotoxic to p53 expressing HCT116 (IC_{50} = 2.8 μM) than p53-null HCT116 cells (IC_{50} = 5.5 μM), suggesting the interference on p53 activity [258]. In that same year, the cytotoxic activity of compound (**98**) was also again studied in HCT116 $p53^{+/+}$ cells, showing an IC_{50} value of 1.49 μM[259]. According to Achanta *et al.* the cytotoxic activity of diarylpentanoid **98** was associated with the accumulation of p53[259]. This accumulation seemed to be caused by the inhibition of the 20S proteasome by AM114 (**98**), which in turn lead to the accumulation of ubiquitinated p53 and p21. However, this compound was not able to significantly disrupt the interaction between p53 and MDM2. Curiously, AM114 (**98**) was preferentially toxic to cells expressing wild-type p53, while on the other hand, the combination of this boronic diarylpentanoid with ionizing radiation enhanced the cytotoxic activity of the radiation in both wild-type p53 and p53-null cells[259].

In 2007, EF24 (**99**) was studied for its ability to inhibit the proliferation of cisplatin (CR) resistant human ovary tumor cells. EF24 (**99**) increased PTEN expression in human ovarian tumor cells. The upregulation of PTEN resulted in a decrease in Akt and MDM2 and an increase in the expression of p53, thereby inducing G_2/M arrest and apoptosis[260].

Later, Selvendiran *et al.* (2010) verified that N-hydroxypyrroline derivative HO-3867 (**100**) showed a preferential toxicity toward ovarian tumor cells while sparing healthy cells[261]. Compound **100** induced G_2/M cell cycle arrest in A2780 cells by modulating several cell cycle regulatory molecules (p53, p21, p27, cyclin-dependent kinase 2, and cyclin), and promoted apoptosis by caspase-8 and caspase-3 activation. In 2011, it was verified once again that diarylpentanoid **100** induced G_2/M cell-cycle arrest in A2780 cells by modulating the same cell cycle regulatory proteins by Kálai *et al.* and promoted apoptosis by caspase-8 and caspase-3 activation[262].

In 2011, Anchoori *et al.*[263] tested a series of diarylpentanoids known as RAMBs, including RAMB1 (**102**). Treatment of CaSki cervical tumor cells with 10 μM RAMB1 (**102**) led to the accumulation and stabilization of p53. This stabilization caused suppression of cyclin D1 transcription, which indicated that these cells, upon treatment with RAMB1 (**102**) failed to enter the S phase of the cell cycle, resulting in loss of viability[263].

***Table 4**: Diarylpentanoids as inducers of p53-dependent apoptosis and/or cell cycle arrest.*

Diarylpentanoids	Molecular targets in apoptotic/cell cycle cellular processes	Cytotoxic effect (IC_{50})/ p53 activation (Ref) (Method)
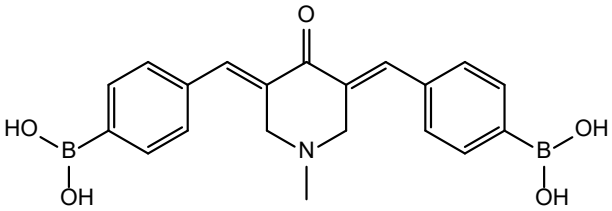 **AM114** (**98**)	Accumulation of p21 Inhibition of 20S proteasome activity	HCT116 $p53^{+/+}$[258]: IC_{50} = 2.8 µM p53 activity* = 2.8 µM (MTT) HCT116 $p53^{+/+}$[259]: IC_{50} = 1.49 µM p53 activity* = 1 µM (Western Blot)
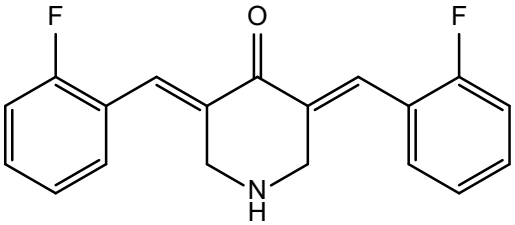 **EF24** (**99**)	Upregulation of PTEN Decrease of Akt Increase of p53 expression	CR[260]: IC_{50} = 0.65 µM p53 activity* = 2 µM (Western Blot)

Table 4 *(cont.)*

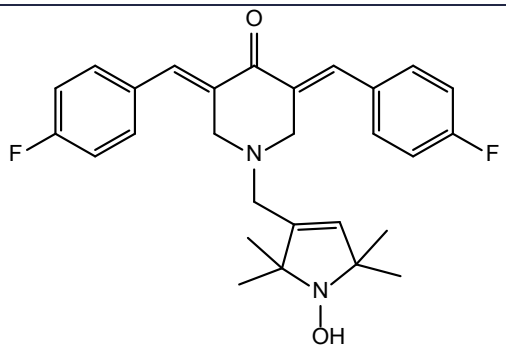 **HO-3867** (**100**)	Upregulation of p53 and p21 Decrease of cdk2 , Cyclin-A, STAT3 (Tyr705) and JAK1 phosphorylation Increase of Fas/CD95 Activation of caspase-3 and -8	A2780[261]: IC_{50} = n.d. p53 activity* = 10 µM (Western Blot)
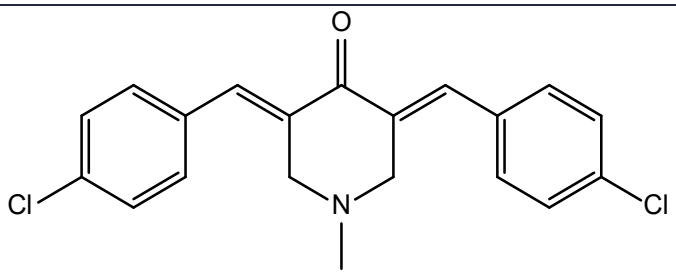 **RAMB1** (**101**)	Increase in p53 levels and caspase-3 activity Decrease of cyclin D1 expression PARP cleavage	CaSki[263]: IC_{50} = n.d. p53 activity* = 2 µM (Western Blot)

4. Aims and overview

As a result of the search for new bioactive compounds with antitumor activity by CIIMAR and LAQV/REQUIMTE, chalcones **84**, **85**, and **92-95** (Figure 19), possessing 4-methoxy, 3,4-dimethoxy, 3,4,5-trimethoxy and 4-bromophenyl B rings have been identified as promising p53-MDM2 inhibitors using a yeast cell assay. Moreover, some of these compounds revealed to be potent growth inhibitors of human tumor cell lines (GI_{50} ≤10 μM), as well as of co-transformed yeasts co-expressing p53 and MDM2.

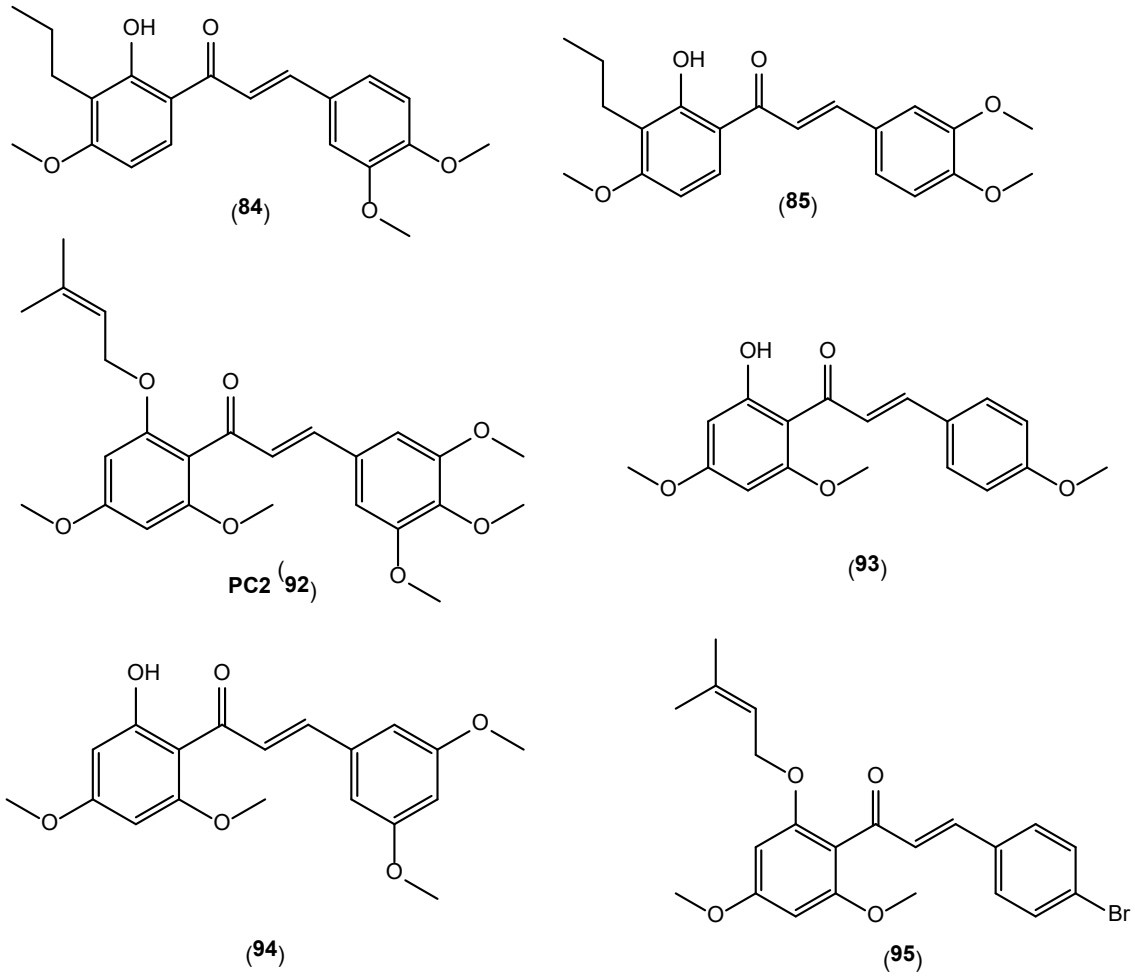

***Figure 19**: Chemical structures of chalcones identified as p53-MDM2 inhibitors.*

The main purpose of this dissertation was to obtain new potent p53-MDM2/X dual inhibitors with diarylpropanoid scaffold using compounds **84**, **85** and **92-95** as models.

To fulfill this, a series of diarylpentanoids structure related with **84**, **85** and **92-95** were synthesized and their p53-MDM2/X dual inhibitory activity were evaluated using yeast cell assays. For the most promising compounds identified in yeast, it was investigated the antitumor activity and molecular mechanism of action in human tumor cell lines.

CHAPTER II

Results and discussion

1. Results

1.1. Chemistry

1.1.1. Synthesis

A series of 3,5-di((*E*)-benzylidene)tetrahydro-4*H*-pyran-4-one derivatives were synthesized through a reaction between tetrahydro-4*H*-pyran-4-one (**AP**) and seven suitably substituted benzaldehydes (**M4**, **MA4**, **B4**, **F4**, **EA4**, **M34** and **M345**). The synthetic strategy involved four steps, starting with the formation of the enolate ion, its nucleophilic addition to the benzaldehyde, formation of an aldol and, finally, the formation of a α,β-unsaturated ketone through dehydration (Figure 20).

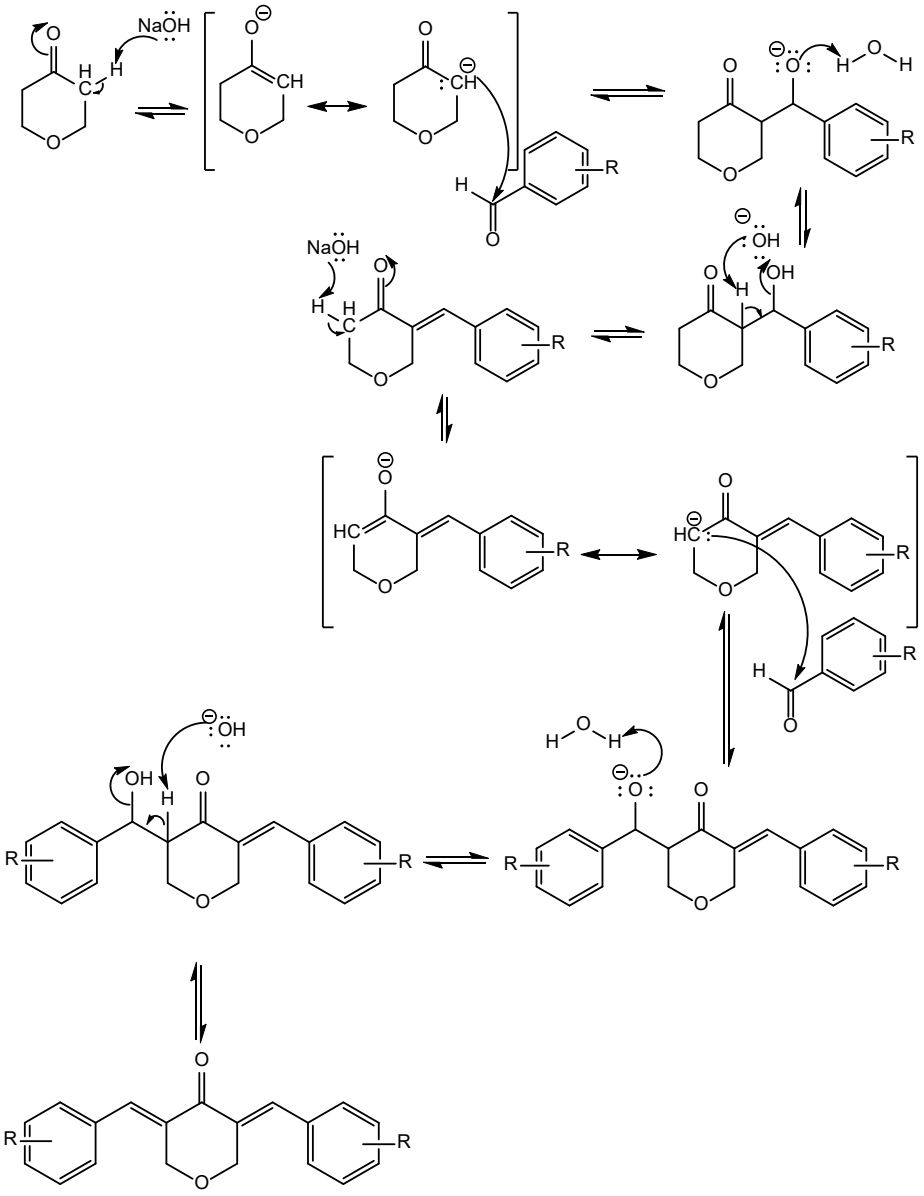

***Figure 20**: Claisen-Schmidt condensation mechanism for the synthesis of 3,5-di((E)-benzylidene)tetrahydro-4H-pyran-4-ones under basic conditions.*

The reaction conditions, obtained products and the respective yields are depicted in Table 1.

***Table 5**: Reaction conditions, obtained compounds and their respective yields.*

Ketone	Benzaldehyde	Reaction conditions	Product	Yield (%)
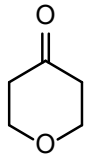 **(AP)**	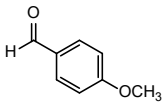 (**M4**)	MeOH, 40% NaOH, r.t., 22.5 h	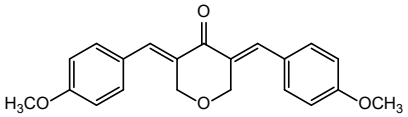 **BP-M4**	58.9
	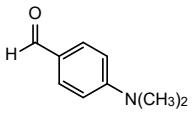 (**MA4**)	MeOH, 40% NaOH, r.t., 7 days	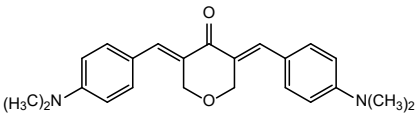 **BP-MA4**	1.1
	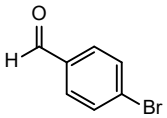 (**B4**)	MeOH, 40% NaOH, r.t., 3 days	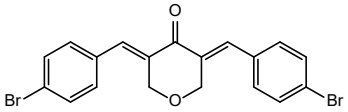 **BP-B4**	47.1
	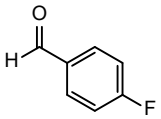 (**F4**)	MeOH, 40% NaOH, r.t., 3 days	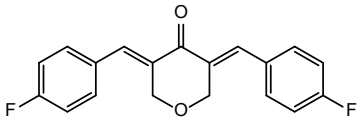 **BP-F4**	50.7
	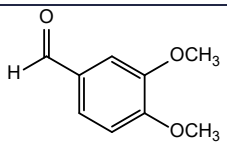 (**M34**)	MeOH, 40% NaOH, r.t., 3 days	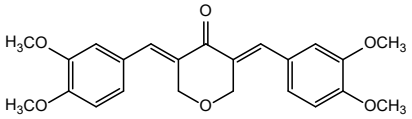 **BP-M34**	32.4
	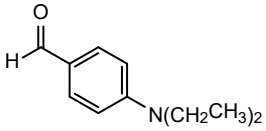 (**EA4**)	MeOH, 40% NaOH, r.t., 7 days	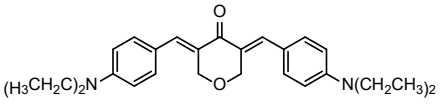 **BP-EA4**	3
	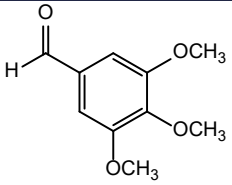 (**M345**)	MeOH, 40% NaOH, r.t., 3 days	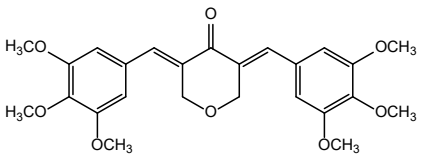 **BP-M345**	40

r.t.: room temperature.

The expected diarylpentanoids were obtained with moderate yields for almost all reactions (22.6% to 58.9%). However, the reactions performed with amino-benzaldehydes had very low yields (1.1% for **BP-MA4** and 3% for **BP-EA4**), because in addition to the desirable products, other impurities hard to separate from **BP-MA4** and **BP-EA4** were observed, being necessary to purify the compounds by preparative thin layer chromatography.

1.1.2. Structure elucidation

The structure elucidation of the obtained compounds was performed through IR and NMR techniques. ^{13}C NMR assignments were determined by 2D heteronuclear single quantum correlation (HSQC) and heteronuclear multiple bond correlation (HMBC) experiments.

The numbering concerning the NMR assignments of the synthesized compounds is presented in Figure 21.

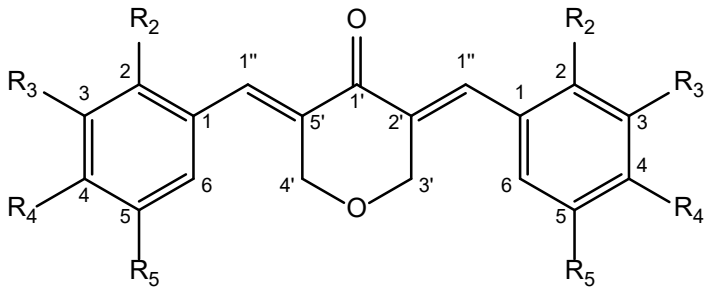

R_2=R_3=R_5=H; R_4=OCH_3: **BP-M4**
R_2=R_3=R_5=H; R_4=$N(CH_3)_2$: **BP-MA4**
R_2=R_3=R_5=H; R_4=Br: **BP-B4**
R_2=R_3=R_5=H; R_4=F: **BP-F4**
R_2=R_5=H; R_3=R_4=OCH_3: **BP-M34**
R_2=R_3=R_5=H; R_4=$N(CH_2CH_3)_2$: **BP-EA4**
R_2=H; R_3=R_4=R_5=OCH_3: **BP-M345**

Figure 21: *Structure of synthesized compounds **BP-M4**, **BP-MA4**, **BP-B4**, **BP-F4**, **BP-M34**, **BP-EA4** and **BP-M345**.*

The IR data of the eight synthesized compounds is presented in Table 6 and is in accordance with their predicted structures. As such, the IR spectra of all compounds showed bands of stretching vibration between 1723 cm^{-1} and 1667 cm^{-1}, indicating the presence of a α-β-unsaturated ketone moiety. The IR spectra also showed bands at 2957-2807 cm^{-1} (aliphatic C-H) and 1617-1416 cm^{-1} (C=C). Additionally, all spectra showed bands characteristic of C-O bonds between 1293 cm^{-1} and 1255 cm^{-1}, revealing the presence of the ether group between carbons 3' and 4', as well as the methoxy groups for **BP-M4**, **BP-M34**, and **BP-M345**. Furthermore, the spectra of **BP-MA4** and **BP-EA4** suggested the presence of C-N bonds, as shown by the presence bands of stretching vibration between 1376 cm^{-1} and 1176 cm^{-1}. On the other hand, for **BP-B4** and **BP-F4** a band at 832 cm^{-1} and 1155 cm^{-1}, respectively, was observed, suggesting the presence of C-Br and C-F bonds for each of these two compounds.

***Table 6**: IR data of **BP-M4**, **BP-MA4**, **BP-B4**, **BP-M34**, **BP-EA4** and **BP-M345**.*

Groups	υ (cm^{-1})						
	BP-M4	BP-MA4	BP-B4	BP-F4	BP-M34	BP-EA4	BP-M345
Aliphatic C-H	2920	2957 2917 2848	2921 2831 2807	2919 2830	2939 2838	2957 2917 2848	2669 2641 2828
C=O	1668	1723	1669	1670	1671	1723	1667
C=C	1596 1567 1509 1420	1584 1518 1472 1463	1577 1559 1486 1439	1576 1507 1450	1594 1578 1515 1462	1548 1518 1472 1463	1578 1504 1458 1416
C-O	1256	1270	1263	1293	1278	1270	1255
C-N	-	1369 1237	-	-	-	1376 1176	-
C-F	-	-	-	1155	-	-	-
C-Br	-	-	667	-	-	-	-

The ^{1}H and ^{13}C NMR data of **BP-M4**, **BP-MA4**, **BP-B4**, **BP-F4**, **BP-M34**, **BP-EA4** and **BP-M345** are represented in Table 7 and Table 8, respectively.

The ^{1}H spectra of all compounds showed one singlet at δ_H 8.04-7.75 (H-1'') and a doublet at δ_H 4.98-4.79 (*J* = 1.9-1.6 Hz, H-3', 4') characteristic of two equivalent vinylic and oxymethylenic protons, respectively, confirming the formation of a dienone. As the precursor, the spectra of **BP-M4**, **BP-MA4**, **BP-B4** and **BP-EA4** displayed signals that put in evidence the presence of two pairs of aromatic protons with *ortho* coupling (H-2, -6: δ_H 7.29-7.18 d, *J* = 8.9-8.5 Hz, H-3, -5: δ_H 7.56-6.67 d, *J* = 8.9-8.5 Hz). As expected for **BP-F4**, instead of these two doublets, two multiplets were observed for the pairs of *ortho* coupled aromatic protons H-2,6 (δ_H 7.34-7.29) and H-3,5 (δ_H 7.15-7.10). On the contrary, the ^{1}H spectra of **BP-M34** and **BP-M345** showed characteristic signals of two 3,4-dimethoxy- and 3,4,5- trimethoxy- rings. Instead of the singlets at δ_H 3.93-3.82 characteristic of methoxy groups, the ^{1}H NMR spectrum of **BP-MA4** indicated the presence of two dimethylamine groups (δ_H 3.03 s). On the other hand, in the spectrum of **BP-EA4**, a quartet at δ_H 3.40 (*J* = 7.1 Hz) coupled with a triplet at δ_H 1.20 (*J* = 7.1 Hz) was observed for the ethylamine side chains.

***Table 7**: [1]H NMR data of **BP-M4**, **BP-MA4**, **BP-B4**, **BP-F4**, **BP-M34**, **BP-EA4** and **BP-M345**.*

	BP-M4	BP-MA4	BP-B4	BP-F4	BP-M34	BP-EA4	BP-M345
H-1''	7.79 (brs)	7.77 (s)	7.75 (brs)	7.80 (brs)	7.78 (brs)	7.75 (s)	7.77 (brs)
H-3',-4'	4.93 (d, *J* = 1.8)	4.96 (d, *J* = 1.6)	4.88 (d, *J* = 1.9)	4.90 (d, J = 1.9)	4.96 (d, *J* = 1.8)	4.95 (d, *J* = 1.6)	4.98 (d, *J* = 1.8)
H-2	7.29 (d, *J* = 8.8)	7.26 (d, *J* = 8.9)	7.18 (d, *J* = 8.5)	7.34-7.29 (m)	6.87 (brd)	7.24 (d, *J* = 8.9)	6.55 (s)
H-3	6.95 (d, *J* = 8.8)	6.71 (d, *J* = 8.9)	7.56 (d, *J* = 8.5)	7.15-7.10 (m)	-	6.67 (d, *J* = 8.9)	-
H-4	-	-	-	-	-	-	-
H-5	6.95 (d, *J* = 8.8)	6.71 (d, *J* = 8.9)	7.56 (d, *J* = 8.5)	7.15-7.10 (m)	6.91 (brd)	6.67 (d, *J* = 8.9)	-
H-6	7.29 (d, *J* = 8.8)	7.26 (d, *J* = 8.9)	7.18 (d, *J* = 8.5)	7.34-7.29 (m)	6.91 (brd)	7.24 (d, *J* = 8.9)	6.55 (s)
2-OCH_3	-	-	-	-	-	-	-
3-OCH_3		-	-	-	3.93 (s)	-	3.89 (s)
4-OCH_3	3.85 (s)	-	-	-	3.91 (s)	-	3.90 (s)
5-OCH_3	-	-	-	-	-	-	3.89 (s)
4-$N\underline{C}H_2CH_3$	-	-	-	-	-	3.40 (q, *J* = 7.1)	-
4-NCH_3	-	3.03 (s)	-	-	-	-	-
4-$NCH_2\underline{C}H_3$	-	-	-	-	-	1.20 (t, *J* = 7.1)	-

The ^{13}C NMR data of all compounds were in accordance with their predicted structure. ^{13}C NMR assignments were confirmed by HSQC and HMBC spectra. The main correlations observed in the HMBC spectra of synthesized compounds are illustrated in Figure 22. The assignments of ^{13}C NMR signals of aromatic moieties were made considering the effect of substituents and were after confirmed by 2D NMR techniques.

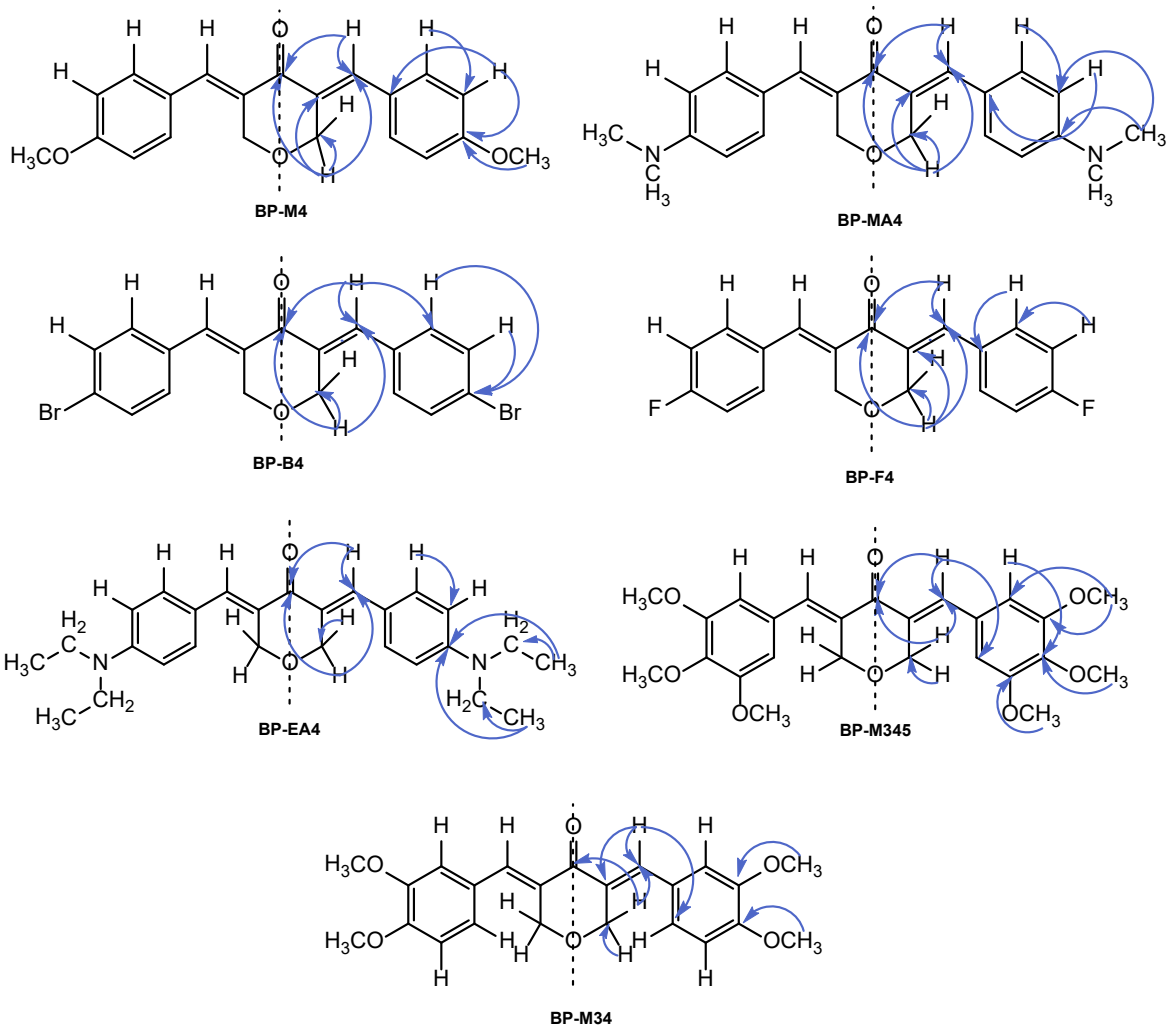

***Figure 22**: Main correlations found in HMBC spectra of **BP-M4**, **BP-MA4**, **BP-B4**, **BP-F4**, **BP-EA4**, **BP-M345** and **BP-M34**.*

The correlation observed in the HSQC spectra between the singlet at δ_H 8.04-7.75 (H-1'') and the signals at δ_C 137.2-135.5 allowed to attribute these δ_C values to the vinylic carbons at position 1''. The correlation observed in the HMBC spectra between the doublet at δ_H 4.98-4.79 (J = 1.9-1.6 Hz, 4H, H-3',4') and the signals at δ_C 137.2-135.5 (C-1''), as well as between the singlet at δ_H 8.04-7.75 (H-1'') and the signals at δ_C 69.3-68.2 (C-3',4') also confirmed the formation of a dienone (Figure 22).

The HRMS data of all synthesized compounds were in accordance with the structure proposed for the compounds.

***Table 8**: ^{13}C data of compounds **BP-M4**, **BP-MA4**, **BP-B4**, **BP-M34**, **BP-F4**, **BP-EA4** and **BP-M345**.*

	BP-M4	BP-MA4	BP-B4	BP-M34	BP-F4	BP-EA4	BP-M345
C=O	185.6	185.4	185.2	185.0	185.4	185.6	185.7
C-1''	136.1	136.4	135.5	136.0	135.5	136.6	137.2
C-2', 5'	131.4	129.3	133.6	131.1	132.8	129.1	132.8
C-3', 4'	68.2	69.0	68.6	68.4	68.6	69.3	69.1
C-1	127.7	123.1	133.5	127.5	131.0	122.5	130.7
C-2	132.6	132.8	132.1	113.3	132.6	133.4	108.5
C-3	114.4	111.9	132.0	149.9	116.2	111.5	153.7
C-4	160.7	150.9	124.1	148.6	165.0	148.7	140.0
C-5	114.4	111.9	132.0	123.8	116.2	111.5	153.7
C-6	132.6	132.8	132.1	110.7	132.6	133.4	108.5
3-OCH_3	-	-	-	55.6	-	-	56.8
4-OCH_3	55.5	-	-	55.6	-	-	61.6
5-OCH_3	-	-	-	-	-	-	56.8
4-$N\underline{C}H_2CH_3$	-	-	-	-	-	44.8	-
4-NCH_3	-	40.3	-	-	-	-	-
4-$NCH_2\underline{C}H_3$	-	-	-	-	-	13.0	-

1.2. Biological activity

1.2.1. Identification of potential inhibitors of the p53-MDM2/MDMX interactions using a yeast-based assay

As discussed in the previous section, 7 compounds were synthesized and tested for their effect on the p53-MDM2 interaction. Besides these, more 11 structure related compounds already synthesized were also tested (Figure 23).

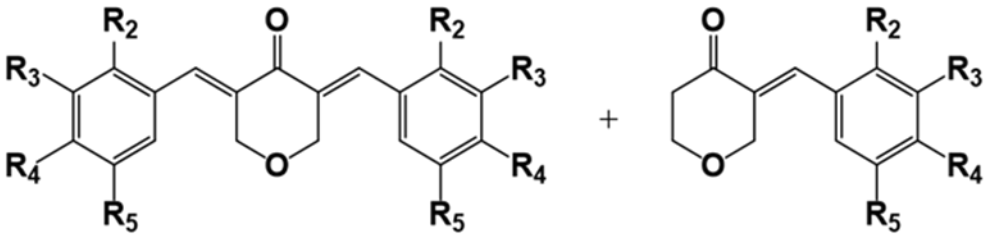

BP-M4: R_2=R_3=R_5=H; R_4=OCH_3

BP-MA4: R_2=R_3=R_5=H; R_4=$N(CH_3)_2$

BP-C4: R_2=R_3=R_5=H; R_4=Cl

BP-MP4: R_2=R_3=R_5=H; R_4=-$NCH_2CH_2OCH_2CH_2$-

BP-B4: R_2=R_3=R_5=H; R_4=Br

BP-F4: R_2=R_3=R_5=H; R_4=F

BP-EA4: R_2=R_3=R_5=H; R_4=$N(CH_2CH_3)_2$

BP-FM4: R_2=R_3=R_5=H; R_4=FCH_3

BP-C2: R_3=R_4=R_5=H; R_2=Cl

BP-M2: R_3=R_4=R_5=H; R_2=OCH_3

BP-F2: R_3=R_4=R_5=H; R_2=F

BP-M24: R_3=R_5=H; R_2=R_4= OCH_3

BP-M34: R_2=R_5=H; R_3=R_4= OCH_3

BP-M345: R_2=H; R_3=R_4=R_5=OCH_3

BP-M245: R_3=H; R_2=R_4=R_5=OCH_3

CP-MA4: R_2=R_3=R_5=H; R_4=$N(CH_3)_2$

CP-MP4: R_2=R_3=R_5=H; R_4=-$NCH_2CH_2OCH_2CH_2$-

CP-EA4: R_2=R_3=R_5=H; R_4=$N(CH_2CH_3)_2$

***Figure 23**: Chemical structures of all tested compounds.*

The effect on the p53-MDM2 interaction was assessed through a previously developed yeast-based screening assay[264–267]. In this assay, the growth of treated co-transformed yeasts is compared to the growth of both co-transformed yeasts treated with solvent (DMSO) and p53-expressing yeasts[256,265–267]. The growth observed in p53-expressing yeasts represents the desired effect, since p53 induces growth inhibition proportional to its activity in co-transformed yeasts. This can be quantified by quantification methods of optical density or by counting colony formation units (CFUs)[268–270].

The activity of the aforementioned series of compounds was evaluated at 10 and 25 µM on yeast cells co-expressing p53 and MDM2, and their growth was compared to that of control yeasts (transformed with the empty vector and expressing p53 only; (Figure 24)). Compounds **BP-C4**, **BP-C2**, **BP-M2**, **BP-F2** and **BP-M245** inhibited the growth of co-transformed yeast cells. These compounds showed growth inhibitory activity at the concentration of 25 µM. The only exception occurred with **BP-M245**, which inhibited cell growth at 10 µM and had no effect at 25 µM. **BP-C4** showed the most interesting effect, as yeasts treated with 25 µM **BP-C4** showed a growth percentage of 70.54% ± 6.52, a value that is closer to that obtained with wt p53-expressing yeast (70.81% ± 4.57).

To assess whether this inhibitory effect was due to an effective p53-MDM2 interaction disruption or due to yeast cytotoxicity, these five compounds were then tested on yeasts transformed with the empty vector (25 µM for **BP-C4**, **BP-C2**, **BP-M2** and **BP-F2**; 10 µM for **BP-M245**) (Figure 25A). Yeasts treated with **BP-C4** and **BP-M245** showed a high growth percentage, indicating no cytotoxicity and a potential selectivity towards the p53-MDM2 interaction. However, **BP-C2**, **BP-M2** and **BP-F2** proved to be cytotoxic, as shown by the decrease of yeast growth. This also explains why the co-transformed yeasts treated with these three compounds showed low growth percentages. The growth inhibition in these cases was not due to the disruption of the p53-MDM2 interaction, but rather due to cytotoxicity.

BP-C4 and **BP-M245** were further investigated in yeast cells expressing p53 only, in order to determine if these compounds have effect on p53 itself (Figure 25B). **BP-C4** (25 µM) did not interfere with the growth of p53-expressing yeasts. On the other hand, **BP-M245** (10 µM) seemed to stimulate the growth of p53-expressing yeasts, as yeasts treated with this compound showed a higher growth percentage than the control yeasts.

Based on these results, **BP-C4** was selected to be tested on yeasts co-expressing p53 and MDMX in order to investigate whether this derivative had effect on the p53-MDMX interaction (Figure 25C). Yeasts treated with 25 µM **BP-C4** showed a decrease in growth when compared to control yeasts (82.79 % ± 4.06). In fact, the growth percentage of treated

yeasts was proximate to that of yeasts expressing p53 only (77.52 % ± 4.93), which indicates that **BP-C4** was able to cause a MDMX inhibition of approximately 82.2 % (data not shown).

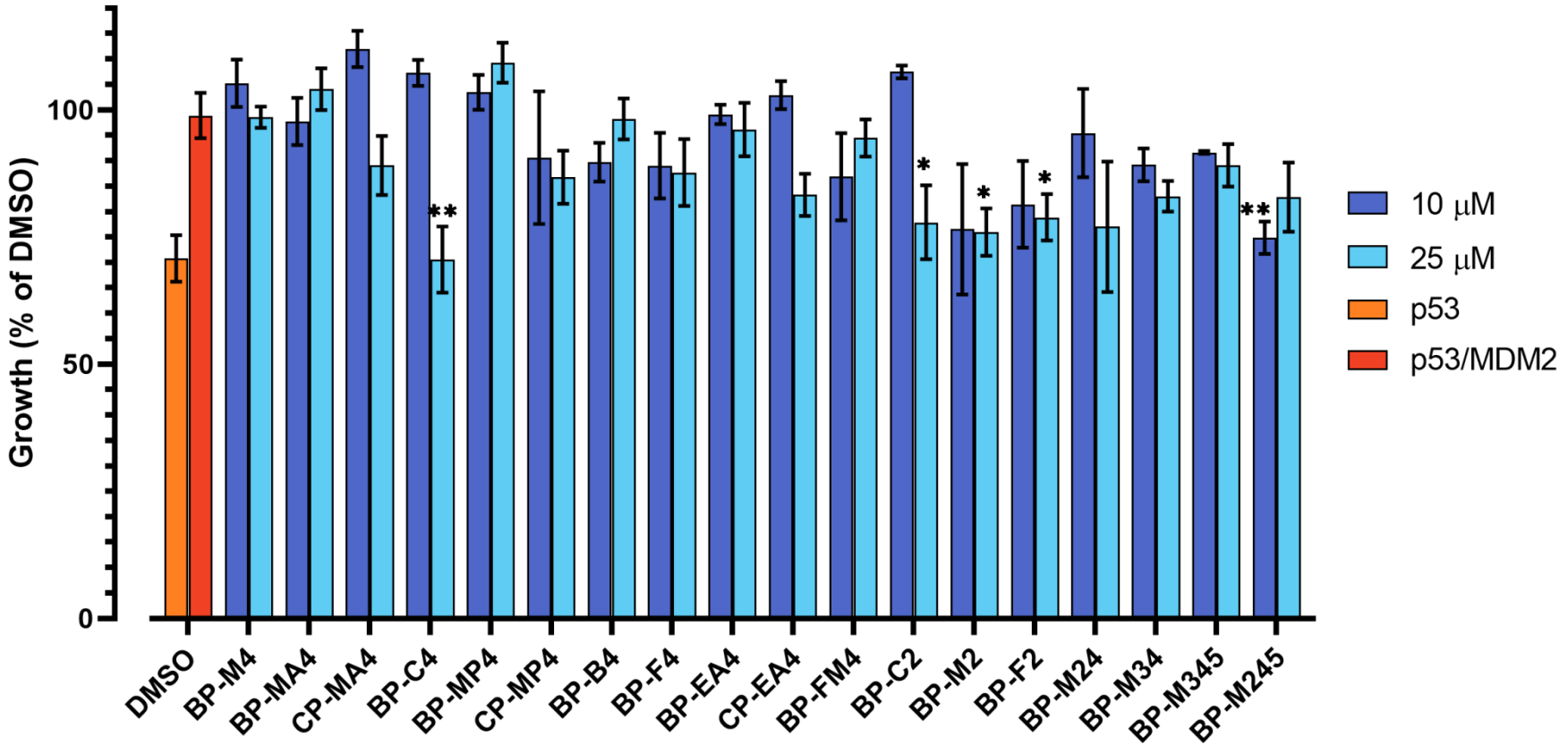

***Figure 24**: Effect of compounds **BP-M4**, **BP-MA4**, **CP-MA4**, **BP-C4**, **BP-MP4**, **CP-MP4**, **BP-B4**, **BP-F4**, **BP-EA4**, **CP-EA4, BP-FM4, BP-C2, BP-M2, BP-F2, BP-M24, BP-M34, BP-M345** and **BP-M245** (10 μM and 25 μM) on percentage of growth of yeasts expressing p53 and MDM2, after 48 h treatment. The DMSO-treated cells co-expressing p53 and MDM2 were considered as 100%. Data are mean ± SEM of at least three independent experiments; values significantly different from DMSO are indicated (*p<0.05; **p<0.01). The unpaired student t-test was used.*

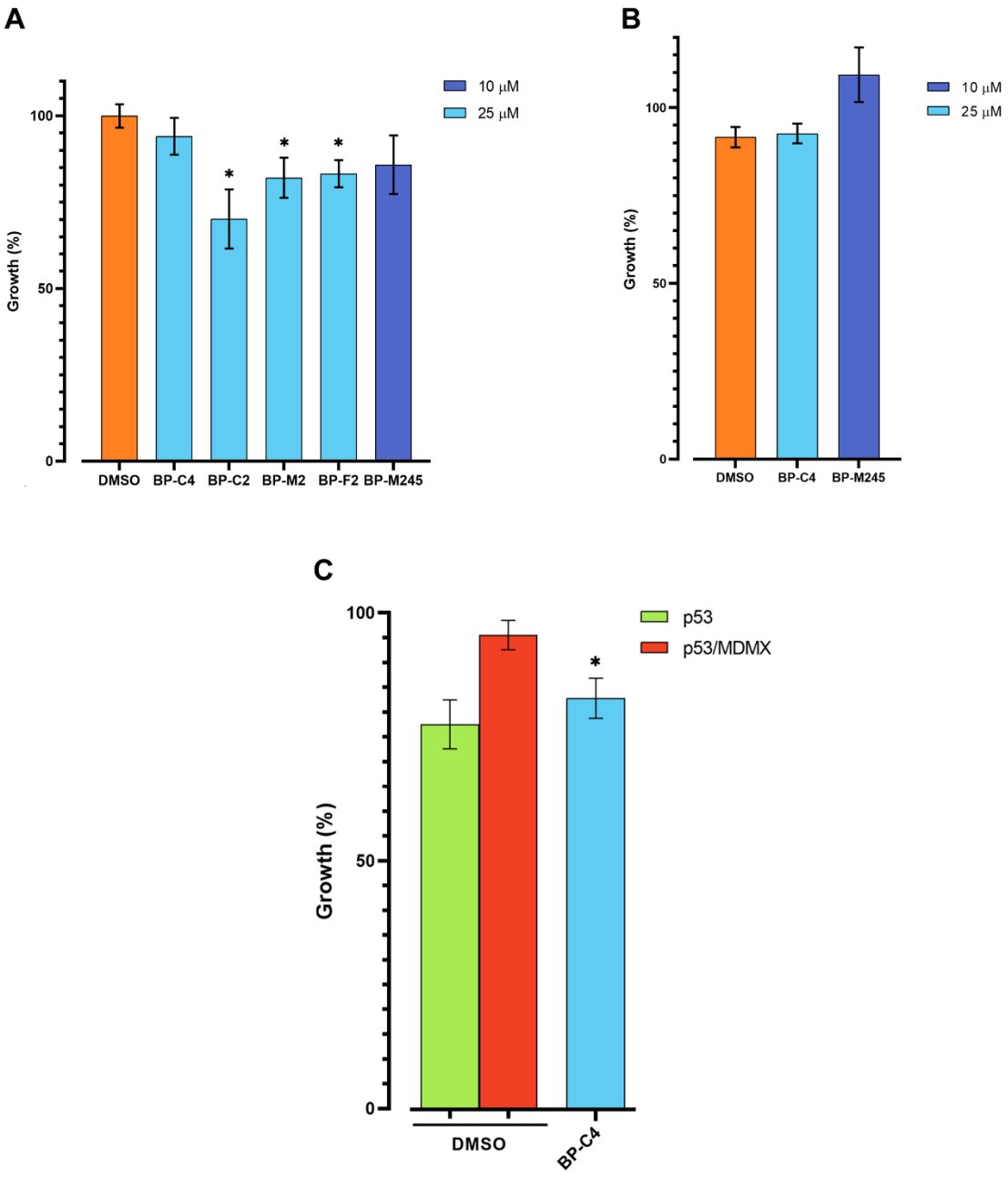

***Figure 25**: **BP-C4** shows no cytotoxic effects on yeast cells, exhibiting potential dual inhibitory effects on the p53-MDMX interaction. (A) Effect of compounds **BP-C4**, **BP-C2**, **BP-M2**, **BP-F2** and **BP-M245** on the growth of yeast cells transformed with the empty vector, after 48 hours treatment. The results obtained with non-treated cells were considered as 100%. Data are mean ± SEM of at least three independent experiments; values significantly different from DMSO are indicated (*p<0.05). (B) Effect of compounds **BP-C4** and **BP-M245** (25 and 10 µM, respectively) on the growth of yeast cells expressing p53, after 48 hours treatment. The DMSO-treated cells were considered as 100%. Data are mean ± SEM of at least three independent experiments. (C) Effect of 25 µM **BP-C4** on the growth of yeasts expressing p53 and MDMX, after 48 hours treatment. The DMSO-treated cells co-expressing p53 and MDMX were considered as 100%. Data are mean ± SEM of five independent experiments; values significantly different from DMSO are indicated (* p<0.05). The unpaired t-test was used.*

Altogether, the results obtained in yeast suggested that **BP-C4** was a potential dual inhibitor of the p53-MDM2/MDMX interactions.

1.2.2. Evaluation on human cell lines

1.2.2.1. Evaluation of the *in vitro* growth inhibitory effect

Considering the results obtained in the yeast screening assay, **BP-C4** was selected for tests on HCT116 $p53^{+/+}$ and $p53^{-/-}$ and MDA-MB-231 tumor cell lines, along with **BP-F2** (used as a cytotoxic control) and **BP-M245** (a second non-cytotoxic compound selected for the SRB assay) (Figure 26). These tests were carried out using the sulforhodamine B (SRB) assay. The SRB assay is a colorimetric assay that has been used since 1990[271] as a relatively economic method of performing several screening assays for cytotoxicity evaluation[272]. This method relies on the binding of SRB to proteins under mildly acid conditions, which can then be extracted under basic conditions. The color intensity can be used as a cellular mass indicator, which can then be extrapolated for measurement of cellular proliferation. This assay is limited to manual or semiautomatic screening assays and can be used as an effective way of testing chemotherapeutic drug candidates on adherent cells. It is also useful for evaluation of genic expression modulation (knockdown, increase of genic expression, etc.), as well as in the study of miRNA substitution on cell proliferation[273]. The GI_{50} values for each compound are shown in Table 9.

As obtained in yeast, the results confirm the ability of **BP-C4** to induce growth inhibition in the presence of p53. In the absence of p53, **BP-C4** showed a reduction of the growth inhibitory effect when compared to p53-expressing cells (Figure 26A). However, even in these conditions, **BP-C4** is able to inhibit the growth of p53-null cells, suggesting that this derivative may have an additional mechanism that is independent of p53. On the other hand, **BP-C4** seems to have no effect on MDA-MB-231 cells, which expresses mutp53 R280K. These results suggest that **BP-C4** does not act on the mutp53 pathway, but rather has some selectivity towards the wt p53 pathway.

BP-F2 displayed the highest growth inhibition among the selected compounds on the tested tumor cell lines (Figure 26B). This derivative induced a strong growth inhibition of the HCT116 cells, regardless of p53 status, and also notably decreased the growth of MDA-MB-231 cells, albeit with a higher GI_{50} value than the obtained in HCT116 cells (Table 5). These results are in accordance with those obtained in yeast, supporting a p53-independent growth inhibitory effect of **BP-F2**.

BP-M245 showed high GI_{50} values in the three tumor cell lines (Table 9), indicating a low antiproliferative effect against tumor cells, particularly on MDA-MB-231 cells (Figure 26C). As such, although this derivative showed promising activity in the yeast, it was not effective on tumor cells.

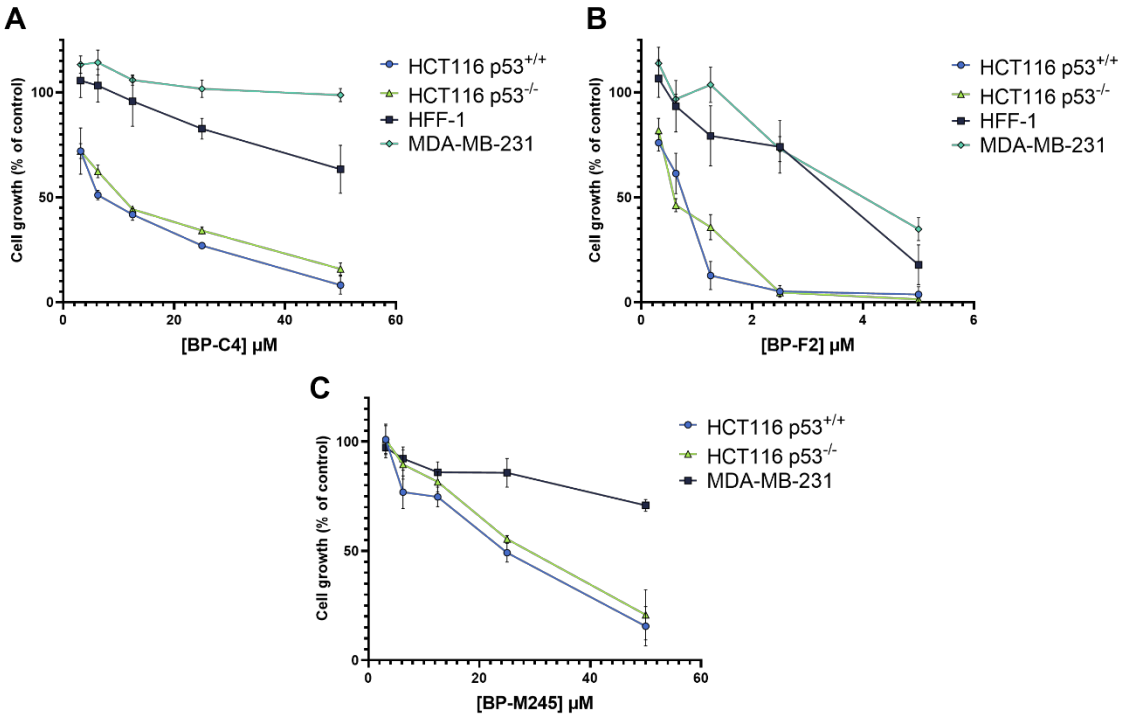

***Figure 26**: Dose-response curves for the three selected compounds. (A) Dose-response curves for the growth inhibitory activity of 3.13 – 50.0 µM **BP-C4** in $p53^{+/+}$ and $p53^{-/-}$ HCT116 cells, HFF-1 and MDA-MB-231 cells, determined by SRB assay, after 48 hours treatment. Data are mean ± SEM (n=3). (B) Dose-response curves for the growth inhibitory activity of 0.313 – 5.00 µM **BP-F2** in $p53^{+/+}$ and $p53^{-/-}$ HCT116 cells, HFF-1 and MDA-MB-231 cells, determined by SRB assay, after 48h treatment. Data are mean ± SEM (n=3). (C) Dose-response curves for the growth inhibitory activity of 3.13 – 50.0 µM **BP-M245** in $p53^{+/+}$ and $p53^{-/-}$ HCT116 cells and MDA-MB-231 cells, determined by SRB assay, after 48h treatment. Data are mean ± SEM (n=3)*

Given these results, the antiproliferative effect of **BP-C4** and **BP-F2** was tested on human fibroblasts HFF-1 cells in order to assess their cytotoxic towards normal cells. **BP-M245** was excluded from this test due to its high GI_{50} values in tumor cells. **BP-C4** proved to have low cytotoxicity towards HFF-1 cells, as its GI_{50} value for these cells is much higher than that for HCT116 cells (Table 9). However, **BP-F2** was cytotoxic towards these cells, confirming its unspecific cytotoxic effect observed in yeast.

***Table 9**: GI_{50} values obtained for the compounds **BP-C4**, **BP-F2** and **BP-M245** in tumor and normal cells.*

	GI_{50} (μM)		
	BP-C4	**BP-F2**	**BP-M245**
HCT116 $p53^{+/+}$	5.85 ± 0.67	0.69 ± 0.21	25.00 ± 2.52
HCT116 $p53^{-/-}$	10.13 ± 0.47**	0.70 ± 0.12	29.33 ± 2.40
MDA-MB-231	> 50**	3.97 ± 0.41**	> 50
HFF-1	44 ± 4.90**	1.61 ± 0.70	*ND*

*Results are expressed as GI_{50} (μM) values, tested using HCT116 $p53^{+/+}$, HCT116 $p53^{-/-}$, MDA-MB-231, and HFF-1 cell lines. Data represent mean ± SEM of three independent experiments; values significantly different from HCT116 $p53^{+/+}$ cells are indicated (**p<0.01). *ND – Not Determined.*

Altogether, **BP-C4** showed to be the most promising compound, as it showed some selectivity towards the wt p53 pathway and showed no cytotoxicity towards normal cells. This derivative was further studied using the colony formation assays on the HCT116 $p53^{+/+}$ cells in order to confirm its antiproliferative activity. The colony formation assay, or clonogenic assay, is a survival assay based on the ability of a single cell to grow into a colony of cells[274]. This assay essentially tests every cell in the population for its ability to multiply indefinitely. The clonogenic assay is a method to determine cell reproductive death in order to determine the effectiveness of cytotoxic agents[274]. **BP-C4** inhibited the formation of colonies up to 100% relative to DMSO at the concentration of 2.00 μM, a value lower than the GI_{50} value determined for these cells (Figure 27). However, it should be noted that this is an ongoing work, and as such, these results correspond to preliminary data.

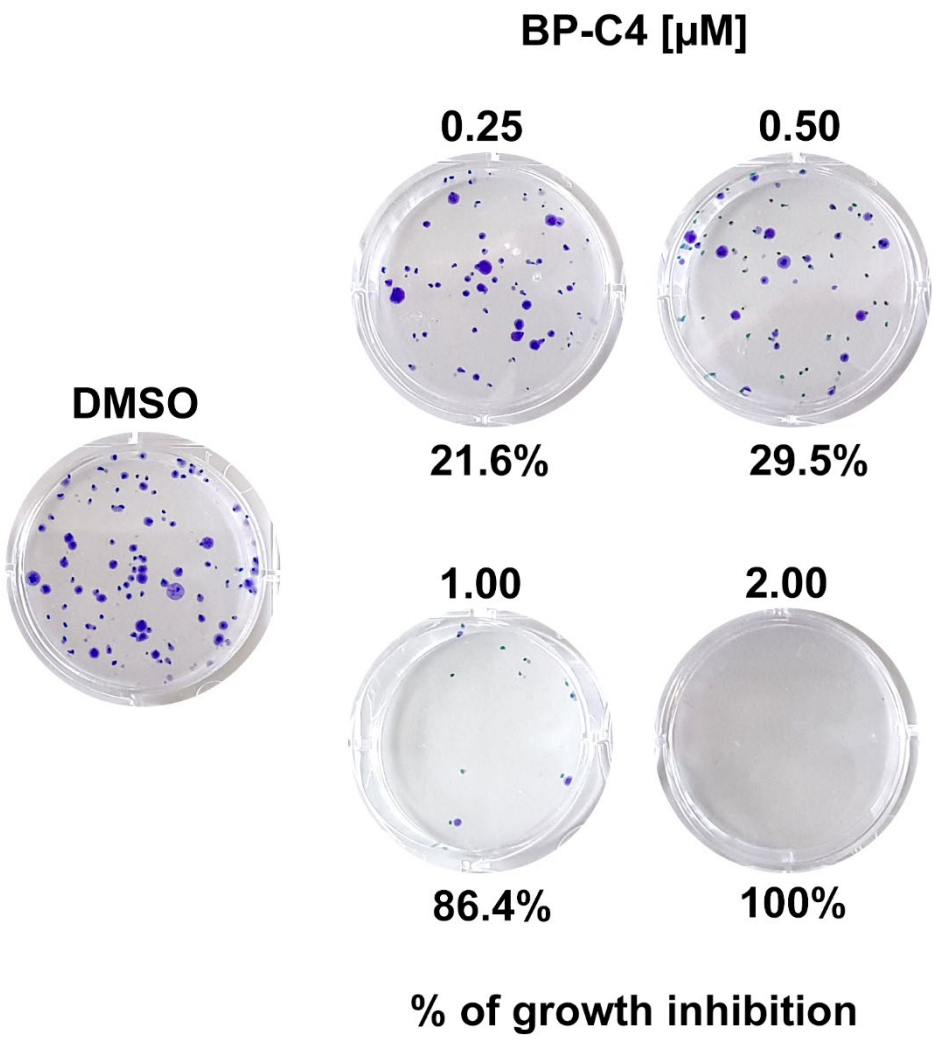

***Figure 27**: Colony formation assay for HCT116 p53$^{+/+}$ cells treated with **BP-C4**. The DMSO-treated cells were considered as 0% of growth inhibition; images correspond to a representative experiment (ongoing work).*

1.2.2.2. Cell cycle and apoptosis analysis

For the most promising compound **BP-C4,** it was thereafter analyzed its impact on cell cycle and apoptosis of HCT116 $p53^{+/+}$ cells. For that, these tumor cells were incubated with 12 µM **BP-C4** (approximately twice of its GI_{50} value) for 48 hours. **BP-C4** was able to induce apoptosis by approximately 24% (Figure 28A) and it also caused cell cycle arrest mainly at the G_0/G_1 phase (Figure 28B), as shown by the increase of cells in this phase when compared to the solvent.

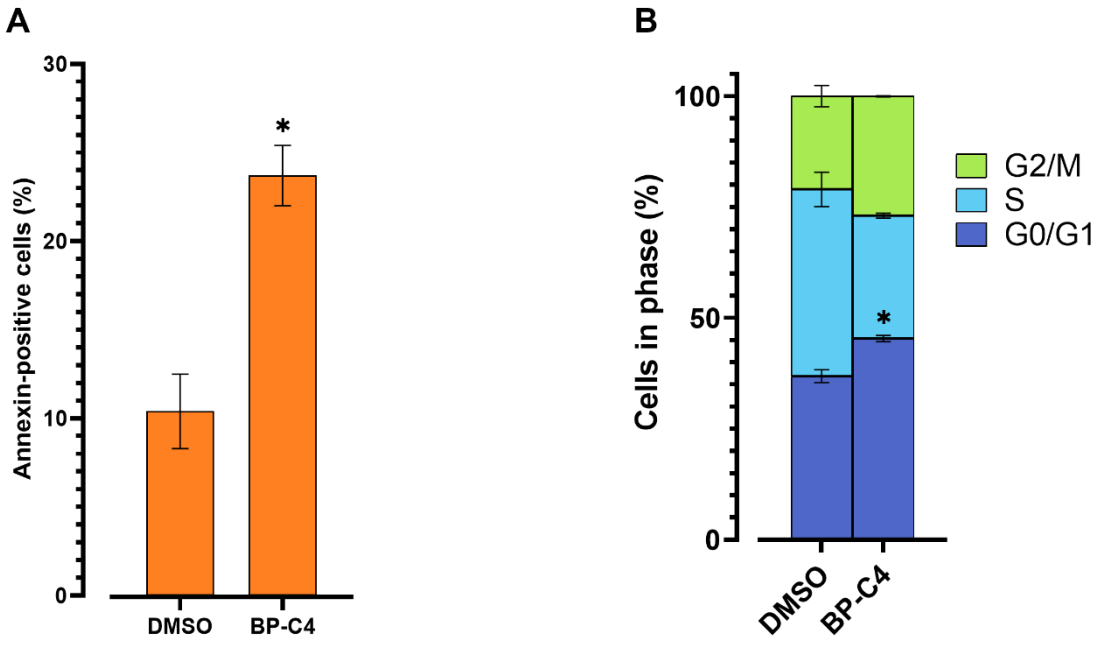

***Figure 28**: Effect of **BP-C4** on cell cycle and apoptosis of HCT115 $p53^{+/+}$ cells. (A) Effect of 12µM **BP-C4** on apoptosis of HCT116 $p53^{+/+}$ cells after 48h treatment. Data are mean ± SEM (n=3). (B) Effect of 12µM **BP-C4** on cell cycle progression of HCT116 $p53^{+/+}$ cells after 48h treatment. Data are mean ± SEM (n=3); values significantly different from DMSO: *p<0.05. The unpaired student t-test was used.*

1.2.2.3. Effect on p53 activity by analysis of its transcriptional targets

To better understand the underlying mechanisms of **BP-C4**-induced apoptosis and cell cycle arrest, the expression levels of p53 and transcriptional targets (p21 and PUMA), as well as PARP cleavage were analyzed through Western Blot on HCT116 $p53^{+/+}$ cells (Figure 29). Western blot is a frequently used technique for separation and identification of proteins. This method consists on the separation of a mixture of proteins based on molecular weight (and consequently by type) through gel electrophoresis. These results are transferred to a membrane, which produces a band for each protein. This membrane is incubated with label antibodies that are specific to the protein of interest[275]. The unbound antibody is then washed off, which leaves only the bound antibody to the desired protein. These antibodies are then detected by developing the film. Since the antibodies only bind to the desired protein, only one band for each protein should be visible. The thickness of the obtained band corresponds to the amount of protein that is present, so by comparing it to a control (like GAPDH), it is possible to indicate the amount of protein present[275].

As predicted, **BP-C4** increased the levels of p53, as well as of p21 and PUMA. On the other hand, the induction of apoptosis is mediated by an upregulation of PUMA levels. **BP-C4** also led to the cleavage of PARP.

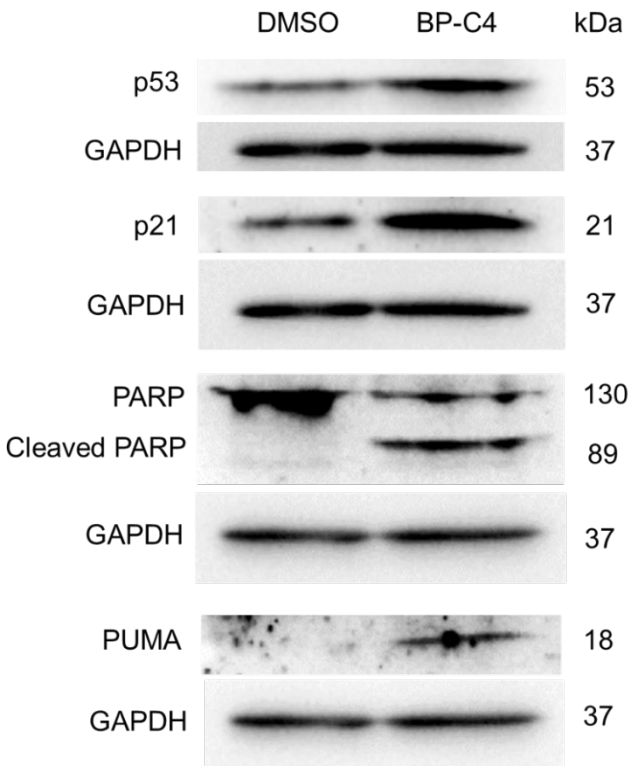

***Figure 29**: Protein levels of p53 transcriptional targets in HCT116 $p53^{+/+}$ cells after 48h treatment with 12 μM **BP-C4** or DMSO, visualized by Western Blot. Immunoblots represent one of two independent experiments; GAPDH was used as a loading control.*

2. Discussion

For many years, cancer therapy has relied on conventional chemotherapeutic agents like antimetabolites, alkylating agents and other types of chemicals that target rapid proliferating cells through different mechanisms, such as microtubule polymerization, DNA intercalation or topoisomerase inhibition[276]. Because of its inherent unspecific cytotoxic nature, and with no other options available, conventional chemotherapy has countless side effects, ranging from fatigue and hair loss, to anemia and gastrointestinal distress, as well as myelosuppression, immunosuppression, neuropathy and organ failure. With the advance in molecular and genetic techniques, there was a better understanding of the mechanisms that regulate cancer, and the tools to target signaling pathways were improved[277]. Rational drug design and targeted therapy brought the possibility of creating “magic bullets” that could target tumor cells without the adverse side effects of conventional chemotherapy[278,279]. The key role of p53 in tumor suppression makes the p53-targeting strategies highly appealing. As mentioned in chapter I, the disruption of the p53-MDM2/MDMX interaction in wtp53-expressing tumor cells can result in a more effective tumor regression when compared to that based on MDM2-only inhibitors[280,281].

Chalcones and diarylpentanoids are two classes of compounds with several representatives as p53-targeting compounds (reviewed in chapter I). Here, the synthesized diarylpentanoids were obtained through a Claisen-Schmidt condensation. This reaction is one of the most classical reactions in organic chemistry[282]. The catalysts are either strong acids or strong bases, being more common the use of bases. When using a base catalyst, the chalcone is produced from the aldol product *via* dehydration in an enolate mechanism, while in the case of acid catalysis, it is generated *via* an enol mechanism[283]. The main disadvantage of this reaction is its slow reaction rate, as it generally needs several days for completion. It could also result in a complex mixture containing byproducts and even sometimes starting materials among the desirable product. Thus, the yield could vary drastically, ranging from <10% to near 100% conversion, depending on the reactants and catalysts[283,284]. However, this reaction has been used in most publications. Széll *et al.* synthesized a series of nitrochalcones and demonstrated that the presence of electron-donating groups in the aldehyde favored condensation by acid catalysis, while in the other hand, the base catalysis was favored by electron-withdrawing substituents[285].

A library of 18 diarylpentanoids were screened for their ability to disrupt the p53-MDM2 interaction using a yeast-based assay.

As mentioned before, the compounds with the most promising activities were **BP-C4**, **BP-C2**, **BP-M2**, **BP-F2** and **BP-M245**. When comparing the results of the

monosubstituted diarylpentanoids, the presence of chlorine on carbon 4 of rings A and B seems to favor the growth inhibitory activity of co-transformed yeasts, as shown by the growth inhibitory activity of **BP-C4**. Also, this substitution pattern does not interfere with the growth of control yeasts and yeasts expressing p53 only. **BP-C4** also induced a lower growth percentage than the remaining halogenated diarylpentanoids **BP-B4**, **BP-F4**, **BP-C2**, **BP-F2** and **BP-FM4**. In fact, **BP-C4** induced the lowest growth percentage of the 18 compounds and thus the closest growth percentage to that obtained with wt p53-expressing yeasts, which may suggest that this diarylpentanoid was able to successfully free p53 from the p53-MDM2 complex, allowing it to play its role as a growth suppressor. On the other hand, the presence of substituents only on carbon 2 of rings A and B results in yeast cytotoxicity, as demonstrated by the results of **BP-C2**, **BP-M2** and **BP-F2**, which decreased the growth of co-transformed yeasts and control yeasts. Regarding the methoxylated diarylpentanoids, the results indicate that the presence of three methoxy groups on positions 2, 4 and 5 on both rings is more favorable than the presence of one or two methoxy groups, as shown by the results of **BP-M245**. This compound also showed better results than **BP-M345**, a diarylpentanoid with three methoxy groups in carbons 3, 4 and 5 on both rings. Considering the compounds with only one ring, the lowest growth percentage was achieved with **CP-EA4**, which possesses an ethylamine group on carbon 4. The corresponding diarylpentanoid, **BP-EA4**, induced a higher growth percentage than **CP-EA4**, which indicates that the presence of only one ring can slightly improve the growth inhibitory effect of co-transformed yeasts in the presence of the ethylamine group on position 4. This effect is also observed with **BP-MA4** and **CP-MA4**, the other two aminated compounds with a methylamine group on carbon 4 instead of an ethylamine group. The presence of a methylamine or an ethylamine group in the aminated diarylpentanoids **BP-MA4** and **BP-EA4** seems to induce no differences in the growth of co-transformed yeasts. However, **CP-EA4** induced a lower growth percentage than **CP-MA4**. **CP-MP4** also showed better results than its corresponding diarylpentanoid **BP-MP4**. The presence of the morpholine ring on position 4 seems to improve the growth inhibitory activity only in the presence of one aromatic ring, as showed by the results obtained with **CP-MP4** and **BP-MP4**.

Since **BP-C4** induced the most interesting results in this initial screening, this compound was tested on p53-MDMX co-expressing yeasts to investigate if it could display dual-inhibitory activity. **BP-C4** inhibited the growth of the co-transformed yeasts to a value that was very close to that observed in p53-expressing yeasts. This indicates that **BP-C4** not only can inhibit the p53-MDM2 interaction, but can also inhibit the p53-MDMX, behaving as a potential dual inhibitor of the p53-MDM2/MDMX interactions.

The yeast assay allows the selection of potential p53-MDM2/MDMX inhibitors, which antitumor activity and molecular mechanism of action is thereafter validated in human cell lines. For this, the SRB assay was used.

Comparing the GI_{50} values of **BP-C4**, **BP-F2**, and **BP-M245**, the lowest GI_{50} values were obtained with **BP-F2** for all tested cell lines, including HFF-1. The yeast screening assay allowed predicting this result, as this diarylpentanoid showed to be cytotoxic in control yeasts. On the other hand, the high GI_{50} values of **BP-M245** rendered **BP-C4** the most promising of the 18 compounds. **BP-C4** induced cell cycle and apoptosis in HCT116 $p53^{+/+}$ cells, and upregulation of p53 and respective targets as p21, PUMA and PARP.

The cell cycle arrest observed in the G_0/G_1 phase is in accordance with an upregulation of p21 observed by Western Blot. In fact, the cell cycle arrest in G_0/G_1 phase requires the induction of p21 by binding of the cyclin/cdk complex, which leads to accumulation of an unphosphorylated form of RB that arrests cells in G_1 by preventing the release of E2F (required for the G_1-S transition) from its complex with RB[286,287]. In some cases, the overexpression of E2F could lead to apoptosis instead of cell cycle arrest[287].

Another upregulated target was PUMA. After activation by p53, PUMA interacts with the Bcl-2 family proteins, which have anti-apoptotic properties. These proteins will then free BAX and/or BAK, which in turn will signal apoptosis to the mitochondria. This mitochondrial stress will activate the caspase cascade, which ultimately leads to cell death[288]. Mitochondria from tumor cells are structurally and functionally different from their normal counterparts. In fact, tumor cells are more susceptible to mitochondrial perturbations than normal cells, and therefore many mitochondria-targeting strategies have emerged as a way to selectively induce death in tumor cells[289]. Although it was not proven that **BP-C4** targets the mitochondria, its ability to upregulate PUMA may be related to an eventual mitochondrial stress and may explain its apoptotic effects. When BAX is released, it is translocated from the cytosol to mitochondria, where it triggers mitochondrial membrane permeabilization (MMP)[289,290]. This, in turn, will release pro-apoptotic factors into the cytosol, such as cyt *c*[289].

BP-C4 also leads to the PARP cleavage. The PARP-family proteins respond to DNA damage by attempting to repair it *via* recruitment and modification of several proteins, including DNA helicases, topoisomerases and histones. However, by doing so, they can lead to depletion of cellular ATP, which leads to cell death by necrosis[288] unless they are inactivated. PARP proteins are normally inactivated by caspases, which naturally cleave them in cases where the DNA damage is too extensive[291]. Since the caspase pathway was already activated by PUMA *via* release of cyt c to the cytosol, these caspase proteins will

cleave PARP, leading to an increase in its levels. Altogether, based on the obtained results, a mechanism of action is proposed for **BP-C4** (Figure 30).

These results are in accordance with that observed in other studies with chalcone derivatives in HCT116 cells[255], as well as in S-KN-SH[243], MCF-7[253] and CCRF-CEM[292] cells.

BP-C4 has a similar chemical structure to another diarylpentanoid, the compound **RAMB1** mentioned in chapter I[263]. Like **BP-C4**, **RAMB1** has a chlorine atom bound to carbons 4 of both A and B rings, and the only difference lies in the presence of a tertiary amine connecting carbons 3' and 4' instead of an oxygen atom. Some studies suggest that the α,β-unsaturated carbonyl system, present in chalcones and in diarylpentanoids like **BP-C4** and **RAMB1**, are determinant in the inhibition of ubiquitin-mediated protein degradation upstream of the 20S proteasome[293–297], which is known to degrade p53 after polyubiquitination by MDM2[263]. Like **BP-C4**, **RAMB1** was also reported to increase the levels of p53 and PARP cleavage[263]. **RAMB1** also inhibited ubiquitin-dependent protein degradation without compromising the catalytic activity of the 20S proteasome, and led to p53 stabilization. It also triggered synergistic cell death when combined with the lysosome inhibitor chloroquine in cervical cancer cells[263]. **AM114**, also mentioned in chapter I, is a boronic diarylpentanoid with the same scaffold as **RAMB1**, having $B(OH)_2$ groups instead of chlorine in carbons 4. **AM114** induced a more potent response in HCT116 $p53^{+/+}$ cells than **BP-C4**, with an IC_{50} value of 1.49 μM[259], indicating that the antiproliferative activity increased with the presence of the tertiary amine between carbons 3' and 4' and the $B(OH_2)$ groups on carbons 4. Like **RAMB1**, **AM114** also inhibited the 20S proteasome activity, which might be related to the α, β unsaturated carbonyl moiety like mentioned earlier, and had synergistic effect with ionizing radiation[259].

Other chalcone derivatives showed similar results, like prenylchalcones[255,257], aminochalcones[251], a boronic chalcone[259] and several others (reviewed in chapter I). Natural chalcones like the unsubstituted chalcone[218] and isoliquiritigenin[224] also induced cleavage of PARP and up-regulation of p21, along with increased p53 levels.

Although it was not proven whether **BP-C4** binds to p53 or to the MDMs in order to induce the results here presented, it is interesting to note that its A and B rings bear some resemblance to the 6-chloroindole group of **WK 298**, mentioned in chapter I as a dual inhibitor of the p53-MDMs interactions[155]. The 6-chloroindole group of **WK 298** binds to the Trp23 subpocket of both MDM2 and MDMX. However, in order to increase the binding ability, the occupancy of the three subpockets of Phe19, Trp23 and Leu26 appear to be a requirement[155]. Additionally, the Phe19 subpocket must be filled with large-surface hydrophobic groups. The Leu26 subpocket poses the greatest challenge for the design of

dual MDM2/MDMX inhibitors, as MDM2 and MDMX differ significantly in the shape and properties of residues surrounding this pocket[298].

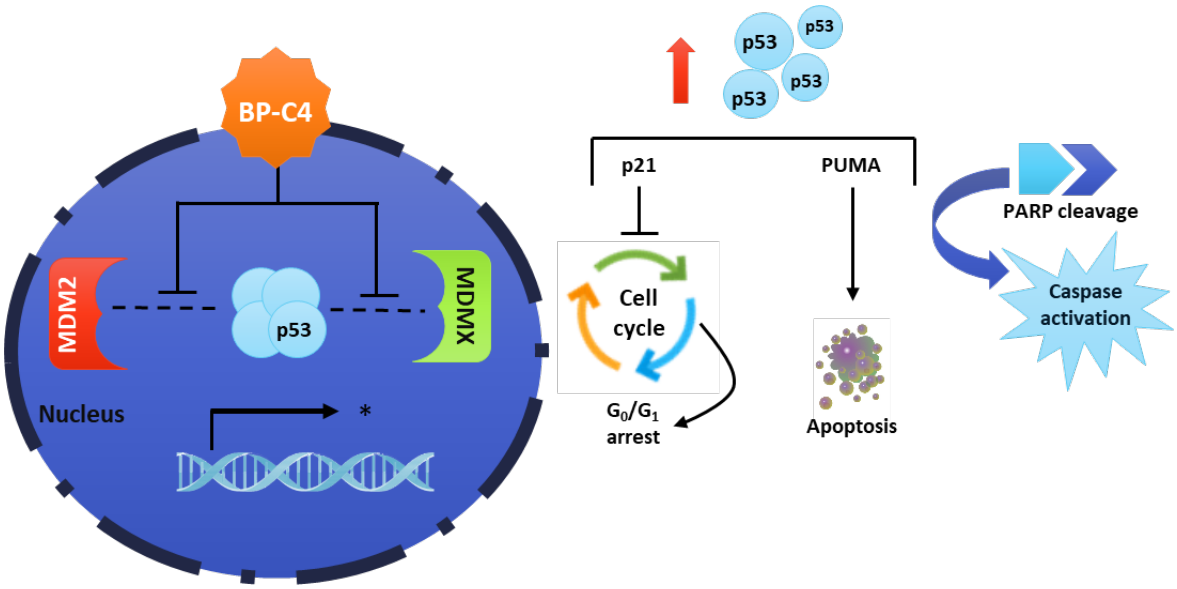

***Figure 30**: Hypothetical mechanism of action of **BP-C4** in HCT116 p53$^{+/+}$ cells. As a dual inhibitor of the p53 interaction with MDM2 and MDMX, **BP-C4** increases p53 levels and activates p53 transcriptional activity, increasing the levels of the p53 target proteins p21 and PUMA. The observed PARP cleavage indicates a potential activation of the caspase pathway. *p53 target genes.*

CHAPTER III

Experimental

1. Synthesis

1.1. General methods

All reagents and solvents used were purchased from Sigma Aldrich.

Solvents were evaporated using rotary evaporators under reduced pressure (Buchi Waterchath B-480).

The reactions were supervised by TLC carried out on precoated plates with 0.2 mm of thickness (Merck silica gel 60 (GF254)).

The obtained chromatograms were visualized under UV radiation at 254 and 365 nm.

The purification of the synthesized compounds was performed either by crystallization, or by preparative chromatography (Macherey-Nagel silica gel 60 (GF254)).

Melting Points were obtained in a Köfler microscope and are uncorrected.

IR spetra were obtained in KBr microplates in a FTIR spectrometer Nicolet iS10 from Thermo Scientific with Smart OMNI-Transmisson accessory (software OMNIC 8.3 for Microsoft Windows XP).

All NMR spectra were obtained at University of Aveiro, Department of Chemistry, using $CDCl_3$ (Deutero GmbH) at room temperature at frequencies of 300.13 MHz for ^{1}H and 75.47 MHz for ^{13}C (Bruker Avance 300 spectrometer).

1.2. Synthesis of **BP-M4**

An aqueous solution of 40% sodium hydroxide was added to a solution of tetrahydro-4*H*-pyran-4-one (100 mg, 0.99 mmol) in methanol until pH 13–14. Then, a solution of 2.99 mmol (392.1 mg) 4-methoxybenzaldehyde in methanol was slowly added to the reaction mixture. The reaction was left at room temperature for 22.5 hours and was monitored by TLC. After completion, the reaction mixture was poured into ice and neutralized with diluted HCl. A precipitate was formed upon cooling to room temperature. This was filtered, washed with water, and crystallized with chloroform. A light yellow solid corresponding to 3,5-bis((E)-4-methoxybenzylidene)tetrahydro-4*H*-pyran-4-one (**BP-M4**) was obtained.

3,5-bis((*E*)-4-methoxybenzylidene)tetrahydro-4*H*-pyran-4-one (BP-M4): Yield: 58.9%; mp (chloroform): 179-180 ºC; IR (kBr) υmáx (cm^{-1}): 2920, 1668, 1596-1420, 1256; ^{1}H NMR ($CDCl_3$ 300.13 MHz) δ= 7.79 (brs, H-1''), 7.29 (d, J = 8.8, H-2,-6), 6.95 (d, J = 8.8,

H-3,-5), 4.93 (d, J = 1.8, H-3',-4''), 3.85 (s, 4-OCH_3); ^{13}C NMR ($CDCl_3$, 75.47 MHz): δ= 185.6 (C=O), 160.7 (C-4), 136.1 (C-1''),132.6 (C-2, 6), 131.4 (C-2', 5'), 127.7 (C-1), 114.4 (C-3, 5), 68.2 (C-3', 4''), 55.5 (4-OCH_3); ESI-TOF-HRMS (+) m/z: Anal. Calc. for $C_{21}H_{21}O_4$ ($M+H^+$): 337.14344; found: 337.14272.

1.3. Synthesis of **BP-MA4**

An aqueous solution of 40% sodium hydroxide was added to a solution of tetrahydro-4*H*-pyran-4-one (100 mg, 0.99 mmol) in methanol until pH 13–14. Then a solution of 2.99 mmol (443.1 mg) 4-dimethylaminobenzaldehyde in methanol was slowly added to the reaction mixture. The reaction was left at room temperature for 7 days and was monitored by TLC. After completion, the reaction mixture was poured into ice and neutralized with diluted HCl. A precipitate was formed upon cooling to room temperature. This was filtered and washed with water and further purified by preparative TLC (SiO_2, n-hexane/ethyl acetate 7:3) . An orange gum corresponding to 3,5-bis((*E*)-4-dimethylaminobenzylidene)tetrahydro-4*H*-pyran-4-one (**BP-MA4**) was obtained.

3,5-bis((E)-4-dimethylaminobenzylidene)tetrahydro-4*H*-pyran-4-one (**BP-MA4**): Yield: 1.1% as orange gum; IR (kBr) υmáx (cm^{-1}): 2957-2848, 1723, 1584-1463, 1369-1237, 1270; ^1H NMR ($CDCl_3$ 300.13 MHz) *δ*= 7.77 (s H-1''), 7.26 (d, *J* = 8.8 Hz, H-2,-6), 6.71 (d, *J* = 8.9 Hz, H-3,-5), 4.96 (d, *J* = 1.6 Hz, H-3',-4''), 3.03 (s, 4-NCH_3); ^{13}C NMR ($CDCl_3$, 75.47 MHz): δ= 185.4 (C=O), 150.9 (C-4), 136.4 (C-1''), 132.8 (C-2, 6), 129.3 (C-2', 5'), 123.1 (C-1), 111.9 (C-3, 5), 69.0 (C-3', 4''), 40.3 (4-NCH_3); ESI-TOF-HRMS (+) m/z: Anal. Calc. for $C_{23}H_{27}N_2O_2$ ($M+H^+$): 363.20670; found: 363.20545.

1.4. Synthesis of **BP-B4**

An aqueous solution of 40% sodium hydroxide was added to a solution of tetrahydro-4*H*-pyran-4-one (100 mg, 0.99 mmol) in methanol until pH 13–14. Then, a solution of 2.99 mmol (551.4 mg) 4-bromobenzaldehyde in methanol was slowly added to the reaction mixture. The reaction was left at room temperature for 4 days and was monitored by TLC. After completion, the reaction mixture was poured into ice and neutralized with diluted HCl. The solution was then extracted with ethyl acetate (3 x 50 mL). The organic phase was collected and further rinsed with water, dried over with anhydrous sodium sulfate and concentrated under reduced pressure. The crude material was purified by crystallization

with ethyl acetate. A light yellow solid corresponding to 3,5-bis((*E*)-4-bromobenzylidene)tetrahydro-4*H*-pyran-4-one (**BP-B4**) was obtained.

3,5-bis((E)-4-bromobenzylidene)tetrahydro-4*H*-pyran-4-one (**BP-B4**): Yield: 47.1%; mp (ethyl acetate): 203-206ºC; IR (kBr) υmáx (cm^{-1}): 2921-2807, 1669, 1577-1439, 1263; ^{1}H NMR ($CDCl_3$ 300.13 MHz) *δ* = 7.75 (brs, H-1''), 7.56 (d, *J* = 8.5 Hz, H-3,-5), 7.18 (d, *J* = 8.5 Hz, H-2,-6), 4.88 (d, *J* = 1.9 Hz, H-3',-4'). ^{13}C NMR ($CDCl_3$, 75.47 MHz): δ= 185.2 (C=O), 135.5 (C-1''), 133.6 (C-2', 5'), 133.5 (C-1), 132.1 (C-2, 6), 132.0 (C-3, 5), 124.1 (C-4), 68.6 (C-3', 4'). ESI-TOF-HRMS (+) m/z: Anal. Calc. for $C_{19}H_{15}Br_2O_2$ ($M+H^+$): 432.94333; found:432.94232.

1.5. Synthesis of **BP-M34**

An aqueous solution of 40% sodium hydroxide was added to a solution of tetrahydro-4*H*-pyran-4-one (100 mg, 0.99 mmol) in methanol until pH 13–14. Then, a solution of 2.99 mmol (496.85 mg) 3,4-dimethoxybenzaldehyde in methanol was slowly added to the reaction mixture. The reaction was left at room temperature for 3 days and was monitored by TLC. After completion, the reaction mixture was poured into ice and neutralized with diluted HCl. The solution was then extracted with ethyl acetate (3 x 50 mL). The organic phase was collected and further rinsed with water, dried over with anhydrous sodium sulfate and concentrated under reduced pressure. The crude material was purified by crystallization from ethyl acetate. A solid corresponding to 3,5-bis((*E*)-3,4-dimethoxybenzylidene)tetrahydro-4*H*-pyran-4-one (**BP-M34**) was obtained.

3,5-bis((E)-3,4-dimethoxybenzylidene)tetrahydro-4*H*-pyran-4-one (**BP-M34**): Yield: 32.4%; mp (ethyl acetate): 163-165ºC; IR (kBr) υmáx (cm^{-1}): 2939-2838, 1671, 1594-1462. 1278; ^{1}H NMR ($CDCl_3$ 300.13 MHz) *δ*= 7.78 (brs, H-1''), 6.91 (brd, H-5, -6), 6.87 (brd, H-2), 4.96 (d, *J* = 1.8 Hz, H-3', -4'), 3.93 (s, 3-OCH_3), 3.91 (4-OCH_3); ^{13}C NMR ($CDCl_3$, 75.47 MHz): δ= 185.0 (C=O), 149.9 (C-3), 148.6 (C-4), 136.0 (C-1''), 131.1 (C-2', -5'), 127.5 (C-1), 123.8 (C-5), 113.3 (C-2), 110.7 (C-6), 55.6 (3-, 4-OCH_3).); ESI-TOF-HRMS (+) m/z: Anal. Calc. for $C_{23}H_{25}O_6$ ($M+H^+$): 397.16456; found: 397.16371.

1.6. Synthesis of **BP-F4**

An aqueous solution of 40% sodium hydroxide was added to a solution of tetrahydro-4*H*-pyran-4-one (100 mg, 0.99 mmol) in methanol until pH 13–14. Then, a solution of 2.99

mmol (371.9 mg) 4-fluorobenzaldehyde in methanol was slowly added to the reaction mixture. The reaction was left at room temperature for 3 days and was monitored by TLC. After completion, the reaction mixture was poured into ice and neutralized with diluted HCl. The solution was then extracted with ethyl acetate (3 x 50 mL). The organic phase was collected and further rinsed with water, dried over with anhydrous sodium sulfate and concentrated under reduced pressure. The crude material was purified by crystallization from chloroform. A yellow solid corresponding to 3,5-bis((*E*)-4-fluorobenzylidene)tetrahydro-4H-pyran-4-one (**BP-F4**) was obtained.

3,5-bis((E)-4-fluorobenzylidene)tetrahydro-4H-pyran-4-one (**BP-F4**): Yield: 50.7%; mp (chloroform): 175-177ºC; IR (kBr) υmáx (cm^{-1}): 2919-2830, 1670, 1576-1450, 1293, 1155; ^{1}H NMR ($CDCl_3$ 300.13 MHz) *δ*= 7.80 (brs, H-1''), 7.34-7.29 (m, H-2, -6), 7.15-7.10 (m, H-3, -5), 4.90 (d, *J* = 1.9, H-3', 4'); ^{13}C NMR ($CDCl_3$, 75.47 MHz): δ= 185.4 (C=O), 165.0 (C-4), 135.5 (C-1''), 132.8 (C-2', -5'), 132.6 (C-2, -6), 131.0 (C-1), 116.2 (C-3, -5), 68.6 (C-3', -4'); ESI-TOF-HRMS (+) m/z: Anal. Calc. for $C_{19}H_{15}F_2O_2$ ($M+H^+$): 313.10346; found: 313.10314.

1.7. Synthesis of **BP-EA4**

An aqueous solution of 40% sodium hydroxide was added to a solution of tetrahydro-4*H*-pyran-4-one (100 mg, 0.99 mmol) in methanol until pH 13–14. Then, a solution of 2.99 mmol (526 mg) 4-diethylaminobenzaldehyde in methanol was slowly added to the reaction mixture. The reaction was left at room temperature for 7 days and was monitored by TLC. After completion, the reaction mixture was poured into ice and neutralized with diluted HCl. A precipitate was formed upon cooling to room temperature. This was filtered and washed with water and further purified by preparative TLC (SiO_2; n-hexane/ethyl acetate 7:3). An orange gum corresponding to 3,5-bis((E)-4-diethylaminobenzylidene)tetrahydro-4*H*-pyran-4-one (**BP-EA4**) was obtained.

3,5-bis((E)-4-diethylaminobenzylidene)tetrahydro-4*H*-pyran-4-one (**BP-EA4**). Yield: 3% as orange gum; IR (kBr) υmáx (cm^{-1}): 2957-2848, 1671, 1594-1462, 1278; ^{1}H NMR ($CDCl_3$ 300.13 MHz) *δ*= ^{1}H NMR ($CDCl_3$, 300 MHz) δ 7.75 (s, H-1''), 7.24 (d, *J* = 8.9 Hz, H-2,-6), 6.67 (d, *J* = 9.0 Hz, H-3,-5), 4.95 (d, *J* = 1.6 Hz, H-3',-4'), 3.40 (q, *J* = 7.1 Hz, 4-NCH2-), 1.20 (t, *J* = 7.0 Hz, 4-CH_3); ^{13}C NMR ($CDCl_3$, 75.47 MHz): δ= 185.6 (C=O=, 148.7 (C-4), 136.6 (C-1''), 133.4 (C-2, -6), 129.1 (C-2', -5'), 122.5 (C-1), 111.5 (C-3, -6), 69.3 (C-3', -4'), 44.8 (4-N<u>C</u>$H_2$$CH_3$), 13.0 (4-$NCH_2$<u>C</u>$H_3$); ESI-TOF-HRMS (+) m/z: Anal. Calc. for $C_{27}H_{35}N_2O_2$ ($M+H^+$): 419.26930; found: 419.26852.

1.8. Synthesis of **BP-M345**

An aqueous solution of 40% sodium hydroxide was added to a solution of tetrahydro-4H-pyran-4-one (100 mg, 0.99 mmol) in methanol until pH 13–14. Then, a solution of 2.99 mmol (490.68 mg) 3,4,5-trimethoxybenzaldehyde in methanol was slowly added to the reaction mixture. The reaction was left at room temperature for 3 days and was monitored by TLC. After completion, the reaction mixture was poured into ice and neutralized with diluted HCl. The solution was then extracted with ethyl acetate (3 x 50 mL). The organic phase was collected and further rinsed with water, dried over with anhydrous sodium sulfate and concentrated under reduced pressure. The crude material was purified by preparative TLC (SiO_2; n-hexane/ethyl acetate 7:3). A solid corresponding to 3,5-bis((*E*)-3,4,5-trimethoxybenzylidene)tetrahydro-4*H*-pyran-4-one (**BP-M345**) was obtained.

3,5-bis((E)-3,4,5-trimethoxybenzylidene)tetrahydro-4*H*-pyran-4-one (**BP-M345**): Yield: 10%; mp (ethyl acetate): 193-196ºC; IR (kBr) υmáx (cm^{-1}): 2669-2828, 1667, 1578-1416, 1255; ^{1}H NMR ($CDCl_3$ 300.13 MHz) δ= 7.77 (brs, H-1''), 6.55 (s, H-2,-6), 4.98 (d, *J* = 1.8 Hz, H-3',-4'), 3.90 (s, 4-OCH3), 3.89 (s, 3-,5-OCH3); ^{13}C NMR ($CDCl_3$, 75.47 MHz): δ= 185.7 (C=O), 153.7 (C-3, -5), 140.0 (C-4), 137.2 (C-1'') 132.8 (C-2', -5'), 130.7 (C-1), 108.5 (C-2, -6), 69.1 (C-3', -4'), 61.6 (4-OCH_3), 56.8 (3, 5-OCH_3); ESI-TOF-HRMS (+) m/z: Anal. Calc. for $C_{25}H_{29}O_8$ ($M+H^+$): 457.18569; found: 457.18492.

2. Biological activity

2.1. Compounds

Details concerning the synthesis of compounds **BP-M4**, **BP-MA4**, **BP-B4**, **BP-M34**, **BP-F4**, **BP-EA4** and **BP-M345** are discussed in chapters 3 and 5. In addition to the eight synthesized bischalcones, 10 other structure related compounds **BP-C4**, **BP-MP4**, **BP-FM4**, **BP-C2**, **BP-M2**, **BP-F2**, **BP-M24**, **BP-M245**, **CP-MA4**, **CP-MP4** and **CP-EA4** previously synthesized were also tested. All compounds were dissolved in dimethyl sulfoxide (DMSO; Sigma-Aldrich, Sintra, Portugal) and stored at -20 ºC.

2.2. Yeast screening assay

2.2.1. Yeast strains and growth conditions

Saccharomyces cerevisiae cells expressing human wt p53 alone or co-expressed with human MDM2 or MDMX were used, as previously described[256,265–267]. For the selection of transformed yeast, cells were grown in glucose minimal selective medium with 2% (w/v) glucose (Panreac Química, Barcelona, Spain) 0.67% (w/v) yeast nitrogen base without amino acids (Difco; Quilaban, Sintra, Portugal) and all the amino acids required for yeast growth (50 µg/mL) except leucine and tryptophan, and incubated at 30 ºC, under continuous orbital shaking (170 r.p.m.). To induce the expression of human proteins, yeast cultures were diluted to 0.05 optical density at 600 nm (OD_{600}) in induction selective medium containing 2% (w/v) galactose (Sigma-Aldrich, Sintra, Portugal) and 1% glycerol (JMGS, Odivelas, Portugal) and grown at 30 ºC under continuous shaking. Briefly, yeast cells expressing the human protein and control yeast (transformed with the empty vector) were grown in induction selective medium for up to 48 hours for growth curves experiments. Yeast growth was analyzed by counting the number of colony-forming units per mL (CFU/mL) after 2 days incubation at 30 ºC on Sabouraud Dextrose Agar (Liofilchem; Frilabo, Porto, Portugal) plates.

2.2.2. Effect of the compounds on yeast cell growth

In yeast assays with p53 and MDM2/MDMX, the cells expressing p53 alone were used as positive control. To analyze the effect of compounds on yeast cell growth, transformed cells were incubated in induction selective medium in the presence of 10 or 25 µM compounds or DMSO only (0.1%). Cells were incubated to approximately 0.4 OD_{600} (achieved with each transformant incubated with DMSO only), and the cell growth was

analyzed as described above. For each culture, the percentage of drug-induced growth inhibition was estimated considering 100% growth the number of CFU obtained with yeast expressing both p53 and MDM2 or MDMX.

2.3. Human cell lines assays

2.3.1. Growth conditions

The human cell lines used in this work are listed in Table 1. All tumor cell lines were routinely cultured in RPMI-1640 medium with glutamine from Corning (VWR, Carnaxide, Portugal) supplemented with 10% fetal bovine serum (FBS) from Biowest (Labclinics, Barcelona, Spain). All cells were maintained in a humidified incubator at 37 ºC with 5% CO_2.

***Table 10**: Human cell lines used in the present work.*

Cell line	Tissue/Disease	p53 status	Supplier
HCT116 p53$^{+/+}$	Human colon adenocarcinoma	wt	ATCC (American Type Culture Collection)
HCT116 p53$^{-/-}$		Null (knock out)	
MDA-MB-231	Human breast adenocarcinoma	Mutant p53R280K	
HFF-1	Human foreskin fibroblasts	wt	

2.3.2. Sulforhodamine B (SRB) assay

Human cell lines were incubated in 96-well plates at a final density of 4.0×10^3 cells/well (for HFF-1 cells), 5.0×10^3 cells/well (for HCT116 cell lines), and 1.0×10^4 cells/well (for MDA-MB-231 cells) for 24 hours. Cells were then treated with serial dilutions (0.313 µM to 50 µM) of compounds for 48 hours. The effect of these compounds on *in vitro* growth was assessed using the SRB assay. Cells were fixated with 2.5% TCA for 1 hour at 4 ºC. Plates were then stained with 0.25% SRB (Sigma-Aldrich, Sintra, Portugal) and washed with 1% acetic acid. The bound dye was solubilized in 0.12% Tris Base and the absorbance was measured at 510 nm in a microplate reader (Biotek Instruments Inc., Synergy MX, USA). The maximum concentration of solvent used in this assay (1% DMSO) was included as control. The concentration of compound that induces 50% growth inhibition (GI_{50}) was then determined.

2.3.3. Colony formation assay

HCT116 $p53^{+/+}$ cells were seeded in 6-well plates at a density of 1.0×10^3 cells/well, followed by incubation with 0.25, 0.50, 1.00 and 2.00 μM **BP-C4** for 11 days. Formed colonies were fixed with 10% MeOH and 10% AcOH for 10 min, and then stained with 0.5% crystal violet (Sigma-Aldrich, Sintra, Portugal) in 1:1 MeOH/H_2O for 15 min. Colonies containing more than 20 cells were counted.

2.3.4. Cell cycle and apoptosis analysis

HCT116 $p53^{+/+}$ cells were incubated in 6-well plates at a density of 1.5×10^5 cells/well for 24 hours. Cells were then treated with **BP-C4** or DMSO only for 48 hours. For cell cycle analysis, cells were fixed in ice-cold 70% ethanol and incubated at 37 ºC with RNAse A (Sigma-Aldrich, Sintra, Portugal) at a final concentration of 20 μg/mL for 15 minutes, and further incubated with 50 μg/mL propidium iodide (PI; Sigma-Aldrich, Sintra, Portugal) for 30 minutes, followed by flow cytometry analysis; cells were analysed by flow cytometry and cell cycle phases were identified and quantified using the FlowJo X 10.0.7 Software (Treestar, Ashland, OR, USA) for Microsoft Windows 8. As for apoptosis assessment, flow cytometry was performed using the *Annexin V-FITC Apoptosis Detection Kit I* from BD Biosciences (Enzifarma, Porto, Portugal), according to the manufacturer's instructions. The AccuriTM C6 flow cytometer and the BD Accuri C6 software (BD Biosciences) for Microsoft Windows 7 were used.

2.3.5. Western Blot analysis

HCT116 $p53^{+/+}$ cells were seeded in 6-well plates at a density of 1.5×10^5 cells/well for 24 hours, followed by treatment with 12 μM **BP-C4**. Protein extracts were quantified using the Bradford reagent (Sigma-Aldrich, Sintra, Portugal). Proteins were run in SDS-PAGE and transferred to a Whatman nitrocellulose membrane from Protan (VWR, Carnaxide, Portugal). After blocking, proteins were identified using specific primary antibodies followed by HRP-conjugated secondary antibodies (Table 2). GAPDH was used as loading control. The signal was detected with the ECL Amersham kit from GE Healthcare (VWR, Carnaxide, Portugal). The ChemiDoc™ XRS Imaging System from Bio-Rad Laboratories (Amadora, Portugal) for Microsoft Windows 10 was used for detection. Band intensities were quantified using the Image Lab (version 6.0.1; Bio-Rad Laboratories) software for Microsoft Windows 10. Signal intensity is relative to the respective loading and normalized to control (DMSO), set as 1.

***Table 11**: Antibodies used in Western Blot.*

Antigen	Final Dilution	Supplier
Primary antibodies		
p53 (DO-1) (mouse monoclonal)	1:5000	Santa Cruz Biotechnology (Frilabo, Porto, Portugal)
p21 (C-19) (rabbit polyclonal)	1:100	
PARP (C2-10) (mouse monoclonal)	1:50	
PUMA (B-6) (mouse monoclonal)	1:500	
Secondary antibodies		
Anti-mouse horseradish-peroxidase (HRP)-conjugated	1:5000	Santa Cruz Biotechnology (Frilabo, Porto, Portugal)
Anti-rabbit horseradish-peroxidase (HRP)-conjugated	1:5000	

2.4. Statistical analysis

Data were analyzed statistically using the GraphPad Prism (La Jolla, CA, USA; version 8.0.2) software for Microsoft Windows 10 and differences between means were tested for significance using the unpaired Student's t-test (*$p < 0.05$; **$p < 0.01$).

CHAPTER IV

Conclusions and perspectives

Diarylpentanoids are a class of compounds with many interesting properties, namely antiproliferative activities on tumor cells, with hundreds of cases reported. Some of these compounds were reported to target the p53 pathway, resulting in the upregulation of p53 targets, as well as in proteasome inhibition and in caspase activation.

In this work, seven diarylpentanoids inspired in chalcone scaffolds were synthesized through the Claisen-Schmidt condensation and their ability to disrupt the p53-MDM2 interaction was then evaluated.

The work developed in this dissertation led to the potential identification of a novel p53-MDM2/MDMX dual inhibitor. From a chemical standpoint, it would be interesting to optimize some of the tested diarylpentanoids, either for reduction of cytotoxicity, as is the case of **BP-F2**, or for enhancement of growth inhibitory activity. The new compounds that would be obtained from these modifications would be tested for comparison with the results obtained with the starting materials. Moreover, other assays should be performed in order to further understand the mechanism of action of **BP-C4** in wt p53-expressing cells. For instance, a Co-IP assay in yeast and in human tumor cells is necessary to prove the disruption of the p53-MDM2/MDMX complex by **BP-C4**. The effect of this compound should also be tested in different wt-p53 expressing cell lines, like HepG2 and SJSA-1 cell lines, which overexpress MDM2, and MCF-7, which overexpresses MDMX. Additionally, a CETSA assay would be useful to predict a potential binding of **BP-C4** to p53 or MDMs.

CHAPTER V

References

(1) Hafner, A.; Bulyk, M. L.; Jambhekar, A.; Lahav, G. The Multiple Mechanisms That Regulate P53 Activity and Cell Fate. *Nat. Rev. Mol. Cell Biol.* **2019**, *20*, 199–210.

(2) Lane, D. P.; Crawford, L. V. T Antigen Is Bound to a Host Protein in SV40-Transformed Cells. *Nature* **1979**, *278*, 261–263.

(3) Barker, D.; White, R.; Ledbetter, D.; Preisinger, A.; Fearon, E.; Nakamura, Y.; Baker, S.; Nigro, J.; Vogelstein, B.; Jessup, J.; et al. Chromosome 17 Deletions and P53 Gene Mutations in Colorectal Carcinomas. *Science (80-.).* **1989**, *244* (4901), 217–221.

(4) Hollstein, M.; Sidransky, D.; Vogelstein, B.; Curtis, C. P53 Mutation Human Cancers. *Science (80-.).* **1991**, *253* (July), 49–53.

(5) Kandoth, C.; McLellan, M. D.; Vandin, F.; Ye, K.; Niu, B.; Lu, C.; Xie, M.; Zhang, Q.; McMichael, J. F.; Wyczalkowski, M. A.; et al. Mutational Landscape and Significance across 12 Major Cancer Types. *Nature* **2013**, *502* (7471), 333–339.

(6) Lawrence, M. S.; Stojanov, P.; Mermel, C. H.; Robinson, J. T.; Garraway, L. A.; Golub, T. R.; Meyerson, M.; Gabriel, S. B.; Lander, E. S.; Getz, G. Discovery and Saturation Analysis of Cancer Genes across 21 Tumour Types. *Nature* **2014**, *505* (7484), 495–501.

(7) McBride, O. W.; Merry, D.; Givol, D. The Gene for Human P53 Cellular Tumor Antigen Is Located on Chromosome 17 Short Arm (17p13). *Proc. Natl. Acad. Sci. U. S. A.* **1986**, *83* (1), 130–134.

(8) Isobe, M.; Emanuel, B. S.; Givol, D.; Oren, M.; Croce, C. M. Localization of Gene for Human P53 Tumour Antigen to Band 17p13. *Nature* **1986**, *320* (6057), 84–85.

(9) May, P.; May, E. Twenty Years of P53 Research: Structural and Functional Aspects of the P53 Protein. *Oncogene* **1999**, *18* (53), 7621–7636.

(10) Raycroft, L.; Wu, H.; Lozano, G. Transcriptional Activation by Wild-Type but Not Transforming Mutants of the P53 Anti-Oncogene. *Science (80-.).* **1990**, *249* (4972), 1049–1051.

(11) Fields, S.; Jang, S. K. E. Y. Presence of a Potent Transcription Activating Sequence in the P53 Protein. *Science (80-.).* **1990**, *249* (4972), 1046–1049.

(12) Scolnick, D. M.; Darpino, P.; Berger, S. L.; Halazonetis, T. D.; Candau, R.; Ying, C. Y. Two Tandem and Independent Sub-Activation Domains in the Amino Terminus of P53 Require the Adaptor Complex for Activity. *Oncogene* **2002**, *15* (7), 807–816.

(13) Karnezis, A. N.; Broz, D. K.; Brady, C. A.; Jiang, D.; Attardi, L. D.; Johnson, T. M.; Kozak, M. M.; Jarvis, L. A.; Basak, S.; McLaughlin, M. E.; et al. Distinct P53 Transcriptional Programs Dictate Acute DNA-Damage Responses and Tumor Suppression. *Cell* **2011**, *145* (4), 571–583.

(14) Kamada, R.; Toguchi, Y.; Nomura, T.; Imagawa, T.; Sakaguchi, K. Tetramer Formation of Tumor Suppressor Protein P53: Structure, Function, and Applications. *Biopolymers* **2016**, *106* (4), 598–612.

(15) Joerger, A. C.; Fersht, A. R. The Tumor Suppressor P53: From Structures to Drug Discovery. *Cold Spring Harb Perspect Biol* **2010**, *2* (6), a000919.

(16) Karni-Schmidt, O.; Lokshin, M.; Prives, C. The Roles of MDM2 and MDMX in Cancer. *Annu. Rev. Pathol. Mech. Dis.* **2016**, *11* (1), 617–644.

(17) Walker, K. K.; Levine, A. J. Identification of a Novel P53 Functional Domain That Is Necessary for Efficient Growth Suppression. *Proc. Natl. Acad. Sci.* **1996**, *93* (26), 15335–15340.

(18) Pavletich, N. P.; Chambers, K. A.; Pabo, C. O. The DNA-Binding Domain of P53 Contains the Four Conserved Regions and the Major Mutation Hot Spots. *Genes Dev.* **1993**, *7* (12 B), 2556–2564.

(19) Kitayner, M.; Rozenberg, H.; Kessler, N.; Rabinovich, D.; Shaulov, L.; Haran, T. E.; Shakked, Z. Structural Basis of DNA Recognition by P53 Tetramers. *Mol. Cell* **2006**, *22* (6), 741–753.

(20) Kitayner, M.; Rozenberg, H.; Rohs, R.; Suad, O.; Rabinovich, D.; Honig, B.; Shakked, Z. Diversity in DNA Recognition by P53 Revealed by Crystal Structures with Hoogsteen Base Pairs. *Nat. Struct. Mol. Biol.* **2010**, *17* (4), 423–429.

(21) Cho, Y.; Gorina, S.; Jeffrey, P. D.; Pavletich, N. P. Tumor of a P53 Structure Crystal Complex : Suppressor- DNA Tumorigenic Mutations Understanding. *Adv. Sci.* **2010**, *265* (5170), 346–355.

(22) Veprintsev, D. B.; Freund, S. M. V.; Andreeva, A.; Rutledge, S. E.; Tidow, H.; Cañadillas, J. M. P.; Blair, C. M.; Fersht, A. R. Core Domain Interactions in Full-Length P53 in Solution. *Proc. Natl. Acad. Sci.* **2006**, *103* (7), 2115–2119.

(23) Clore, G. M.; Ernst, J.; Clubb, R.; Omichinski, J. G.; Kennedy, W. M. P.; Kazuya. Refined Solution Structure of the Oligomerization Domain of the Tumour Suppressor P53. *Nat. Struct. Mol. Biol.* **1995**, *2*, 312–333.

(24) Davison, T. S.; Yin, P.; Nie, E.; Kay, C.; Arrowsmith, C. H. Characterization of the Oligomerization Defects of Two P53 Mutants Found in Families with Li-Fraumeni and Li-Fraumeni-like Syndrome. *Oncogene* **1998**, *17* (5), 651–656.

(25) Imagawa, T.; Terai, T.; Yamada, Y.; Kamada, R.; Sakaguchi, K. Evaluation of Transcriptional Activity of P53 in Individual Living Mammalian Cells. *Anal. Biochem.* **2009**, *387* (2), 249–256.

(26) Kawaguchi, T.; Kato, S.; Otsuka, K.; Watanabe, G.; Kumabe, T.; Tominaga, T.; Yoshimoto, T.; Ishioka, C. The Relationship among P53 Oligomer Formation, Structure and Transcriptional Activity Using a Comprehensive Missense Mutation Library. *Oncogene* **2005**, *24* (46), 6976–6981.

(27) Bell, S.; Klein, C.; Müller, L.; Hansen, S.; Buchner, J. P53 Contains Large Unstructured Regions in Its Native State. *J. Mol. Biol.* **2002**, *322* (5), 917–927.

(28) Gu, W.; Roeder, R. G. Activation of P53 Sequence-Specific DNA Binding by Acetylation of the P53 C-Terminal Domain. *Cell* **1997**, *90* (4), 595–606.

(29) Hupp, T. R.; Meek, D. W.; Midgley, C. A.; Lane, D. P. Regulation of the Specific DNA Binding Function of P53. *Cell* **1992**, *71* (5), 875–886.

(30) Luo, J.; Laszkowska, M.; Li, M.; Gu, W.; Roeder, R. G.; Tang, Y. Acetylation of P53 Augments Its Site-Specific DNA Binding Both in Vitro and in Vivo. *Proc. Natl. Acad. Sci.* **2004**, *101* (8), 2259–2264.

(31) Ayed, A.; Mulder, F. A. A.; Yi, G.; Lu, Y.; Kay, L. E.; Arrowsmith, C. H. Latent and Active P53 Are Identical in Conformation. *Nat. Struct. Mol. Biol.* **2001**, *8*, 756–760.

(32) Anderson, M. E.; Woelker, B.; Reed, M.; Wang, P.; Tegtmeyer, P. Reciprocal Interference between the Sequence-Specific Core and Nonspecific C-Terminal DNA Binding Domains of P53: Implications for Regulation. *Mol. Cell. Biol.* **1997**, *17* (11), 6255–6264.

(33) Kim, H.; Kim, K.; Choi, J.; Heo, K.; Baek, H. J.; Roeder, R. G.; An, W. P53 Requires an Intact C-Terminal Domain for DNA Binding and Transactivation. *J. Mol. Biol.* **2012**, *415* (5), 843–854.

(34) McKinney, K.; Mattia, M.; Gottifredi, V.; Prives, C. P53 Linear Diffusion along DNA Requires Its C Terminus. *Mol. Cell* **2004**, *16* (3), 413–424.

(35) van Oijen, A. M.; Tafvizi, A.; Fersht, A. R.; Huang, F.; Mirny, L. A. A Single-Molecule Characterization of P53 Search on DNA. *Proc. Natl. Acad. Sci.* **2010**, *108* (2), 563–

568.

(36) Tafvizi, A.; Huang, F.; Leith, J. S.; Fersht, A. R.; Mirny, L. A.; Van Oijen, A. M. Tumor Suppressor P53 Slides on DNA with Low Friction and High Stability. *Biophys. J.* **2008**, *95* (1), 1–3.

(37) Walter, K.; Göhler, T.; Deppert, W.; Cherny, D.; Warnecke, G.; Reimann, M.; Kim, E. Specific Interaction of P53 with Target Binding Sites Is Determined by DNA Conformation and Is Regulated by the C-Terminal Domain. *J. Biol. Chem.* **2002**, *277* (43), 41192–41203.

(38) McKinney, K.; Prives, C. Efficient Specific DNA Binding by P53 Requires Both Its Central and C-Terminal Domains as Revealed by Studies with High-Mobility Group 1 Protein. *Mol. Cell. Biol.* **2002**, *22* (19), 6797–6808.

(39) Espinosa, J. M.; Emerson, B. M. Transcriptional Regulation by P53 through Intrinsic DNA/Chromatin Binding and Site-Directed Cofactor Recruitment. *Mol. Cell* **2001**, *8* (1), 57–69.

(40) Moll, U. M.; Petrenko, O. The MDM2-P53 Interaction. *Mol. Cancer Res.* **2003**, *1* (14), 1001–1008.

(41) Hong, B.; van den Heuvel, a P. J.; Prabhu, V. V; Zhang, S.; El-Deiry, W. S. Targeting Tumor Suppressor P53 for Cancer Therapy: Strategies, Challenges and Opportunities. *Curr. Drug Targets* **2014**, *15* (1), 80–89.

(42) Kruse, J. P.; Gu, W. Modes of P53 Regulation. *Cell* **2009**, *137* (4), 609–622.

(43) Sane, S.; Rezvani, K. Essential Roles of E3 Ubiquitin Ligases in P53 Regulation. *Int. J. Mol. Sci.* **2017**, *18* (2).

(44) Zhao, Y.; Yu, H.; Hu, W. The Regulation of MDM2 Oncogene and Its Impact on Human Cancers. *Acta Biochim. Biophys. Sin. (Shanghai).* **2014**, *46* (3), 180–189.

(45) Kawai, H.; Wiederschain, D.; Yuan, Z.-M. Critical Contribution of the MDM2 Acidic Domain to P53 Ubiquitination. *Mol. Cell. Biol.* **2003**, *23* (14), 4939–4947.

(46) Meulmeester, E.; Frenk, R.; Stad, R.; de Graaf, P.; Marine, J.-C.; Vousden, K. H.; Jochemsen, A. G. Critical Role for a Central Part of Mdm2 in the Ubiquitylation of P53. *Mol. Cell. Biol.* **2003**, *23* (14), 4929–4938.

(47) Manfredi, J. J. The Mdm2–P53 Relationship Evolves: Mdm2 Swings Both Ways as an Oncogene and a Tumor Suppressor. *Genes Dev.* **2010**, *53* (15), 1580–1589.

(48) Poyurovsky, M. V.; Priest, C.; Kentsis, A.; Borden, K. L. B.; Pan, Z. Q.; Pavletich, N.; Prives, C. The Mdm2 RING Domain C-Terminus Is Required for Supramolecular Assembly and Ubiquitin Ligase Activity. *EMBO J.* **2007**, *26* (1), 90–101.

(49) Uldrijan, S.; Pannekoek, W. J.; Vousden, K. H. An Essential Function of the Extreme C-Terminus of MDM2 Can Be Provided by MDMX. *EMBO J.* **2007**, *26* (1), 102–112.

(50) Clegg, H. V.; Itahana, K.; Zhang, Y. Unlocking the Mdm2-P53 Loop: Ubiquitin Is the Key. *Cell Cycle* **2008**, *7* (3), 287–292.

(51) Lin, J.; Chen, J.; Elenbaas, B.; Levine, A. J. Several Hydrophobic Amino Acids in the P53 Amino-Terminal Domain Are Required for Transcriptional Activation, Binding to Mdm-2 and the Adenovirus 5 E1B 55-KD Protein. *Genes Dev.* **1994**, *8* (10), 1235–1246.

(52) Kussie, P. H.; Gorina, S.; Marechal, V.; Elenbaas, B.; Moreau, J.; Levine, A. J.; Pavletich, N. P. Structure of the MDM2 Oncoprotein Bound to the P53 Tumor Suppressor Transctivation Domain. *Science (80-.).* **1996**, *274* (5289), 948–953.

(53) Blommers, M. J. J.; Fendrich, G.; Garcia-Echeverria, C.; Chene, P. On the Interaction between P53 and MDM2: Transfer NOE Study of a P53-Derived Peptide Ligated to MDM2. *J. Am. Chem. Soc.* **1997**, *119* (14), 3425–3426.

(54) Yu, G. W.; Rudiger, S.; Veprintsev, D.; Freund, S.; Fernandez-Fernandez, M. R.; Fersht, A. R. The Central Region of HDM2 Provides a Second Binding Site for P53. *Proc. Natl. Acad. Sci. U. S. A.* **2006**, *103* (5), 1227–1232.

(55) Wallace, M.; Worrall, E.; Pettersson, S.; Hupp, T. R.; Ball, K. L. Dual-Site Regulation of MDM2 E3-Ubiquitin Ligase Activity. *Mol. Cell* **2006**, *23* (2), 251–263.

(56) Shimizu, H.; Burch, L. R.; Smith, A. J.; Dornan, D.; Wallace, M.; Ball, K. L.; Hupp, T. R. The Conformationally Flexible S9-S10 Linker Region in the Core Domain of P53 Contains a Novel MDM2 Binding Site Whose Mutation Increases Ubiquitination of P53 in Vivo. *J. Biol. Chem.* **2002**, *277* (32), 28446–28458.

(57) Ma, J.; Martin, J. D.; Zhang, H.; Auger, K. R.; Ho, T. F.; Kirkpatrick, R. B.; Grooms, M. H.; Johanson, K. O.; Tummino, P. J.; Copeland, R. A.; et al. A Second P53 Binding Site in the Central Domain of Mdm2 Is Essential for P53 Ubiquitination. *Biochemistry* **2006**, *45* (30), 9238–9245.

(58) Cross, B.; Chen, L.; Cheng, Q.; Li, B.; Yuan, Z. M.; Chen, J. Inhibition of P53 DNA Binding Function by the MDM2 Protein Acidic Domain. *J. Biol. Chem.* **2011**, *286* (18), 16018–16029.

(59) Poyurovsky, M. V.; Katz, C.; Laptenko, O.; Beckerman, R.; Lokshin, M.; Ahn, J.; Byeon, I. J. L.; Gabizon, R.; Mattia, M.; Zupnick, A.; et al. The C Terminus of P53 Binds the N-Terminal Domain of MDM2. *Nat. Struct. Mol. Biol.* **2010**, *17* (8), 982–989.

(60) Lam, S.; de Lange, J.; Teunisse, A.; Wolf, A.; Lodder, K.; Lenos, K.; Bartel, F.; Emaduddin, M.; Darley, M.; Richter, J.; et al. HDMX-L Is Expressed from a Functional P53-Responsive Promoter in the First Intron of the HDMX Gene and Participates in an Autoregulatory Feedback Loop to Control P53 Activity. *J. Biol. Chem.* **2010**, *285* (38), 29111–29127.

(61) Popowicz, G. M.; Czarna, A.; Holak, T. A. Structure of the Human Mdmx Protein Bound to the P53 Tumor Suppressor Transactivation Domain. *Cell Cycle* **2008**, *7* (15), 2441–2443.

(62) Sharp, D. A.; Kratowicz, S. A.; Sank, M. J.; George, D. L. Stabilization of the MDM2 Oncoprotein by Interaction with the Structurally Related MDMX Protein. *J. Biol. Chem.* **1999**, *274* (53), 38189–38196.

(63) Tanimura, S.; Ohtsuka, S.; Mitsui, K.; Shirouzu, K.; Yoshimura, A.; Ohtsubo, M. MDM2 Interacts with MDMX through Their RING Finger Domains. *FEBS Lett.* **1999**, *447* (1), 5–9.

(64) Shadfan, M.; Lopez-Pajares, V.; Zhi-Min, Y. MDM2 and MDMX: Alone and Together in Regulation of P53. *Transl. Cancer Res.* **2012**, *1* (2), 88–89.

(65) Priest, C.; Prives, C.; Poyurovsky, M. V. Deconstructing Nucleotide Binding Activity of the Mdm2 RING Domain. *Nucleic Acids Res.* **2010**, *38* (21), 7587–7598.

(66) Poyurovsky, M. V.; Jacq, X.; Ma, C.; Karni-Schmidt, O.; Parker, P. J.; Chalfie, M.; Manley, J. L.; Prives, C. Nucleotide Binding by the MDM2 RING Domain Facilitates Arf-Independent MDM2 Nucleolar Localization. *Mol. Cell* **2003**, *12* (4), 875–887.

(67) Stevens, C.; Pettersson, S.; Wawrzynow, B.; Wallace, M.; Ball, K.; Zylicz, A.; Hupp, T. R. ATP Stimulates MDM2-Mediated Inhibition of the DNA-Binding Function of E2F1. *FEBS J.* **2008**, *275* (19), 4875–4886.

(68) Singh, R. K.; Iyappan, S.; Scheffner, M. Hetero-Oligomerization with MdmX Rescues the Ubiquitin/Nedd8 Ligase Activity of RING Finger Mutants of Mdm2. *J. Biol. Chem.* **2007**, *282* (15), 10901–10907.

(69) Bista, M.; Petrovich, M.; Fersht, A. R. MDMX Contains an Autoinhibitory Sequence Element. *Proc. Natl. Acad. Sci.* **2013**, *110* (44), 17814–17819.

(70) Iwakuma, T.; Lozano, G. MDM2, An Introduction. *Mol. Biol. Rep.* **2003**, *1* (December), 993–1000.

(71) Meek, D. W.; Anderson, C. W. Post-Translational Modification of P53. *Cold Spring Harb. Perspect. Biol.* **2009**, 1–16.

(72) Jain, A. K.; Barton, M. C. Making Sense of Ubiquitin Ligases That Regulate P53. *Cancer Biol. Ther.* **2010**, *10* (7), 665–672.

(73) Soares, J.; Loureiro, J. B.; Saraiva, L. Chapter 1 Keeping P53 Active : The Challenge of Cancer Therapy. In *Advances in Drug Discovery and Development*; 2017; pp 2–87.

(74) Kulikov, R.; Letienne, J.; Kaur, M.; Grossman, S. R.; Arts, J.; Blattner, C. Mdm2 Facilitates the Association of P53 with the Proteasome. *Proc. Natl. Acad. Sci.* **2010**, *107* (22), 10038–10043.

(75) Barak, Y.; Gottlieb, E.; Juven-Gershon, T.; Oren, M. Regulation of Mdm2 Expression by P53: Alternative Promoters Produce Transcripts with Nonidentical Translation Potential. *Genes Dev.* **1994**, *8* (15), 1739–1749.

(76) Wu, X.; Bayle, J. H.; Olson, D.; Levine, A. J. The P53-Mdm-2 Autoregulatory Feedback Loop. *Genes Dev.* **1993**, *53*, 1126–1132.

(77) Lev Bar-Or, R.; Maya, R.; Segel, L. A.; Alon, U.; Levine, A. J.; Oren, M. Generation of Oscillations by the P53-Mdm2 Feedback Loop: A Theoretical and Experimental Study. *Proc. Natl. Acad. Sci.* **2002**, *97* (21), 11250–11255.

(78) Lahav, G.; Rosenfeld, N.; Sigal, A.; Geva-Zatorsky, N.; Levine, A. J.; Elowitz, M. B.; Alon, U. Dynamics of the P53-Mdm2 Feedback Loop in Individual Cells. *Nat. Genet.* **2004**, *36* (2), 147–150.

(79) Wei, C. L.; Wu, Q.; Vega, V. B.; Chiu, K. P.; Ng, P.; Zhang, T.; Shahab, A.; Yong, H. C.; Fu, Y. T.; Weng, Z.; et al. A Global Map of P53 Transcription-Factor Binding Sites in the Human Genome. *Cell* **2006**, *124* (1), 207–219.

(80) Zhang, Y.; Xiong, Y.; Yarbrough, W. G. ARF Promotes MDM2 Degradation and Stabilizes P53: ARF-INK4a Locus Deletion Impairs Both the Rb and P53 Tumor Suppression Pathways. *Cell* **1998**, *92* (6), 725–734.

(81) Sherr, C. J.; Weber, J. D. The ARF/P53 Pathway. *Curr. Opin. Genet. Dev.* **2000**, *10* (1), 94–99.

(82) Christophorou, M. A.; Ringshausen, I.; Finch, A. J.; Swigart, L. B.; Evan, G. I. The

Pathological Response to DNA Damage Does Not Contribute to P53-Mediated Tumour Suppression. *Nature* **2006**, *443* (7108), 214–217.

(83) Efeyan, A.; Murga, M.; Martinez-Pastor, B.; Ortega-Molina, A.; Soria, R.; Collado, M.; Fernandez-Capetillo, O.; Serrano, M. Limited Role of Murine ATM in Oncogene-Induced Senescence and P53-Dependent Tumor Suppression. *PLoS One* **2009**, *4* (5).

(84) Kojima, K.; Konopleva, M.; McQueen, T.; O'Brien, S.; Plunkett, W.; Andreeff, M. Mdm2 Inhibitor Nutlin-3a Induces P53-Mediated Apoptosis by Transcription-Dependent and Transcription-Independent Mechanisms and May Overcome Atm-Mediated Resistance to Fludarabine in Chronic Lymphocytic Leukemia. *Blood* **2006**, *108* (3), 993–1000.

(85) Simerzin, A.; Zorde-Khvalevsky, E.; Rivkin, M.; Adar, R.; Zucman-Rossi, J.; Couchy, G.; Roskams, T.; Govaere, O.; Oren, M.; Giladi, H.; et al. The Liver-Specific MicroRNA-122*, the Complementary Strand of MicroRNA-122, Acts as a Tumor Suppressor by Modulating the P53/Mouse Double Minute 2 Homolog Circuitry. *Hepatology* **2016**, *64* (5), 1623–1636.

(86) Shangary, S.; Qin, D.; McEachern, D.; Liu, M.; Miller, R. S.; Qiu, S.; Nikolovska-Coleska, Z.; Ding, K.; Wang, G.; Chen, J.; et al. Temporal Activation of P53 by a Specific MDM2 Inhibitor Is Selectively Toxic to Tumors and Leads to Complete Tumor Growth Inhibition. *Proc. Natl. Acad. Sci. U. S. A.* **2008**, *105* (10), 3933–3938.

(87) Dar, A. A.; Majid, S.; Rittsteuer, C.; De Semir, D.; Bezrookove, V.; Tong, S.; Nosrati, M.; Sagebiel, R.; Miller, J. R.; Kashani-Sabet, M. The Role of MiR-18b in MDM2-P53 Pathway Signaling and Melanoma Progression. *J. Natl. Cancer Inst.* **2013**, *105* (6), 433–442.

(88) Xiao, J.; Lin, H.; Luo, X.; Luo, X.; Wang, Z. MiR-605 Joins P53 Network to Form a P53:MiR-605:Mdm2 Positive Feedback Loop in Response to Stress. *EMBO J.* **2011**, *30* (3), 524–532.

(89) Yang, H.-Y.; Wen, Y.-Y.; Chen, C.-H.; Lozano, G.; Lee, M.-H. 14-3-3{sigma} Positively Regulates P53 and Suppresses Tumor Growth. *Mol. Cell. Biol.* **2003**, *23* (20), 7096–7107.

(90) Stevenson, L. F.; Sparks, A.; Allende-Vega, N.; Xirodimas, D. P.; Lane, D. P.; Saville, M. K. The Deubiquitinating Enzyme USP2a Regulates the P53 Pathway by Targeting Mdm2. *EMBO J.* **2007**, *26* (4), 976–986.

(91) Zhang, Y.; Wolf, G. W.; Bhat, K.; Jin, A.; Allio, T.; Burkhart, W. A.; Xiong, Y. Ribosomal Protein L11 Negatively Regulates Oncoprotein MDM2 and Mediates a P53-Dependent Ribosomal-Stress Checkpoint Pathway. *Mol. Cell. Biol.* **2003**, *23* (23), 8902–8912.

(92) Zheng, J.; Lang, Y.; Zhang, Q.; Cui, D.; Sun, H.; Jiang, L.; Chen, Z.; Zhang, R.; Gao, Y.; Tian, W.; et al. Structure of Human MDM2 Complexed with RPL11 Reveals the Molecular Basis of P53 Activation. *Genes Dev.* **2015**, *29* (14), 1524–1534.

(93) Sasaki, M.; Kawahara, K.; Nishio, M.; Mimori, K.; Kogo, R.; Hamada, K.; Itoh, B.; Wang, J.; Komatsu, Y.; Yang, Y. R.; et al. Regulation of the MDM2-P53 Pathway and Tumor Growth by PICT1 via Nucleolar RPL11. *Nat. Med.* **2011**, *17* (8), 944–951.

(94) Sui, G.; Affar, E. B.; Shi, Y.; Brignone, C.; Wall, N. R.; Yin, P.; Donohoe, M.; Luke, M. P.; Calvo, D.; Grossman, S. R.; et al. Yin Yang 1 Is a Negative Regulator of P53. *Cell* **2004**, *117* (7), 859–872.

(95) Gottlieb, T. M.; Martinez Leal, J. F.; Seger, R.; Taya, Y.; Oren, M. Cross-Talk between Akt, P53 and Mdm2: Possible Implications for the Regulation of Apoptosis. *Oncogene* **2002**, *21* (8), 1299–1303.

(96) Xirodimas, D. P.; Saville, M. K.; Bourdon, J. C.; Hay, R. T.; Lane, D. P. Mdm2-Mediated NEDD8 Conjugation of P53 Inhibits Its Transcriptional Activity. *Cell* **2004**, *118* (1), 83–97.

(97) Wade, M.; Wahl, G. M. Targeting Mdm2 and Mdmx in Cancer Therapy: Better Living through Medicinal Chemistry? *Mol. Cancer Res.* **2009**, *7* (1), 1–11.

(98) Parant, J.; Chavez-Reyes, A.; Little, N. A.; Yan, W.; Reinke, V.; Jochemsen, A. G.; Lozano, G. Rescue of Embryonic Lethality in Mdm4-Null Mice by Loss of Trp53 Suggests a Nonoverlapping Pathway with MDM2 to Regulate P53. *Nat. Genet.* **2001**, *29* (1), 92–95.

(99) Marine, J. C.; Francoz, S.; Maetens, M.; Wahl, G.; Toledo, F.; Lozano, G. Keeping P53 in Check: Essential and Synergistic Functions of Mdm2 and Mdm4. *Cell Death Differ.* **2006**, *13* (6), 927–934.

(100) Steinman, H. A.; Hoover, K. M.; Keeler, M. L.; Sands, A. T.; Jones, S. N. Rescue of Mdm4-Deficient Mice by Mdm2 Reveals Functional Overlap of Mdm2 and Mdm4 in Development. *Oncogene* **2005**, *24* (53), 7935–7940.

(101) Wang, Y. V.; Wade, M.; Wong, E.; Li, Y.-C.; Rodewald, L. W.; Wahl, G. M. Quantitative Analyses Reveal the Importance of Regulated Hdmx Degradation for

P53 Activation. *Proc. Natl. Acad. Sci.* **2007**, *104* (30), 12365–12370.

(102) Wang, X.; Wang, J.; Jiang, X. MdmX Protein Is Essential for Mdm2 Protein-Mediated P53 Polyubiquitination. *J. Biol. Chem.* **2011**, *286* (27), 23725–23734.

(103) Linke, K.; Mace, P. D.; Smith, C. A.; Vaux, D. L.; Silke, J.; Day, C. L. Structure of the MDM2/MDMX RING Domain Heterodimer Reveals Dimerization Is Required for Their Ubiquitylation in Trans. *Cell Death Differ.* **2008**, *15* (5), 841–848.

(104) Kawai, H.; Lopez-Pajares, V.; Kim, M. M.; Wiederschain, D.; Yuan, Z. M. RING Domain-Mediated Interaction Is a Requirement for MDM2's E3 Ligase Activity. *Cancer Res.* **2007**, *67* (13), 6026–6030.

(105) Li, C.; Chen, L.; Chen, J. DNA Damage Induces MDMX Nuclear Translocation by P53-Dependent and -Independent Mechanisms. *Mol. Cell. Biol.* **2002**, *22* (21), 7562–7571.

(106) Pan, Y.; Chen, J. MDM2 Promotes Ubiquitination and Degradation of MDMX. *Mol. Cell. Biol.* **2003**, *23* (15), 5113–5121.

(107) Kawai, H.; Wiederschain, D.; Kitao, H.; Stuart, J.; Tsai, K. K. C.; Yuan, Z. M. DNA Damage-Induced MDMX Degradation Is Mediated by MDM2. *J. Biol. Chem.* **2003**, *278* (46), 45946–45953.

(108) Huang, L.; Yan, Z.; Liao, X.; Li, Y.; Yang, J.; Wang, Z.-G.; Zuo, Y.; Kawai, H.; Shadfan, M.; Ganapathy, S.; et al. The P53 Inhibitors MDM2/MDMX Complex Is Required for Control of P53 Activity in Vivo. *Proc. Natl. Acad. Sci.* **2011**, *108* (29), 12001–12006.

(109) Pant, V.; Xiong, S.; Iwakuma, T.; Quintas-Cardama, A.; Lozano, G. Heterodimerization of Mdm2 and Mdm4 Is Critical for Regulating P53 Activity during Embryogenesis but Dispensable for P53 and Mdm2 Stability. *Proc. Natl. Acad. Sci.* **2011**, *108* (29), 11995–12000.

(110) Tollini, L. A.; Jin, A.; Park, J.; Zhang, Y. Regulation of P53 by Mdm2 E3 Ligase Function Is Dispensable in Embryogenesis and Development, but Essential in Response to DNA Damage. *Cancer Cell* **2014**, *26* (2), 235–247.

(111) Di Conza, G.; Mancini, F.; Buttarelli, M.; Pontecorvi, A.; Trimarchi, F.; Moretti, F. MDM4 Enhances P53 Stability by Promoting an Active Conformation of the Protein upon DNA Damage. *Cell Cycle* **2012**, *11* (4), 749–760.

(112) Toledo, F.; Wahl, G. M. Regulating the P53 Pathway: In Vitro Hypotheses, in Vivo Veritas. *Nat. Rev. Cancer* **2006**, *6* (12), 909–923.

(113) Perry, M. E. The Regulation of the P53-Mediated Stress Response by MDM2 and MDM4. *Cold Spring Harb. Perspect. Biol.* **2010**, No. 2.

(114) Yu, Q.; Li, Y.; Mu, K.; Li, Z.; Meng, Q.; Wu, X.; Wang, Y.; Li, L. Amplification of Mdmx and Overexpression of MDM2 Contribute to Mammary Carcinogenesis by Substituting for P53 Mutations. *Diagn. Pathol.* **2014**, *9* (1), 1–8.

(115) Matijasevic, Z.; Krzywicka-Racka, A.; Sluder, G.; Jones, S. N. MdmX Regulates Transformation and Chromosomal Stability in P53-Deficient Cells. *Cell Cycle* **2008**, *7* (19), 2967–2973.

(116) Matijasevic, Z.; Steinman, H. A.; Hoover, K.; Jones, S. N. MdmX Promotes Bipolar Mitosis To Suppress Transformation and Tumorigenesis in P53-Deficient Cells and Mice. *Mol. Cell. Biol.* **2007**, *28* (4), 1265–1273.

(117) Mancini, F.; Di Conza, G.; Pellegrino, M.; Rinaldo, C.; Prodosmo, A.; Giglio, S.; D'Agnano, I.; Florenzano, F.; Felicioni, L.; Buttitta, F.; et al. MDM4 (MDMX) Localizes at the Mitochondria and Facilitates the P53-Mediated Intrinsic-Apoptotic Pathway. *EMBO J.* **2009**, *28* (13), 1926–1939.

(118) Xue, W.; Zender, L.; Miething, C.; Dickins, R. A.; Hernando, E.; Krizhanovsky, V.; Cordon-Cardo, C.; Lowe, S. W. Senescence and Tumour Clearance Is Triggered by P53 Restoration in Murine Liver Carcinomas. *Nature* **2007**, *445* (7128), 656–660.

(119) Ventura, A.; Kirsch, D. G.; McLaughlin, M. E.; Tuveson, D. A.; Grimm, J.; Lintault, L.; Newman, J.; Reczek, E. E.; Weissleder, R.; Jacks, T. Restoration of P53 Function Leads to Tumour Regression in Vivo. *Nature* **2007**, *445* (7128), 661–665.

(120) Brosh, R.; Rotter, V. When Mutants Gain New Powers: News from the Mutant P53 Field. *Nat. Rev. Cancer* **2009**, *9* (10), 701–713.

(121) Willis, A.; Jung, E. J.; Wakefield, T.; Chen, X. Mutant P53 Exerts a Dominant Negative Effect by Preventing Wild-Type P53 from Binding to the Promoter of Its Target Genes. *Oncogene* **2004**, *23* (13), 2330–2338.

(122) Kern, S. E.; Pietenpol, J. A.; Thiagalingam, S.; Seymour, A.; Kinzler, K. W.; Vogelstein, B. Oncogenic Forms of P53 Inhibit P53-Regulated Gene Expression. *Science* **1992**.

(123) Milner, J.; Medcalf, E. A. Cotranslation of Activated Mutant P53 with Wild Type Drives the Wild-Type P53 Protein into the Mutant Conformation. *Cell* **1991**, *65* (5), 765–774.

(124) Dittmer, D.; Pati, S.; Zambetti, G.; Chu, S.; Teresky, A. K.; Moore, M.; Finlay, C.;

Levine, A. J. Gain of Function Mutations in P53. *Nat. Genet.* **1993**, *4* (1), 42–46.

(125) Vikhanskaya, F.; Lee, M. K.; Mazzoletti, M.; Broggini, M.; Sabapathy, K. Cancer-Derived P53 Mutants Suppress P53-Target Gene Expression - Potential Mechanism for Gain of Function of Mutant P53. *Nucleic Acids Res.* **2007**, *35* (6), 2093–2104.

(126) Bossi, G.; Lapi, E.; Strano, S.; Rinaldo, C.; Blandino, G.; Sacchi, A. Mutant P53 Gain of Function: Reduction of Tumor Malignancy of Human Cancer Cell Lines through Abrogation of Mutant P53 Expression. *Oncogene* **2006**, *25* (2), 304–309.

(127) Yan, W.; Liu, G.; Scoumanne, A.; Chen, X. Suppression of Inhibitor of Differentiation 2, a Target of Mutant P53, Is Required for Gain-of-Function Mutations. *Cancer Res.* **2008**, *68* (16), 6789–6796.

(128) Zhu, H.-B.; Yang, K.; Xie, Y.-Q.; Lin, Y.-W.; Mao, Q.-Q.; Xie, L.-P. Silencing of Mutant P53 by SiRNA Induces Cell Cycle Arrest and Apoptosis in Human Bladder Cancer Cells. *World J. Surg. Oncol.* **2013**, *11* (1), 22.

(129) Olive, K. P.; Tuveson, D. A.; Ruhe, Z. C.; Yin, B.; Willis, N. A.; Bronson, R. T.; Crowley, D.; Jacks, T. Mutant P53 Gain of Function in Two Mouse Models of Li-Fraumeni Syndrome. *Cell* **2004**, *119* (6), 847–860.

(130) Robles, A. I.; Harris, C. C. Clinical Outcomes and Correlates of TP53 Mutations and Cancer. *Cold Spring Harb. Perspect. Biol.* **2009**, *2* (3), a001016–a001016.

(131) Goh, A. M.; Coffill, C. R.; Lane, D. P. The Role of Mutant P53 in Human Cancer. *J. Pathol.* **2011**, *223* (2), 116–126.

(132) Jung, M. S.; Yun, J.; Chae, H. D.; Kim, J. M.; Kim, S. C.; Choi, T. S.; Shin, D. Y. P53 and Its Homologues, P63 and P73, Induce a Replicative Senescence through Inactivation of NF-Y Transcription Factor. *Oncogene* **2001**, *20*, 5818–5825.

(133) Chin, K. V; Ueda, K.; Pastan, I.; Gottesman, M. M. Modulation of Activity of the Promoter of the Human MDR1 Gene by Ras and P53. *Science* **1992**, *255* (December), 459–462.

(134) Khromova, N. V.; Kopnin, P. B.; Stepanova, E. V.; Agapova, L. S.; Kopnin, B. P. P53 Hot-Spot Mutants Increase Tumor Vascularization via ROS-Mediated Activation of the HIF1/VEGF-A Pathway. *Cancer Lett.* **2009**, *276* (2), 143–151.

(135) Stegh, A. H. Targeting the P53 Signaling Pathway in Cancer Therapy – the Promises, Challenges and Perils. *Expert Opin. Ther. Targets* **2012**, *16* (1), 67–83.

(136) Liu, Y.; Wang, X.; Wang, G.; Yang, Y.; Yuan, Y.; Ouyang, L. The Past, Present and

Future of Potential Small-Molecule Drugs Targeting P53-MDM2/MDMX for Cancer Therapy. *Eur. J. Med. Chem.* **2019**, *176*, 92–104.

(137) Vassilev, L. T. Small-Molecule Antagonists of P53-MDM2 Binding: Research Tools and Potential Therapeutics. *Cell Cycle* **2004**, *3* (4), 419–421.

(138) Shangary, S.; Ding, K.; Qiu, S.; Nikolovska-coleska, Z.; Bauer, J. A.; Liu, M.; Wang, G.; Lu, Y.; Mceachern, D.; Bernard, D.; et al. Reactivation of P53 by a Specific MDM2 Antagonist (MI-43) Leads to P21-Mediated Cell Cycle Arrest and Selective Cell Death in Colon Cancer. *Mol. Cancer Ther.* **2008**, *7* (June), 1533–1543.

(139) Vassilev, L. T.; Vu, B. T.; Craves, B.; Carvajal, D.; Podlaski, F.; Filipovic, Z.; Kong, N.; Kammlott, U.; Lukacs, C.; Klein, C.; et al. In Vivo Activation of the P53 Pathway by Small-MoleculeAntagonists of MDM2. *Science (80-.).* **2004**, *303* (5659), 844–848.

(140) Shangary, S.; Wang, S. Small-Molecule Inhibitors of the MDM2-P53 Protein-Protein Interaction to Reactivate P53 Function: A Novel Approach for Cancer Therapy. *Annu. Rev. Pharmacol. Toxicol.* **2009**, *49* (1), 223–241.

(141) Secchiero, P.; Melloni, E.; Di Iasio, M. G.; Tiribelli, M.; Rimondi, E.; Corallini, F.; Gattei, V.; Zauli, G. Nutlin-3 up-Regulates the Expression of Notch1 in Both Myeloid and Lymphoid Leukemic Cells, as Part of a Negative Feedback Antiapoptotic Mechanism. *Blood* **2009**, *113* (18), 4300–4308.

(142) Alimonti, A.; Nardella, C.; Chen, Z.; Clohessy, J. G.; Carracedo, A.; Trotman, L. C.; Cheng, K.; Varmeh, S.; Kozma, S. C.; Thomas, G.; et al. A Novel Type of Cellular Senescence That Can Be Enhanced in Mouse Models and Human Tumor Xenografts to Suppress Prostate Tumorigenesis. *J. Clin. Invest.* **2010**, *120* (3), 681–693.

(143) Zhao, Y.; Aguilar, A.; Bernard, D.; Wang, S. Small-Molecule Inhibitors of the MDM2-P53 Protein-Protein Interaction (MDM2 Inhibitors) in Clinical Trials for Cancer Treatment. *J. Med. Chem.* **2015**, *58* (3), 1038–1052.

(144) Carvajal, D.; Podlaski, F.; Filipovic, Z.; Klein, C.; Fotouhi, N.; Liu, E. A. In Vivo Activation of the P53 Pathway by Small-Molecule Antagonists of MDM2. *Science (80-.).* **2004**, *303* (February), 844–849.

(145) Ray-Coquard, I.; Blay, J. Y.; Italiano, A.; Le Cesne, A.; Penel, N.; Zhi, J.; Heil, F.; Rueger, R.; Graves, B.; Ding, M.; et al. Effect of the MDM2 Antagonist RG7112 on the P53 Pathway in Patients with MDM2-Amplified, Well-Differentiated or Dedifferentiated Liposarcoma: An Exploratory Proof-of-Mechanism Study. *Lancet Oncol.* **2012**, *13* (11), 1133–1140.

(146) Holzer, P.; Masuya, K.; Furet, P.; Kallen, J.; Valat-Stachyra, T.; Ferretti, S.; Berghausen, J.; Bouisset-Leonard, M.; Buschmann, N.; Pissot-Soldermann, C.; et al. Discovery of a Dihydroisoquinolinone Derivative (NVP-CGM097): A Highly Potent and Selective MDM2 Inhibitor Undergoing Phase 1 Clinical Trials in P53wt Tumors. *J. Med. Chem.* **2015**, *58* (16), 6348–6358.

(147) Ravandi, F.; Gojo, I.; Patnaik, M. M.; Minden, M. D.; Kantarjian, H.; Johnson-Levonas, A. O.; Fancourt, C.; Lam, R.; Jones, M. B.; Knox, C. D.; et al. A Phase I Trial of the Human Double Minute 2 Inhibitor (MK-8242) in Patients with Refractory/Recurrent Acute Myelogenous Leukemia (AML). *Leuk. Res.* **2016**, *48*, 92–100.

(148) Iancu-Rubin, C.; Mosoyan, G.; Glenn, K.; Gordon, R. E.; Nichols, G. L.; Hoffman, R. Activation of P53 by the MDM2 Inhibitor RG7112 Impairs Thrombopoiesis. *Exp. Hematol.* **2014**, *42* (2), 137-145.e5.

(149) Neklesa, T. K.; Winkler, J. D.; Crews, C. M. Targeted Protein Degradation by PROTACs. *Pharmacol. Ther.* **2017**, *174*, 138–144.

(150) Churcher, I. Protac-Induced Protein Degradation in Drug Discovery: Breaking the Rules or Just Making New Ones? *J. Med. Chem.* **2018**, *61* (2), 444–452.

(151) Zhou, B.; Hu, J.; Xu, F.; Chen, Z.; Bai, L.; Fernandez-Salas, E.; Lin, M.; Liu, L.; Yang, C. Y.; Zhao, Y.; et al. Discovery of a Small-Molecule Degrader of Bromodomain and Extra-Terminal (BET) Proteins with Picomolar Cellular Potencies and Capable of Achieving Tumor Regression. *J. Med. Chem.* **2018**, *61* (2), 462–481.

(152) Li, Y.; Yang, J.; Aguilar, A.; McEachern, D.; Przybranowski, S.; Liu, L.; Yang, C. Y.; Wang, M.; Han, X.; Wang, S. Discovery of MD-224 as a First-in-Class, Highly Potent, and Efficacious Proteolysis Targeting Chimera Murine Double Minute 2 Degrader Capable of Achieving Complete and Durable Tumor Regression. *J. Med. Chem.* **2019**, *62* (2), 448–466.

(153) Gembarska, A.; Luciani, F.; Fedele, C.; Russell, E. A.; Dewaele, M.; Villar, S.; Zwolinska, A.; Haupt, S.; De Lange, J.; Yip, D.; et al. MDM4 Is a Key Therapeutic Target in Cutaneous Melanoma. *Nat. Med.* **2012**, *18* (8), 1239–1247.

(154) Jochemsen, A. G. Reactivation of P53 as Therapeutic Intervention for Malignant Melanoma. *Curr. Opin. Oncol.* **2014**, *26* (1), 114–119.

(155) Popowicz, G. M.; Czarna, A.; Wolf, S.; Wang, K.; Wang, W.; Dömling, A.; Holak, T. A. Structures of Low Molecular Weight Inhibitors Bound to MDMX and MDM2 Reveal New Approaches for P53-MDMX/MDM2 Antagonist Drug Discovery. *Cell Cycle* **2010**,

9 (6), 1104–1111.

(156) Bista, M.; Smithson, D.; Pecak, A.; Salinas, G.; Pustelny, K.; Min, J.; Pirog, A.; Finch, K.; Zdzalik, M.; Waddell, B.; et al. On the Mechanism of Action of SJ-172550 in Inhibiting the Interaction of MDM4 and P53. *PLoS One* **2012**, *7* (6).

(157) Wang, H.; Ma, X.; Ren, S.; Buolamwini, J. K.; Yan, C. A Small-Molecule Inhibitor of MDMX Activates P53 and Induces Apoptosis. *Mol. Cancer Ther.* **2011**, *10* (1), 69–79.

(158) Vaseva, A. V.; Yallowitz, A. P.; Marchenko, N. D.; Xu, S.; Moll, U. M. Blockade of Hsp90 by 17AAG Antagonizes MDMX and Synergizes with Nutlin to Induce P53-Mediated Apoptosis in Solid Tumors. *Cell Death Dis.* **2011**, *2* (5).

(159) Roh, J. L.; Park, J. Y.; Kim, E. H. XI-011 Enhances Cisplatin-Induced Apoptosis by Functional Restoration of P53 in Head and Neck Cancer. *Apoptosis* **2014**, *19* (11), 1594–1602.

(160) Wang, H.; Ma, X.; Ren, S.; Buolamwini, J. K.; Yan, C. A Small-Molecule Inhibitor of MDMX Activates P53 and Induces Apoptosis. *Mol. Cancer Ther.* **2011**, *10* (1), 69–79.

(161) Karan, G.; Wang, H.; Chakrabarti, A.; Karan, S.; Liu, Z.; Xia, Z.; Gundluru, M.; Moreton, S.; Sauntharajah, Y.; Jackson, M. W.; et al. Identification of a Small Molecule That Overcomes HdmX-Mediated Suppression of P53. *Mol. Cancer Ther.* **2016**, *15* (4), 574–582.

(162) Graves, B.; Thompson, T.; Xia, M.; Janson, C.; Lukacs, C.; Deo, D.; Lello, P. Di; Fry, D.; Garvie, C.; Huang, K.; et al. Activation of the P53 Pathway by Small-Molecule-Induced MDM2 and MDMX Dimerization. *Proc. Natl. Acad. Sci. U.S.A.* **2012**, *109* (29), 11788–11793.

(163) Bernal, F.; Wade, M.; Godes, M.; Davis, T. N.; Whitehead, D. G.; Kung, A. L.; Wahl, G. M.; Walensky, L. D. A Stapled P53 Helix Overcomes HDMX-Mediated Suppression of P53. *Cancer Cell* **2010**, *18* (5), 411–422.

(164) Pazgier, M.; Liu, M.; Zou, G.; Yuan, W.; Li, C.; Li, C.; Li, J.; Monbo, J.; Zella, D.; Tarasov, S. G.; et al. Structural Basis for High-Affinity Peptide Inhibition of P53 Interactions with MDM2 and MDMX. *Proc. Natl. Acad. Sci. U. S. A.* **2009**, *106* (12), 4665–4670.

(165) Hu, B.; Gilkes, D. M.; Chen, J. Efficient P53 Activation and Apoptosis by Simultaneous Disruption of Binding to MDM2 and MDMX. *Cancer Res.* **2007**, *67* (18),

8810–8817.

(166) Lehman, J. A.; Hauck, P. M.; Gendron, J. M.; Batuello, C. N.; Eitel, J. A.; Albig, A.; Kadakia, M. P.; Mayo, L. D. Serdemetan Antagonizes the Mdm2-HIF1α Axis Leading to Decreased Levels of Glycolytic Enzymes. *PLoS One* **2013**, *8* (9), 8–12.

(167) Al-Lazikani, B.; Banerji, U.; Workman, P. Combinatorial Drug Therapy for Cancer in the Post-Genomic Era. *Nat. Biotechnol.* **2012**, *30* (7), 679–692.

(168) Bykov, V. J. N.; Issaeva, N.; Shilov, A.; Hultcrantz, M.; Pugacheva, E.; Chumakov, P.; Bergman, J.; Wiman, K. G.; Selivanova, G. Restoration of the Tumor Suppressor Function to Mutant P53 by a Low-Molecular-Weight Compound. *Nat. Med.* **2002**, *8* (3), 282–288.

(169) Lehmann, S.; Bykov, V. J. N.; Ali, D.; Andreń, O.; Cherif, H.; Tidefelt, U.; Uggla, B.; Yachnin, J.; Juliusson, G.; Moshfegh, A.; et al. Targeting P53 in Vivo: A First-in-Human Study with P53-Targeting Compound APR-246 in Refractory Hematologic Malignancies and Prostate Cancer. *J. Clin. Oncol.* **2012**, *30* (29), 3633–3639.

(170) Bykov, V. J. N.; Issaeva, N.; Zache, N.; Shilov, A.; Hultcrantz, M.; Bergman, J.; Selivanova, G.; Wiman, K. G. Reactivation of Mutant P53 and Induction of Apoptosis in Human Tumor Cells by Maleimide Analogs. *J. Biol. Chem.* **2005**, *280* (34), 30384–30391.

(171) Zache, N.; Lambert, J. M. R.; Rökaeus, N.; Shen, J.; Hainaut, P.; Bergman, J.; Wiman, K. G.; Bykov, V. J. N. Mutant P53 Targeting by the Low Molecular Weight Compound STIMA-1. *Mol. Oncol.* **2008**, *2* (1), 70–80.

(172) Boeckler, F. M.; Joerger, A. C.; Jaggi, G.; Rutherford, T. J.; Veprintsev, D. B.; Fersht, A. R. Targeted Rescue of a Destabilized Mutant of P53 by an in Silico Screened Drug. *Proc. Natl. Acad. Sci.* **2008**, *105* (30), 10360–10365.

(173) Yu, X.; Vazquez, A.; Levine, A. J.; Carpizo, D. R. Allele-Specific P53 Mutant Reactivation. *Cancer Cell* **2012**, *21* (5), 614–625.

(174) Foster, B. A.; Coffey, H. A.; Morin, M. J.; Rastinejad, F. Pharmacological Rescue of Mutant P53 Conformation and Function. *Science (80-.).* **1999**, *286* (5449), 2507–2510.

(175) Demma, M.; Maxwell, E.; Ramos, R.; Liang, L.; Li, C.; Hesk, D.; Rossman, R.; Mallams, A.; Doll, R.; Liu, M.; et al. SCH529074, a Small Molecule Activator of Mutant P53, Which Binds P53 DNA Binding Domain (DBD), Restores Growth-Suppressive Function to Mutant P53 and Interrupts HDM2-Mediated Ubiquitination of Wild Type

P53. *J. Biol. Chem.* **2010**, *285* (14), 10198–10212.

(176) Peng, Y.; Li, C.; Chen, L.; Sebti, S.; Chen, J. Rescue of Mutant P53 Transcription Function by Ellipticine. *Oncogene* **2003**, *22* (29), 4478–4487.

(177) Weinmann, L.; Wischhusen, J.; Demma, M. J.; Naumann, U.; Roth, P.; DasMahapatra, B.; Weller, M. A Novel P53 Rescue Compound Induces P53-Dependent Growth Arrest and Sensitises Glioma Cells to Apo2L/TRAIL-Induced Apoptosis. *Cell Death Differ.* **2008**, *15* (4), 718–729.

(178) Rippin, T. M.; Bykov, V. J. N.; Freund, S. M. V; Selivanova, G.; Wiman, K. G.; Fersht, A. R. Characterization of the P53-Rescue Drug CP-31398 in Vitro and in Living Cells. *Oncogene* **2002**, *21* (14), 2119–2129.

(179) Liu, X.; Wilcken, R.; Joerger, A. C.; Chuckowree, I. S.; Amin, J.; Spencer, J.; Fersht, A. R. Small Molecule Induced Reactivation of Mutant P53 in Cancer Cells. *Nucleic Acids Res.* **2013**, *41* (12), 6034–6044.

(180) Punganuru, S. R.; Madala, H. R.; Arutla, V.; Srivenugopal, K. S. Selective Killing of Human Breast Cancer Cells by the Styryl Lactone (R)-Goniothalamin Is Mediated by Glutathione Conjugation, Induction of Oxidative Stress and Marked Reactivation of the R175H Mutant P53 Protein. *Carcinogenesis* **2018**, *39* (11), 1399–1410.

(181) Baud, M. G. J.; Bauer, M. R.; Verduci, L.; Dingler, F. A.; Patel, K. J.; Horil Roy, D.; Joerger, A. C.; Fersht, A. R. Aminobenzothiazole Derivatives Stabilize the Thermolabile P53 Cancer Mutant Y220C and Show Anticancer Activity in P53-Y220C Cell Lines. *Eur. J. Med. Chem.* **2018**, *152*, 101–114.

(182) Salim, K. Y.; Vareki, S. M.; Danter, W. R.; San-Marina, S.; Koropatnick, J. COTI-2, a Novel Small Molecule That Is Active against Multiple Human Cancer Cell Lines *in Vitro* and *in Vivo*. *Oncotarget* **2016**, *7* (27).

(183) Aggarwal, M.; Saxena, R.; Sinclair, E.; Fu, Y.; Jacobs, A.; Dyba, M.; Wang, X.; Cruz, I.; Berry, D.; Kallakury, B.; et al. Reactivation of Mutant P53 by a Dietary-Related Compound Phenethyl Isothiocyanate Inhibits Tumor Growth. *Cell Death Differ.* **2016**, *23* (10), 1615–1627.

(184) Kravchenko, J. E.; Ilyinskaya, G. V.; Komarov, P. G.; Agapova, L. S.; Kochetkov, D. V.; Strom, E.; Frolova, E. I.; Kovriga, I.; Gudkov, A. V.; Feinstein, E.; et al. Small-Molecule RETRA Suppresses Mutant P53-Bearing Cancer Cells through a P73-Dependent Salvage Pathway. *Proc. Natl. Acad. Sci.* **2008**, *105* (17), 6302–6307.

(185) Li, D.; Marchenko, N. D.; Moll, U. M. SAHA Shows Preferential Cytotoxicity in Mutant

P53 Cancer Cells by Destabilizing Mutant P53 through Inhibition of the HDAC6-Hsp90 Chaperone Axis. *Cell Death Differ.* **2011**, *18* (12), 1904–1913.

(186) Hiraki, M.; Hwang, S. Y.; Cao, S.; Ramadhar, T. R.; Byun, S.; Yoon, K. W.; Lee, J. H.; Chu, K.; Gurkar, A. U.; Kolev, V.; et al. Small-Molecule Reactivation of Mutant P53 to Wild-Type-like P53 through the P53-Hsp40 Regulatory Axis. *Chem. Biol.* **2015**, *22* (9), 1206–1216.

(187) Punganuru, S. R.; Madala, H. R.; Venugopal, S. N.; Samala, R.; Mikelis, C.; Srivenugopal, K. S. Design and Synthesis of a C7-Aryl Piperlongumine Derivative with Potent Antimicrotubule and Mutant P53-Reactivating Properties. *Eur. J. Med. Chem.* **2016**, *107*, 233–244.

(188) Soares, J.; Raimundo, L.; Pereira, N. A. L.; Monteiro, Â.; Gomes, S.; Bessa, C.; Pereira, C.; Queiroz, G.; Bisio, A.; Fernandes, J.; et al. Reactivation of Wild-Type and Mutant P53 by Tryptophanolderived Oxazoloisoindolinone SLMP53-1, a Novel Anticancer Small-Molecule. *Oncotarget* **2015**, *7* (4).

(189) Li, X.-L.; Zhou, J.; Chan, Z.-L.; Chooi, J.-Y.; Chen, Z.-R.; Chng, W.-J. PRIMA-1^{Met} (APR-246) Inhibits Growth of Colorectal Cancer Cells with Different P53 Status through Distinct Mechanisms. *Oncotarget* **2015**, *6* (34), 22–25.

(190) Lu, T.; Zou, Y.; Xu, G.; Potter, J. A.; Taylor, G. L.; Duan, Q.; Yang, Q.; Xiong, H.; Qiu, H.; Ye, D.; et al. PRIMA-1^{Met} Suppresses Colorectal Cancer Independent of P53 by Targeting MEK. *Oncotarget* **2016**, *7* (50), 83017–83030.

(191) Peng, X.; Zhang, M. Q. Z.; Conserva, F.; Hosny, G.; Selivanova, G.; Bykov, V. J. N.; Arnér, E. S. J.; Wiman, K. G. APR-246/PRIMA-1MET Inhibits Thioredoxin Reductase 1 and Converts the Enzyme to a Dedicated NADPH Oxidase. *Cell Death Dis.* **2013**, *4* (10), 1–7.

(192) Bykov, V. J. N.; Issaeva, N.; Zache, N.; Shilov, A.; Hultcrantz, M.; Bergman, J.; Selivanova, G.; Wiman, K. G. Reactivation of Mutant P53 and Induction of Apoptosis in Human Tumor Cells by Maleimide Analogs. *J. Biol. Chem.* **2005**, *280* (34), 30384–30391.

(193) Bou-Hanna, C.; Jarry, A.; Lode, L.; Schmitz, I.; Schulze-Osthoff, K.; Kury, S.; Bezieau, S.; Mosnier, J. F.; Laboisse, C. L. Acute Cytotoxicity of MIRA-1/NSC19630, a Mutant P53-Reactivating Small Molecule, against Human Normal and Cancer Cells via a Caspase-9-Dependent Apoptosis. *Cancer Lett.* **2015**, *359* (2), 211–217.

(194) Chan, K. M.; Rajab, N. F.; Siegel, D.; Din, L. Bin; Ross, D.; Inayat-Hussain, S. H.

Goniothalamin Induces Coronary Artery Smooth Muscle Cells Apoptosis: The P53-Dependent Caspase-2 Activation Pathway. *Toxicol. Sci.* **2010**, *116* (2), 533–548.

(195) Bauer, M. R.; Joerger, A. C.; Fersht, A. R. 2-Sulfonylpyrimidines: Mild Alkylating Agents with Anticancer Activity toward P53-Compromised Cells. *Proc. Natl. Acad. Sci.* **2016**, *113* (36), E5271–E5280.

(196) Lambert, J. M. R.; Gorzov, P.; Veprintsev, D. B.; Söderqvist, M.; Segerbäck, D.; Bergman, J.; Fersht, A. R.; Hainaut, P.; Wiman, K. G.; Bykov, V. J. N. PRIMA-1 Reactivates Mutant P53 by Covalent Binding to the Core Domain. *Cancer Cell* **2009**, *15* (5), 376–388.

(197) Wassman, C. D.; Baronio, R.; Demir, Ö.; Wallentine, B. D.; Chen, C.-K.; Hall, L. V; Salehi, F.; Lin, D.-W.; Chung, B. P.; Hatfield, G. W.; et al. Computational Identification of a Transiently Open L1/S3 Pocket for Reactivation of Mutant P53. *Nat. Commun.* **2013**, *4*, 1407.

(198) Adams, D. J.; Dai, M.; Pellegrino, G.; Wagner, B. K.; Stern, A. M.; Shamji, A. F.; Schreiber, S. L. Synthesis, Cellular Evaluation, and Mechanism of Action of Piperlongumine Analogs. *Proc. Natl. Acad. Sci.* **2012**, *109* (38), 15115–15120.

(199) Pettit, G. R.; Singh, S. B.; Hamel, E.; Lin, C. M.; Alberts, D. S.; Garcia-Kendal, D. Isolation and Structure of the Strong Cell Growth and Tubulin Inhibitor Combretastatin A-4. *Experientia* **1989**, *45* (2), 209–211.

(200) Batovska, D. I.; Todorova, I. T. Trends in Utilization of the Pharmacological Potential of Chalcones. *Curr. Clin. Pharmacol.* **2010**, *5*, 1–29.

(201) Singh, P.; Anand, A.; Kumar, V. Recent Developments in Biological Activities of Chalcones: A Mini Review. *Eur. J. Med. Chem.* **2014**, *85*, 758–777.

(202) Karthikeyan, C.; Narayana Moorthy, N. S.; Ramasamy, S.; Vanam, U.; Manivannan, E.; Karunagaran, D.; Trivedi, P. Advances in Chalcones with Anticancer Activities. *Recent Pat. Anticancer. Drug Discov.* **2014**, *10* (February 2016), 97–115.

(203) K. Sahu, N.; S. Balbhadra, S.; Choudhary, J.; V. Kohli, D. Exploring Pharmacological Significance of Chalcone Scaffold: A Review. *Curr. Med. Chem.* **2012**, *19* (2), 209–225.

(204) Zhou, B.; Xing, C. Diverse Molecular Targets for Chalcones with Varied Bioactivities. *Med. Chem. (Los. Angeles).* **2016**, *5* (8), 388–404.

(205) Sebti, S.; Solhy, A.; Smahi, A.; Kossir, A.; Oumimoun, H. Dramatic Activity

Enhancement of Natural Phosphate Catalyst by Lithium Nitrate. An Efficient Synthesis of Chalcones. *Catal. Commun.* **2002**, *3* (8), 335–339.

(206) Mdee, L. K.; Yeboah, S. O.; Abegaz, B. M. Rhuschalcones II-VI, Five New Bichalcones from the Root Bark of Rhus Pyroides. *J. Nat. Prod.* **2003**, *66* (5), 599–604.

(207) Dao, T. T. H.; Linthorst, H. J. M.; Verpoorte, R. Chalcone Synthase and Its Functions in Plant Resistance. *Phytochem. Rev.* **2011**, *10* (3), 397–412.

(208) Hahlbrock, K.; Scheel, D. Biology of Phenylpropanoid Metabolism. *Annu. Rev. Plant Physiol. Plant Mol. Biol.* **1989**, No. 40, 347–369.

(209) Mishra, L.; Sinha, R.; Itokawa, H.; Bastow, K. F.; Tachibana, Y.; Nakanishi, Y.; Lee, K. Anti-HIV and Cytotoxic Activities of Ru (II)/ Ru (III) Polypyridyl as Co-Ligand. *Bioorg. Med. Chem.* **2001**, *9*, 1667–1671.

(210) Coskun, D.; Erkisa, M.; Ulukaya, E.; Coskun, M. F.; Ari, F. Novel 1-(7-Ethoxy-1-Benzofuran-2-Yl) Substituted Chalcone Derivatives: Synthesis, Characterization and Anticancer Activity. *Eur. J. Med. Chem.* **2017**, *136*, 212–222.

(211) Bhale, P. S.; Chavan, H. V.; Dongare, S. B.; Shringare, S. N.; Mule, Y. B.; Nagane, S. S.; Bandgar, B. P. Synthesis of Extended Conjugated Indolyl Chalcones as Potent Anti-Breast Cancer, Anti-Inflammatory and Antioxidant Agents. *Bioorganic Med. Chem. Lett.* **2017**, *27* (7), 1502–1507.

(212) Gomes, M. N.; Braga, R. C.; Grzelak, E. M.; Neves, B. J.; Muratov, E.; Ma, R.; Klein, L. L.; Cho, S.; Oliveira, G. R.; Franzblau, S. G.; et al. QSAR-Driven Design, Synthesis and Discovery of Potent Chalcone Derivatives with Antitubercular Activity. *Eur. J. Med. Chem.* **2017**, *137*, 126–138.

(213) Li, J.; Li, D.; Xu, Y.; Guo, Z.; Liu, X.; Yang, H.; Wu, L.; Wang, L. Design, Synthesis, Biological Evaluation, and Molecular Docking of Chalcone Derivatives as Anti-Inflammatory Agents. *Bioorganic Med. Chem. Lett.* **2017**, *27* (3), 602–606.

(214) Israf, D. A.; Khaizurin, T. A.; Syahida, A.; Lajis, N. H.; Khozirah, S. Cardamonin Inhibits COX and INOS Expression via Inhibition of P65NF-KB Nuclear Translocation and Iκ-B Phosphorylation in RAW 264.7 Macrophage Cells. *Mol. Immunol.* **2007**, *44* (5), 673–679.

(215) Cole, A. L.; Hossain, S.; Cole, A. M.; Phanstiel, O. Synthesis and Bioevaluation of Substituted Chalcones, Coumaranones and Other Flavonoids as Anti-HIV Agents. *Bioorganic Med. Chem.* **2016**, *24* (12), 2768–2776.

(216) Gan, X.; Hu, D.; Wang, Y.; Yu, L.; Song, B. Novel Trans-Ferulic Acid Derivatives Containing a Chalcone Moiety as Potential Activator for Plant Resistance Induction. *J. Agric. Food Chem.* **2017**, *65* (22), 4367–4377.

(217) Silva, G.; Marins, M.; Fachin, A. L.; Lee, S. H.; Baek, S. J. Anti-Cancer Activity of Trans-Chalcone in Osteosarcoma: Involvement of Sp1 and P53. *Mol. Carcinog.* **2016**, *55* (10), 1438–1448.

(218) Silva, G.; Marins, M.; Chaichanasak, N.; Yoon, Y.; Fachin, A. L.; Pinhanelli, V. C.; Regasini, L. O.; Dos Santos, M. B.; Ayusso, G. M.; De Carvalho Marques, B.; et al. Trans-Chalcone Increases P53 Activity via DNAJB1/HSP40 Induction and CRM1 Inhibition. *PLoS One* **2018**, *13* (8), 1–16.

(219) Hsu, Y. L.; Kuo, P. L.; Chiang, L. C.; Lin, C. C. Isoliquiritigenin Inhibits the Proliferation and Induces the Apoptosis of Human Non-Small Cell Lung Cancer A549 Cells. *Clin. Exp. Pharmacol. Physiol.* **2004**, *31* (7), 414–418.

(220) Rao, Y. K.; Kao, T. Y.; Ko, J. L.; Tzeng, Y. M. Chalcone HTMC Causes in Vitro Selective Cytotoxicity, Cell-Cycle G 1 Phase Arrest through P53-Dependent Pathway in Human Lung Adenocarcinoma A549 Cells, and in Vivo Tumor Growth Suppression. *Bioorganic Med. Chem. Lett.* **2010**, *20* (22), 6508–6512.

(221) Zhou, Y.; Ho, W. S. Combination of Liquiritin, Isoliquiritin and Isoliquirigenin Induce Apoptotic Cell Death through Upregulating P53 and P21 in the A549 Non-Small Cell Lung Cancer Cells. *Oncol. Rep.* **2014**, *31* (1), 298–304.

(222) Hsu, Y. L.; Kuo, P. L.; Lin, C. C. Isoliquiritigenin Induces Apoptosis and Cell Cycle Arrest through P53-Dependent Pathway in Hep G2 Cells. *Life Sci.* **2005**, *77* (3), 279–292.

(223) Hsu, Y. L.; Chia, C. C.; Chen, P. J.; Huang, S. E.; Huang, S. C.; Kuo, P. L. Shallot and Licorice Constituent Isoliquiritigenin Arrests Cell Cycle Progression and Induces Apoptosis through the Induction of ATM/P53 and Initiation of the Mitochondrial System in Human Cervical Carcinoma HeLa Cells. *Mol. Nutr. Food Res.* **2009**, *53* (7), 826–835.

(224) Kim, D. H.; Park, J. E.; Chae, I. G.; Park, G.; Lee, S. Y.; Chun, K. S. Isoliquiritigenin Inhibits the Proliferation of Human Renal Carcinoma Caki Cells through the ROS-Mediated Regulation of the Jak2/STAT3 Pathway. *Oncol. Rep.* **2017**, *38* (1), 575–583.

(225) Tang, Y.; Simoneau, A. R.; Xie, J.; Shahandeh, B.; Zi, X. Effects of the Kava

Chalcone Flavokawain A Differ in Bladder Cancer Cells with Wild-Type versus Mutant P53. *Cancer Prev. Res.* **2008**, *1* (6), 439–451.

(226) Fang, S. C.; Hsu, C. L.; Yu, Y. S.; Yen, G. C. Cytotoxic Effects of New Geranyl Chalcone Derivatives Isolated from the Leaves of Artocarpus Communis in SW 872 Human Liposarcoma Cells. *J. Agric. Food Chem.* **2008**, *56* (19), 8859–8868.

(227) Sławińska-Brych, A.; Zdzisińska, B.; Dmoszyńska-Graniczka, M.; Jeleniewicz, W.; Kurzepa, J.; Gagoś, M.; Stepulak, A. Xanthohumol Inhibits the Extracellular Signal Regulated Kinase (ERK) Signalling Pathway and Suppresses Cell Growth of Lung Adenocarcinoma Cells. *Toxicology* **2016**, *357–358*, 65–73.

(228) Lin, E.; Lin, W. H.; Wang, S. Y.; Chen, C. S.; Liao, J. W.; Chang, H. W.; Chen, S. C.; Lin, K. Y.; Wang, L.; Yang, H. L.; et al. Flavokawain B Inhibits Growth of Human Squamous Carcinoma Cells: Involvement of Apoptosis and Cell Cycle Dysregulation in Vitro and in Vivo. *J. Nutr. Biochem.* **2012**, *23* (4), 368–378.

(229) Hsu, Y. L.; Chia, C. C.; Chen, P. J.; Huang, S. E.; Huang, S. C.; Kuo, P. L. Shallot and Licorice Constituent Isoliquiritigenin Arrests Cell Cycle Progression and Induces Apoptosis through the Induction of ATM/P53 and Initiation of the Mitochondrial System in Human Cervical Carcinoma HeLa Cells. *Mol. Nutr. Food Res.* **2009**, *53* (7), 826–835.

(230) Pedrini, F. S.; Chiaradia, L. D.; Licínio, M. A.; De Moraes, A. C. R.; Curta, J. C.; Costa, A.; Mascarello, A.; Creczinsky-Pasa, T. B.; Nunes, R. J.; Yunes, R. A.; et al. Induction of Apoptosis and Cell Cycle Arrest in L-1210 Murine Lymphoblastic Leukaemia Cells by (2 *E*)-3-(2-Naphthyl)-1-(3′-Methoxy-4′-Hydroxy-Phenyl)-2-Propen-1-One. *J. Pharm. Pharmacol.* **2010**, *62* (9), 1128–1136.

(231) Kamal, A.; Dastagiri, D.; Ramaiah, M. J.; Reddy, J. S.; Bharathi, E. V.; Srinivas, C.; Pushpavalli, S. N. C. V. L.; Pal, D.; Pal-Bhadra, M. Synthesis of Imidazothiazole-Chalcone Derivatives as Anticancer and Apoptosis Inducing Agents. *ChemMedChem* **2010**, *5* (11), 1937–1947.

(232) Zhang, Y.; Srinivasan, B.; Xing, C.; Lü, J. A New Chalcone Derivative (E)-3-(4-Methoxyphenyl)-2-Methyl-1-(3,4,5- Trimethoxyphenyl)Prop-2-En-1-One Suppresses Prostate Cancer Involving P53-Mediated Cell Cycle Arrests and Apoptosis. *Anticancer Res.* **2012**, *32* (9), 3689–3698.

(233) De Vasconcelos, A.; Campos, V. F.; Nedel, F.; Seixas, F. K.; Dellagostin, O. A.; Smith, K. R.; De Pereira, C. M. P.; Stefanello, F. M.; Collares, T.; Barschak, A. G. Cytotoxic

and Apoptotic Effects of Chalcone Derivatives of 2-Acetyl Thiophene on Human Colon Adenocarcinoma Cells. *Cell Biochem. Funct.* **2013**, *31* (4), 289–297.

(234) Shin, S. Y.; Yong, Y.; Lee, J.; Ahn, S.; Jung, K. Y.; Koh, D.; Lee, Y. H.; Lim, Y. A Novel Hydroxymethoxynaphthochalcone Induces Apoptosis through the P53-Dependent Caspase-Mediated Pathway in HCT116 Human Colon Cancer Cells. *J. Korean Soc. Appl. Biol. Chem.* **2014**, *57* (4), 413–418.

(235) Lee, J. M.; Lee, M. S.; Koh, D.; Lee, Y. H.; Lim, Y.; Shin, S. Y. A New Synthetic 2'-Hydroxy-2,4,6-Trimethoxy-5',6'-Naphthochalcone Induces G2/M Cell Cycle Arrest and Apoptosis by Disrupting the Microtubular Network of Human Colon Cancer Cells. *Cancer Lett.* **2014**, *354* (2), 348–354.

(236) Wang, J.; Yang, Z.; Wen, J.; Ma, F.; Wang, F.; Yu, K.; Tang, M.; Wu, W.; Dong, Y.; Cheng, X.; et al. SKLB-M8 Induces Apoptosis Through the AKT/MTOR Signaling Pathway in Melanoma Models and Inhibits Angiogenesis With Decrease of ERK1/2 Phosphorylation. *J. Pharmacol. Sci.* **2014**, *126* (3), 198–207.

(237) Lai, C. K.; Rao, Y. K.; Chang, K. R.; Lin, C. W.; Su, H. L.; Chang, C. S.; Lai, C. H.; Tzeng, Y. M. 3,3',4', 5'-Tetramethoxychalcone Inhibits Human Oral Cancer Cell Proliferation and Migration via P53-Mediated Mitochondrial-Dependent Apoptosis. *Anticancer Res.* **2014**, No. 34, 1811–1820.

(238) Qi, Z.; Liu, M.; Liu, Y.; Zhang, M.; Yang, G. Tetramethoxychalcone, a Chalcone Derivative, Suppresses Proliferation, Blocks Cell Cycle Progression, and Induces Apoptosis of Human Ovarian Cancer Cells. *PLoS One* **2014**, *9* (9), 1–11.

(239) Singh, N.; Sarkar, J.; Sashidhara, K. V.; Ali, S.; Sinha, S. Anti-Tumour Activity of a Novel Coumarin-Chalcone Hybrid Is Mediated through Intrinsic Apoptotic Pathway by Inducing PUMA and Altering Bax/Bcl-2 Ratio. *Apoptosis* **2014**, *19* (6), 1017–1028.

(240) Loch-Neckel, G.; Bicca, M. A.; Leal, P. C.; Mascarello, A.; Siqueira, J. M.; Calixto, J. B. In Vitro and in Vivo Anti-Glioma Activity of a Chalcone-Quinoxaline Hybrid. *Eur. J. Med. Chem.* **2015**, *90*, 93–100.

(241) Ma, L.; Ma, R.; Wang, Y.; Zhu, X.; Zhang, J.; Chan, H. C.; Chen, X.; Zhang, W.; Chiu, S. K.; Zhu, G. Chalcoplatin, a Dual-Targeting and P53 Activator-Containing Anticancer Platinum(Iv) Prodrug with Unique Mode of Action. *Chem. Commun.* **2015**, *51* (29), 6301–6304.

(242) Singh, A. K.; Chauhan, S. S.; Singh, S. K.; Verma, V. V.; Singh, A.; Arya, R. K.; Maheshwari, S.; Akhtar, M. S.; Sarkar, J.; Rangnekar, V. M.; et al. Dual Targeting of

MDM2 with a Novel Small Molecule Inhibitor Overcomes TRAIL Resistance in Cancer. *Carcinogenesis* **2016**, *37* (11), 1027–1040.

(243) Fu, D. J.; Zhang, S. Y.; Liu, Y. C.; Yue, X. X.; Liu, J. J.; Song, J.; Zhao, R. H.; Li, F.; Sun, H. H.; Zhang, Y. B.; et al. Design, Synthesis and Antiproliferative Activity Studies of 1,2,3-Triazole-Chalcones. *Medchemcomm* **2016**, *7* (8), 1664–1671.

(244) Fu, D. J.; Zhang, S. Y.; Liu, Y. C.; Zhang, L.; Liu, J. J.; Song, J.; Zhao, R. H.; Li, F.; Sun, H. H.; Liu, H. M.; et al. Design, Synthesis and Antiproliferative Activity Studies of Novel Dithiocarbamate–Chalcone Derivates. *Bioorganic Med. Chem. Lett.* **2016**, *26* (16), 3918–3922.

(245) Shin, S. Y.; Ahn, S.; Koh, D.; Lim, Y. P53-Dependent and -Independent Mechanisms Are Involved in (E)-1-(2-Hydroxyphenyl)-3-(2-Methoxynaphthalen-1-Yl)Prop-2-En-1-One (HMP)-Induced Apoptosis in HCT116 Colon Cancer Cells. *Biochem. Biophys. Res. Commun.* **2016**, *479* (4), 913–919.

(246) Cao, L.; Zhang, L.; Zhao, X.; Zhang, Y. A Hybrid Chalcone Combining the Trimethoxyphenyl and Isatinyl Groups Targets Multiple Oncogenic Proteins and Pathways in Hepatocellular Carcinoma Cells. *PLoS One* **2016**, *11* (8), 1–23.

(247) Iftikhar, S.; Khan, S.; Bilal, A.; Manzoor, S.; Abdullah, M.; Emwas, A. H.; Sioud, S.; Gao, X.; Chotana, G. A.; Faisal, A.; et al. Synthesis and Evaluation of Modified Chalcone Based P53 Stabilizing Agents. *Bioorganic Med. Chem. Lett.* **2017**, *27* (17), 4101–4106.

(248) Cabral, B. L. S.; da Silva, A. C. G.; de Ávila, R. I.; Cortez, A. P.; Luzin, R. M.; Lião, L. M.; de Souza Gil, E.; Sanz, G.; Vaz, B. G.; Sabino, J. R.; et al. A Novel Chalcone Derivative, LQFM064, Induces Breast Cancer Cells Death via P53, P21, KIT and PDGFRA. *Eur. J. Pharm. Sci.* **2017**, *107* (April), 1–15.

(249) Bagul, C.; Rao, G. K.; Makani, V. K. K.; Tamboli, J. R.; Pal-Bhadra, M.; Kamal, A. Synthesis and Biological Evaluation of Chalcone-Linked Pyrazolo[1,5-a]Pyrimidines as Potential Anticancer Agents. *Medchemcomm* **2017**, *8* (9), 1810–1816.

(250) Mu, J.; Wang, X.; Dong, L.; Sun, P. Curcumin Derivative L6H4 Inhibits Proliferation and Invasion of Gastric Cancer Cell Line BGC-823. *J. Cell. Biochem.* **2018**, No. July, 1011–1017.

(251) Seba, V.; Silva, G.; Dos Santos, M. B.; Baek, S. J.; França, S. de C.; Fachin, A. L.; Regasini, L. O.; Marins, M. Chalcone Derivatives 4′-Amino-1-Naphthyl-Chalcone (D14) and 4′-Amino-4-Methyl-1-Naphthyl-Chalcone (D15) Suppress Migration and

Invasion of Osteosarcoma Cells Mediated by P53 Regulating Emt-Related Genes. *Int. J. Mol. Sci.* **2018**, *19* (9), 1–13.

(252) Leroy, B.; Girard, L.; Hollestelle, A.; Minna, J. D.; Gazdar, A. F.; Soussi, T. Analysis of TP53 Mutation Status in Human Cancer Cell Lines: A Reassessment. *Hum. Mutat.* **2014**, *35* (6), 756–765.

(253) Mohamed, M. F.; Hassaneen, H. M.; Abdelhamid, I. A. Cytotoxicity, Molecular Modeling, Cell Cycle Arrest, and Apoptotic Induction Induced by Novel Tetrahydro-[1,2,4]Triazolo[3,4-a] Isoquinoline Chalcones. *Eur. J. Med. Chem.* **2018**, *143*, 532–541.

(254) Stoll, R.; Renner, C.; Hansen, S.; Palme, S.; Klein, C.; Belling, A.; Zeslawski, W.; Kamionka, M.; Rehm, T.; Mühlhahn, P.; et al. Chalcone Derivatives Antagonize Interactions between the Human Oncoprotein MDM2 and P53. *Biochemistry* **2001**, *40* (2), 336–344.

(255) Leão, M.; Soares, J.; Gomes, S.; Raimundo, L.; Ramos, H.; Bessa, C.; Queiroz, G.; Domingos, S.; Pinto, M.; Inga, A.; et al. Enhanced Cytotoxicity of Prenylated Chalcone against Tumour Cells via Disruption of the P53-MDM2 Interaction. *Life Sci.* **2015**, *142*, 60–65.

(256) Pereira, D.; Lima, R. T.; Palmeira, A.; Seca, H.; Soares, J.; Gomes, S.; Raimundo, L.; Maciel, C.; Pinto, M.; Sousa, E.; et al. Design and Synthesis of New Inhibitors of P53-MDM2 Interaction with a Chalcone Scaffold. *Arab. J. Chem.* **2016**.

(257) Brandão, P.; Loureiro, J. B.; Carvalho, S.; Hamadou, M. H.; Cravo, S.; Moreira, J.; Pereira, D.; Palmeira, A.; Pinto, M.; Saraiva, L.; et al. Targeting the MDM2-P53 Protein-Protein Interaction with Prenylchalcones: Synthesis of a Small Library and Evaluation of Potential Antitumor Activity. *Eur. J. Med. Chem.* **2018**, *156*, 711–721.

(258) Modzelewska, A.; Pettit, C.; Achanta, G.; Davidson, N. E.; Huang, P.; Khan, S. R. Anticancer Activities of Novel Chalcone and Bis-Chalcone Derivatives. *Bioorganic Med. Chem.* **2006**, *14* (10), 3491–3495.

(259) Achanta, G.; Modzelewska, A.; Feng, L.; Khan, S. R.; Huang, P. A Boronic-Chalcone Derivative Exhibits Potent Anti-Cancer Activity through Inhibition of the Proteasome. *Mol. Pharmacol.* **2006**, *70* (1), 426–433.

(260) Selvendiran, K.; Tong, L.; Vishwanath, S.; Bratasz, A.; Trigg, N. J.; Kutala, V. K.; Hideg, K.; Kuppusamy, P. EF24 Induces G2/M Arrest and Apoptosis in Cisplatin-Resistant Human Ovarian Cancer Cells by Increasing PTEN Expression. *J. Biol.*

Chem. **2007**, *282* (39), 28609–28618.

(261) Selvendiran, K.; Tong, L.; Bratasz, A.; Kuppusamy, M. L.; Ahmed, S.; Rav, Y.; Trigg, N. J.; Rivera, B. K.; Kálai, T.; Kuppusamy, P.; et al. Anticancer Efficacy of a Difluorodiarylidenyl Piperidone (HO-3867) in Human Ovarian Cancer Cells and Tumor Xenografts. *Mol. Cancer Ther.* **2010**, *9* (5), 1169–1179.

(262) Kálai, T.; Kuppusamy, M. L.; Balog, M.; Selvendiran, K.; Rivera, B. K.; Kuppusamy, P.; Hideg, K. Synthesis of N-Substituted 3,5-Bis(Arylidene)-4-Piperidones with High Antitumor and Antioxidant Activity. *J. Med. Chem.* **2011**, *54* (15), 5414–5421.

(263) Anchoori, R. K.; Khan, S. R.; Sueblinvong, T.; Felthauser, A.; Iizuka, Y.; Gavioli, R.; Destro, F.; Vogel, R. I.; Peng, S.; Roden, R. B. S.; et al. Stressing the Ubiquitin-Proteasome System without 20s Proteolytic Inhibition Selectively Kills Cervical Cancer Cells. *PLoS One* **2011**, *6* (8), 1–10.

(264) Pereira, C.; Bisio, A.; Ciribilli, Y.; Paiva, A. M.; Pinto, M.; Inga, A.; Saraiva, L. Discovery of a New Small-Molecule Inhibitor of P53 – MDM2 Interaction Using a Yeast-Based Approach. *Biochem. Pharmacol.* **2013**, *85*, 1234–1245.

(265) Soares, J.; Espadinha, M.; Raimundo, L.; Ramos, H.; Gomes, A. S.; Gomes, S.; Loureiro, J. B.; Inga, A.; Reis, F.; Gomes, C.; et al. DIMP53-1: A Novel Small-Molecule Dual Inhibitor of P53-MDM2/X Interactions with Multifunctional P53-Dependent Anticancer Properties. *Mol. Oncol.* **2017**, *11* (6), 612–627.

(266) Soares, J.; Pereira, N. A. L.; Monteiro, Â.; Leão, M.; Bessa, C.; Dos Santos, D. J. V. A.; Raimundo, L.; Queiroz, G.; Bisio, A.; Inga, A.; et al. Oxazoloisoindolinones with in Vitro Antitumor Activity Selectively Activate a P53-Pathway through Potential Inhibition of the P53-MDM2 Interaction. *Eur. J. Pharm. Sci.* **2015**, *66* (October), 138–147.

(267) Soares, J.; Raimundo, L.; Pereira, N. A. L.; Dos Santos, D. J. V. A.; Pérez, M.; Queiroz, G.; Leão, M.; Santos, M. M. M.; Saraiva, L. A Tryptophanol-Derived Oxazolopiperidone Lactam Is Cytotoxic against Tumors via Inhibition of P53 Interaction with Murine Double Minute Proteins. *Pharmacol. Res.* **2015**, *95–96*, 42–52.

(268) Pereira, C.; Leão, M.; Soares, J.; Bessa, C.; Saraiva, L. New Therapeutic Strategies for Cancer and Neurodegeneration Emerging from Yeast Cell-Based Systems. *Curr. Pharm. Des.* **2012**, *18*, 4223–4235.

(269) Lea, M.; Pereira, C.; Coutinho, I.; Soares, J. New Insights into Cancer-Related

Proteins Provided by the Yeast Model. *FEBS J.* **2012**, *279*, 697–712.

(270) Guaragnella, N.; Palermo, V.; Galli, A.; Moro, L.; Mazzoni, C.; Giannattasio, S. The Expanding Role of Yeast in Cancer Research and Diagnosis: Insights into the Function of the Oncosuppressors P53 and BRCA1/2. *FEMS Yeast Res* **2014**, *14*, 2–16.

(271) Skehan, P.; Storeng, R.; Scudiero, D.; Monks, A.; Mcmahon, J.; Vistica, D.; Warren, J. T.; Bokesch, H.; Kenney, S.; Boyd, M. R. New Colorimetric Cytotoxicity Assay for Anticancer-Drug Screening. *J. Natl. Cancer Inst.* **1990**, *82* (13), 1107–1112.

(272) Vichai, V.; Kirtikara, K. Sulforhodamine B Colorimetric Assay for Cytotoxicity Screening. *Nat. Protoc.* **2006**, *1* (3), 1112–1116.

(273) Kasinski, A. L.; Kelnar, K.; Stahlhut, C.; Orellana, E.; Zhao, J.; Shimer, E.; Dysart, S.; Chen, X.; Bader, A. G.; Slack, F. J. A Combinatorial MicroRNA Therapeutics Approach to Suppressing Non-Small Cell Lung Cancer. *Oncogene* **2015**, *34* (27), 3547–3555.

(274) Franken, N. A. P.; Rodermond, H. M.; Stap, J.; Haveman, J.; van Bree, C. Clonogenic Assay of Cells in Vitro. *Nat. Protoc.* **2006**, *1* (5), 2315–2319.

(275) Yang, P.-C.; Mahmood, T. Western Blot: Technique, Theory, and Trouble Shooting. *N. Am. J. Med. Sci.* **2012**, *4* (9), 429–434.

(276) Chabner, B. A.; Roberts, T. G. Chemotherapy and the War on Cancer. *Nat. Rev. Cancer* **2005**, *5* (1), 65–72.

(277) Charles Sawyers. Targeted Cancer Therapy. *Nature* **2004**, *432*, 294–297.

(278) Amato, I. Cancer Therapy. Hope for a Magic Bullet That Moves at the Speed of Light. *Science (80-.).* **2006**, *262* (5130), 32–33.

(279) Schnipper, L. E.; Strom, T. B. A Magic Bullet for Cancer — How Near and How Far? *N. Engl. J. Med.* **2002**, *345* (4), 283–284.

(280) Burgess, A.; Chia, K. M.; Haupt, S.; Thomas, D.; Haupt, Y.; Lim, E. Clinical Overview of MDM2/X-Targeted Therapies. *Front. Oncol.* **2016**, *6* (January), 1–7.

(281) Li, Q.; Lozano, G. Molecular Pathways: Targeting Mdm2 and Mdm4 in Cancer Therapy. *Clin. Cancer Res.* **2013**, *19* (1), 34–41.

(282) Powers, D. G.; Casebier, D. S.; Fokas, D.; Ryan, W. J.; Troth, J. R.; Coffen, D. L. Automated Parallel Synthesis of Chalcone-Based Screening Libraries. *Tetrahedron*

1998, *54* (16), 4085–4096.

(283) Nielsen, A. T.; Houlihan, W. J. The Aldol Condensation. In *Organic Reactions*; 1968.

(284) Mukaiyama, T. The Directed Aldol Reaction. In *Organic Reactions*; 1982.

(285) Széll, T.; Sohár, I. New Nitrochalcones. IX. *Can. J. Chem.* **1969**, *47*, 1254−1258.

(286) Qian, H.; Wang, T.; Naumovski, L.; Lopez, C. D.; Brachmann, R. K. Groups of P53 Target Genes Involved in Specific P53 Downstream Effects Cluster into Different Classes of DNA Binding Sites. *Oncogene* **2002**, *21* (51), 7901–7911.

(287) May, P.; May, E. Twenty Years of P53 Research: Structural and Functional Aspects of the P53 Protein. *Oncogene* **1999**, *18* (53), 7621–7636.

(288) Yu, J.; Zhang, L. PUMA, a Potent Killer with or without P53. *Oncogene* **2008**, *27*.

(289) Fulda, S.; Gorman, A. M.; Hori, O.; Samali, A. Cellular Stress Responses: Cell Survival and Cell Death. *Int. J. Cell Biol.* **2010**, *2010*.

(290) Chipuk, J. E.; Kuwana, T.; Bouchier-hayes, L.; Droin, N. M.; Newmeyer, D. D.; Schuler, M.; Green, D. R. Direct Activation of Bax by P53 Mediates Mitochondrial Membrane Permeabilization and Apoptosis Published by : American Association for the Advancement of Science Stable URL : Http://Www.Jstor.Org/Stable/3836137. *Am. Assoc. Adv. Sci.* **2016**, *303* (5660), 1010–1014.

(291) Garnier, P.; Ying, W.; Swanson, R. A. Ischemic Preconditioning by Caspase Cleavage of Poly(ADP-Ribose) Polymerase-1. *J. Neurosci.* **2018**, *23* (22), 7967–7973.

(292) Kuete, V.; Mbaveng, A. T.; Zeino, M.; Fozing, C. D.; Ngameni, B.; Kapche, G. D. W. F.; Ngadjui, B. T.; Efferth, T. Cytotoxicity of Three Naturally Occurring Flavonoid Derived Compounds (Artocarpesin, Cycloartocarpesin and Isobavachalcone) towards Multi-Factorial Drug-Resistant Cancer Cells. *Phytomedicine* **2015**, *22* (12), 1096–1102.

(293) Coffino, P. Ubiquitin-Independent P53 Proteasomal Degradation. *Biochim. Biophys. Acta - Mol. Cell Res.* **2014**, *1843* (1), 216–221.

(294) Mullally, J. E.; Moos, P. J.; Edes, K.; Fitzpatrick, F. A. Cyclopentenone Prostaglandins of the J Series Inhibit the Ubiquitin Isopeptidase Activity of the Proteasome Pathway. *J. Biol. Chem.* **2001**, *276* (32), 30366–30373.

(295) Verbitski, S. M.; Mullally, J. E.; Fitzpatrick, F. A.; Ireland, C. M. Punaglandins,

Chlorinated Prostaglandins, Function as Potent Michael Receptors to Inhibit Ubiquitin Isopeptidase Activity. *J. Med. Chem.* **2004**, *47* (8), 2062–2070.

(296) Colland, F. The Therapeutic Potential of Deubiquitinating Enzyme Inhibitors. *Biochem. Soc. Trans.* **2010**, *38* (1), 137–143.

(297) Daviet, L.; Colland, F. Targeting Ubiquitin Specific Proteases for Drug Discovery. *Biochimie* **2008**, *90* (2), 270–283.

(298) Popowicz, G. M.; Czarna, A.; Holak, T. A. Structure of the Human Mdmx Protein Bound to the P53 Tumor Suppressor Transactivation Domain. *Cell Cycle* **2008**, *7* (15), 2441–2443.